



Gerhard Baur, BSc

Experimental analysis of a brine/water heat pump with speed control and vapour injection

MASTERARBEIT

zur Erlangung des akademischen Grades

Diplom-Ingenieur

Masterstudium Wirtschaftsingenieurwesen-Maschinenbau

eingereicht an der

Technischen Universität Graz

Beurteiler

Ao. Univ.-Prof. Dipl.-Ing. Dr.techn. René Rieberer

Betreuer

Dipl.-Ing. Dr.techn. Andreas Heinz

Dipl.-Ing. Franz Hengel, BSc

Institut für Wärmetechnik

Graz, im Juni 2014

STATUTORY DECLARATION

I declare that I have authored this thesis independently, that I have not used other than the declared sources/resources, and that I have explicitly indicated all material which has been quoted either literally or by content from the sources used. The text document uploaded to TUGRAZonline is identical to the present master's thesis.

Graz, am.....

.....

(Gerhard Baur)

ABSTRACT

Title: Experimental analysis of a brine/water heat pump with speed control and vapour injection

Author: Gerhard Baur

1st keyword: Speed Control

2nd keyword: Economiser

3rd keyword: Desuperheater

This thesis deals with new approaches to improve the heat pump efficiency, especially in cold climates. A heat pump test rig containing a speed controlled scroll compressor for adaptable heating capacity, an economiser for improved cycle performance and a desuperheater for the additional preparation of hot water is analysed.

After the test rig start-up the LabVIEW program, for data acquisition and the control of the whole heat pump system, was extended and different controllers were implemented to ensure a safe and reliable operating of the test rig. A compressor performance map was recorded and evaluated concerning the overall isentropic- and volumetric efficiency. For improving the cycle performance the condenser heat exchanger was replaced and the controlling of the main expansion valve was adapted. Measurements for the evaluation of the cycle performance were performed, with special focus on the influence of the economiser and the desuperheater at various compressor speeds.

The compressor shows a reliable performance for all measured operating points although the overall isentropic- and volumetric efficiency strongly decrease with compressor speeds lower than 2400 rpm. This should be considered in further applications of the compressor. The modifications of the test rig have resulted in a lower condensation temperature for all points and a higher evaporation temperature for small cooling capacities. The use of an economiser shows an increasing improvement in the COP with increasing pressure ratio. This promises high benefits for air source heat pumps in cold regions. Beside the space heating provided by the condenser, the additional use of a desuperheater offers the possibility to produce hot water for DHW preparation without a significant loss in cycle efficiency.

KURZFASSUNG

Titel: Messtechnische Analyse einer Sole/Wasser-Wärmepumpe mit Drehzahlregelung und Dampfeinspritzung

Autor: Gerhard Baur

1. Stichwort: Drehzahlregelung
2. Stichwort: Economiser
3. Stichwort: Desuperheater

In dieser Masterarbeit werden Konzepte zur Effizienzerhöhung einer Sole/Wasser Wärmepumpe experimentell untersucht. Der Fokus liegt dabei auf den Neuerungen im Kältemittelkreislauf. Diese bestehen aus dem drehzahlgeregelten Scrollkompressor für variable Heizleistung, der Economiserschaltung zur Effizienzsteigerung und dem Desuperheater zur Warmwasserbereitung.

Nach der Inbetriebnahme des Prüfstandes wurde das LabVIEW Programm zur Datenerfassung und Regelung des gesamten Systems erweitert. Dabei wurden Regler für die Peripherie implementiert und parametrisiert. Der Kompressor wurde vermessen und mittels gesamtisentroper- und volumetrischen Wirkungsgrades analysiert. Zur Effizienzsteigerung des Wärmepumpenkreislaufes wurde der Kondensator getauscht und das Überhitzungssignal durch Verwendung neuer Regelparameter stabilisiert. Im Anschluss wurde der Kreislauf vermessen, wobei das Hauptaugenmerk auf dem Einfluss des Economisers und des Desuperheaters auf die Leistungszahl bei verschiedenen Drehzahlen lag.

Die Auswertung des Kennfeldes hat ein zuverlässiges Betriebsverhalten des Kompressors für alle vermessenen Punkte ergeben. Auffallend ist dabei der starke Wirkungsgradabfall für Drehzahlen kleiner 2400 min^{-1} , dies sollte bei der Festlegung des Arbeitsbereiches für spätere Anwendungen berücksichtigt werden. Durch den Austausch des Kondensators ist die Kondensationstemperatur für alle Betriebspunkte gesenkt worden. Durch die neuen Parameter für die Regelung der Überhitzung konnte die Verdampfungstemperatur für kleine Kälteleistungen erhöht werden. Die Verwendung eines Economisers zeigt eine steigende COP-Verbesserung mit steigendem Druckverhältnis. Speziell für Außenluftwärmepumpen in kalten Regionen stellt die Verwendung eines Economisers damit eine vielversprechende Technologie dar. Auch die Verwendung eines Desuperheaters zeigt großes Potential, da die Erzeugung von Warmwasser ohne eine wesentliche Verringerung der Leistungszahl ermöglicht wird.

PREFACE

This master thesis was written in the academic year 2013/2014 at the Institute of Thermal Engineering at Graz University of Technology to support the development of a heat pump with speed control, economiser and desuperheater for the project MacSheep: “New **M**aterials and **C**ontrol for a next generation of compact combined **S**olar and **h**eat pump systems with boosted **e**nergetic and **e**xergetic **p**erformance”. The project is part of the Seventh Framework Programme (FP7), which is an approach for research and technological development funded by the European Union.

First of all I would like to thank Ao. Univ.-Prof. Dipl.-Ing. Dr. techn. René Rieberer, who gave me the opportunity to write my master thesis at the Institute of Thermal Engineering at Graz University of Technology and for his support during the writing of this thesis.

I would like to express my special appreciation and thanks to my supervisors Dipl.-Ing. Dr. techn. Andreas Heinz and Dipl.- Ing. Franz Hengel BSc, who were tremendous mentors during all phases of my thesis. This created a perfect and motivating working atmosphere during the whole project. I would also like to thank them for reviewing this thesis and their constructive input.

Furthermore I would like to thank everybody of the Institute of Thermal Engineering who contributed to this work, especially Daniel Treichl BSc, who worked on the build-up of the test rig during the summer and gave me advice in the start-up phase and the whole team of the workshop, who helped during the different modifications of the test rig.

I am grateful to my family, who supported me during all my years of study, my parent Anna and Anton, who made it possible for me to study at Graz University of Technology, as well as my sister Andrea.

I would also like to thank my friends from my home town who started to study with me in Graz, who made it an unforgettable and terrific student time.

Last but not least I would like to thank my girlfriend Britta for her support and understanding during writing this thesis.

Graz, 01.06.2014

Gerhard Baur

CONTENT

1 INTRODUCTION.....	1
1.1 Background.....	1
1.2 Task and outline.....	2
2 FUNDAMENTALS	4
2.1 Heat pump.....	4
2.1.1 Functional principle.....	4
2.1.2 Types.....	5
2.1.3 Heat pump reference process.....	6
2.1.4 Working fluids for compression heat pumps.....	7
2.1.5 Compressor types.....	9
2.1.6 Speed control.....	11
2.1.7 Economiser.....	12
2.1.8 Desuperheater.....	14
2.2 Control.....	15
2.2.1 Principles.....	15
2.2.2 Controller parameter setting by Chien Hornes Reswick.....	17
2.3 Error calculation.....	20
2.3.1 Error of measurement.....	20
2.3.2 Propagation of uncertainty.....	22
3 HEAT PUMP TEST RIG.....	24
3.1 Refrigerant cycle.....	24
3.1.1 Compressor system.....	26
3.1.2 Heat exchangers.....	30
3.1.3 Liquid receiver.....	32
3.1.4 Filter dryer and sight glass.....	32
3.1.5 Electronic expansion valves.....	33
3.1.6 Solenoid Valves.....	34
3.1.7 Pipes.....	34
3.2 Source cycle.....	35
3.3 Sink cycle.....	36
3.4 Measurement equipment.....	38
3.4.1 Temperature.....	40
3.4.2 Pressure.....	42
3.4.3 Flow rate.....	43
3.4.4 Electric meter.....	45
3.5 Data acquisition and visualisation.....	45
3.5.1 Compact RIO hardware.....	46
3.5.2 LabVIEW.....	47

3.6 Control circuits in the system.....	48
4 DATA EVALUATION.....	51
4.1 Compressor efficiency	51
4.1.1 Compressor losses	52
4.1.2 Overall isentropic efficiency.....	52
4.1.3 Volumetric efficiency	55
4.2 Cycle performance.....	56
4.3 Heat exchanger performance.....	58
4.3.1 Evaporator	58
4.3.2 Condenser	59
4.4 Error of measurement for the cycle evaluation	61
5 RESULTS AND DISCUSSION.....	65
5.1 Analysis of the compressor	65
5.1.1 Compressor heat losses	65
5.1.2 Overall isentropic efficiency.....	67
5.1.3 Volumetric efficiency	69
5.1.4 Influence of the vapour injection for the different efficiency's.....	71
5.2 Analysis of the heat pump cycle.....	77
5.2.1 Improvements on the cycle performance.....	77
5.2.2 Cycle performance	83
5.2.3 Influence of the economiser on the heat pump cycle.....	86
5.2.4 Analysis of the desuperheater	90
5.2.5 Results of the error calculation	95
6 SUMMARY AND CONCLUSION	96
REFERENCES	99
SYMBOLS	102
LIST OF FIGURES	104
LIST OF TABLES	107
APPENDIX.....	A-1
A-1 Filling and evacuating the heat pump	A-1
A-1.1 Recycling of the refrigerant.....	A-1

A-1.2	Filling of the refrigerant cycle	A-2
A-2	Considerations for installation.....	A-4
A-2.1	Test rig components	A-4
A-2.2	Measurement devices	A-5
A-2.3	Calibration	A-7
A-3	Configuration of the Input and Output modules	A-9
A-4	Measurement matrixes for compressor and cycle evaluation	A-10
A-4.1	Measurement matrix for the compressor evaluation	A-10
A-4.2	Measurement matrix for the cycle evaluation.....	A-14
A-4.3	Measurement matrix for the cycle evaluation without economiser	A-16
A-4.4	Measurement matrix for the desuperheater evaluation	A-18

1 INTRODUCTION

1.1 Background

The main part of the world's energy demand is covered by the combustion of fossil fuels. While the world's energy consumption is still rising with no end in sight the resources of fossil fuels decline (IEA, 2013). The scarcity of these resources is already recognizable by rising prices for crude oil, gas, and other depleted raw materials. With the consumption of fossil fuels goes the output of large amounts of carbon dioxide, which are responsible for the greenhouse effect and furthermore the global warming. Faced with these problems, low carbon solutions for energy production get more and more important. Beside the ambition to create energy without carbon dioxide emission and as a result of the rising energy prices it is crucial to use the power we produce with the highest possible efficiency. One catchphrase which is on everyone's lips today is sustainability. It means, in coherence to the described energy difficulty, that we use our resources in a way that does not limit the well-being of our next generations. High efforts have to be taken, if this target should be reached one day, which mainly depends on the extended development and use of renewable energy sources.

Heat pumps are one way for the efficient use of electricity. Apart from the needed electricity to run the cycle there are no additional carbon dioxide emissions generated during the operation. Thermal heat pumps change the direction of the spontaneous heat flow by means of external energy. In terms of compression heat pumps this external energy is the energy consumption of the compressor. On the low pressure side the working fluid of the heat pump cycle absorbs the heat at a low temperature level. Then the heat pump compresses the vaporized refrigerant to a higher pressure stage, which makes it possible to condense it at a higher temperature level. As a consequence the heat pump can be used for both cooling at the side where the heat is absorbed and heating at the side where the heat is emitted. Since compression heat pumps have already been in use for a long time the working principle is approved. This thesis deals with possibilities to increase the efficiency of the heat pump cycle.

The development of a new advanced and highly efficient heat pump cycle is only one part of the project called MacSheep. This project is conducted within the 7th framework programme. Framework programs are a financial tool through which the European Union supports research and development in almost all scientific areas (<http://cordis.europa.eu/fp7>, 26.02.2014). MacSheep stands for "New Materials and Control for a next generation of compact combined Solar and heat pump systems with boosted energetic and exergetic performance". The goal of this project is to achieve 25 % energy savings for a combined solar and heat pump system for space heating and water preparation compared to current state of the art systems, with still competitive prices on the market. The project consists of nine work packages, whereby the Institute of Thermal Engineering is responsible for the development of a new advanced heat pump type (FP7, 2011).

Many concepts to increase the efficiency of the combined solar and heat pump system were analysed by the help of simulations with the program Trnsys (Trnsys, 2010). After the evaluation of the results the most promising concepts concerning energetic efficiency and economic

benefits were chosen and implemented in a test rig for further evaluation. The main concepts, which are discussed in this thesis, are the usage of a desuperheater for domestic hot water preparation (DHW) additionally to the space heating and the use of an economiser to improve the efficiency, especially in cold climates. This concept includes the testing of a new scroll compressor, which can work at variable speeds and includes an inlet port for vapour injection. (Heinz et al., 2013a)

1.2 Task and outline

The title of this master thesis is “Experimental analysis of a brine/water heat pump with speed control and vapour injection”. According to the title the focus of this thesis was to perform measurements with the test rig and analyse the results, furthermore to manage and perform modifications on the test rig with the aim of improving the efficiency of the cycle in between the test runs.

The start of this master thesis was in the middle of October 2013 with the start-up of the test rig. It was built over the summer and had its initial operation on the seventh of October in cooperation with the compressor manufacturer Copeland. As follow-up many changes on the test rig had to be made until the first measurements could be started. The program in LabVIEW (NI, 2012), which is used as measurement and control system, had to be extended and updated frequently. One of the bigger challenges was to implement controllers for the periphery, which have to work reliable at different operating points and in this context the determination of control parameters for the whole control system. For analysis of test runs an evaluation sheet had to be set up and continuously extended.

Many changes on the test rig had to be made in order to improve the cycle performance. The ball valves for bypassing the desuperheater were changed with valves with a higher inner diameter to reduce the pressure drop. After first test runs the sensors for temperature measurement had to be replaced to ensure reliable measurements. Each modification of the test rig included the evacuation of the refrigerant of the test rig and the filling of it with prior leak tests of the whole system under high pressure. By the beginning of December the test rig was ready for the measurement of the compressor, whereby a performance map was recorded.

After these measurements further efforts were taken to improve the efficiency of the cycle. The main expansion valve was changed to a smaller model in order to increase the stability of the controlled superheating after the evaporator and also to reduce the superheating. Furthermore new parameters for the control of the expansion valve were used to decrease the superheating. The condenser heat exchanger was replaced with a model with 40 instead of 30 plates to reduce the condensing temperature and with that to minimize the pressure ratio of the cycle. The overall goal was the improvement of the coefficient of performance (COP). After these modifications further measurements were taken, starting with the end of March, to analyse the cycle, especially the influence of the desuperheater and the economiser.

This diploma thesis is divided into six chapters, whereby subsequently an outline of the different chapters is given:

Chapter two deals with the fundamentals needed for this thesis. Since the fundamentals of heat pumps have already been covered many times, only a short introduction about the principles of heat pumps is given and then the focus is on the cycle improvements that are used in the heat pump prototype. Furthermore the basics for control and error calculation are covered.

Chapter three deals with the description of the test rig, which was built up as first prototype of this new and innovative heat pump concept. First it deals with the layout of the heat pump cycle and its components. Then the used measurement equipment is described and also all information needed for reconstructing the measurements, like the placement and types of sensors. Also the hard- and software for data acquisition and visualisation and the control circuits are described.

Chapter four shows how the data evaluation is performed. It describes the calculation of the efficiencies, which are used to determine the compressor performance. Furthermore it deals with the cycle performance and the calculation of the heat transfer coefficients of the used heat exchangers. Finally the basics of chapter 2 are used to calculate the measurement error of the COP.

Chapter five shows the results of the measurements. It starts with the results of the compressor measurements and then continues with the results of the cycle performance with special emphasis to the influence of the economiser and the desuperheater. A discussion of the results is included.

Chapter six gives a summary of the thesis and focuses on the main findings of the previous chapters and points out the improvements of the cycle, which show potential for further use and development.

2 FUNDAMENTALS

2.1 Heat pump

This chapter deals with the fundamentals needed for this thesis. It starts with the working principle of heat pumps and continues with a short overview over different heat pump types, whereby a compression- and an absorption heat pump are compared. Then the reference cycle for the compression heat pump is shown. After the description of the used refrigerant and the working principle of the scroll compressor the main innovations of the used heat pump type are discussed, which are the speed controlled scroll compressor, the economiser circuit and the desuperheater.

2.1.1 Functional principle

Heat pumps and refrigerators use the effect of changing the direction of the spontaneous heat flow from the higher temperature level to the lower by the means of external energy. If the extracted energy from the lower temperature level is used for cooling the machine is called refrigerator, if the heat on the higher temperature level is used the machine is called heat pump. Sometimes it is possible to use both effects at the same time, the cooling and the heating. Figure 2-1 shows the working principle of a heat pump with connected source and sink cycle.

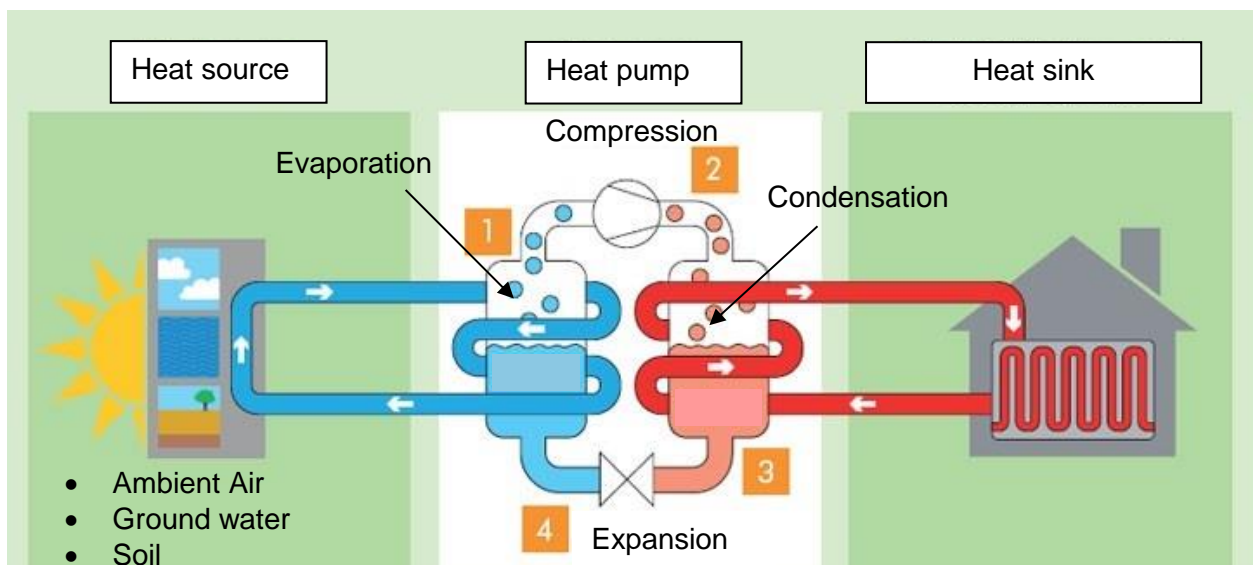


Figure 2-1: Functional principle of a compression heat pump (<http://ecoairsystems.ie/heat-pumps/>, 21.04.2014)

Different heat sources (Figure 2-1) are used to evaporate the working fluid in the heat pump cycle at the low pressure level. The gaseous refrigerant comes to a compressor via the suction line and is compressed. Because of the compression the temperature of the working fluid increases, which makes it possible to use the heat at a higher temperature level. The working fluid gets condensed by transferring the heat to a secondary sink cycle, which is used for heating. After the condensation the working fluid in the refrigerant cycle gets expanded back to the lower pressure level via an expansion valve.

2.1.2 Types

Generally there are two main heat pump concepts to drive the cycle, mechanically and thermally driven. Mechanically driven systems use a compressor, which is usually powered with electricity, to run the cycle and lift the working fluid from the lower temperature level to the higher as already described in chapter 2.1.1. Another important concept is the principle of thermally driven systems, for example the absorption heat pump, whereby the mechanical compressor is replaced with a thermally driven compressor. The comparison of the two different heat pump types can be seen in Figure 2-2. It shows the schematic view of a compression heat pump on the left side and an absorption heat pump on the right side.

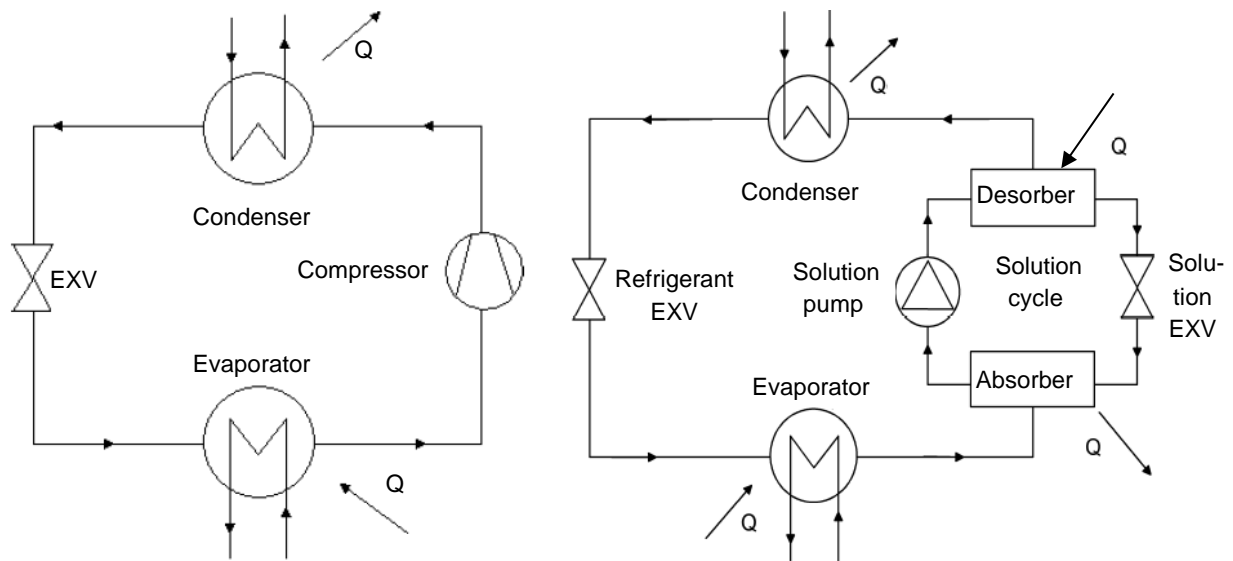


Figure 2-2: Schematic view of a compression heat pump (left) and an absorption heat pump (right) (Rieberer et al., 2009)

For the absorption heat pump a combination of two fluids is needed to run the cycle, the refrigerant itself and a solvent. The evaporated refrigerant is absorbed by the solvent. Then the solution is compressed and transported to desorber by the means of a solution pump, which needs only a fraction of the energy needed in a compression heat pump cycle. The main power input comes from a heat source, which is used to separate the refrigerant out of the solution. That means that the temperature of the input heat has to be higher than the evaporation temperature of the solution. After the evaporation of the refrigerant the solvent is expanded to the lower pressure level with a solvent expansion valve. The refrigerant, which can contain a small part of the solvent depending on the used fluid combination, is lead to the condenser. The further cycle is the same as for the compression heat pump. Two typical used fluid combinations are ammoniac/water for temperatures lower than 0 °C and water/lithium bromide for temperatures higher than 0 °C. (Rieberer et al., 2009)

Since the heat pump covered in this thesis is a mechanically driven compression heat pump the thermally driven heat pumps are not further covered in this thesis. For additional theory about this heat pump type it is referred to the script for heat pump technology of Graz University of Technology (Rieberer et al., 2009).

2.1.3 Heat pump reference process

These fundamentals are based on the script “Heat Pump Technology” of Graz University of Technology (Rieberer et al., 2009). As reference cycle for the heat pump process, the Carnot cycle is used, which consist of two isotherms and two isentropes, as shown in the T/s diagram in Figure 2-3 on the left side.

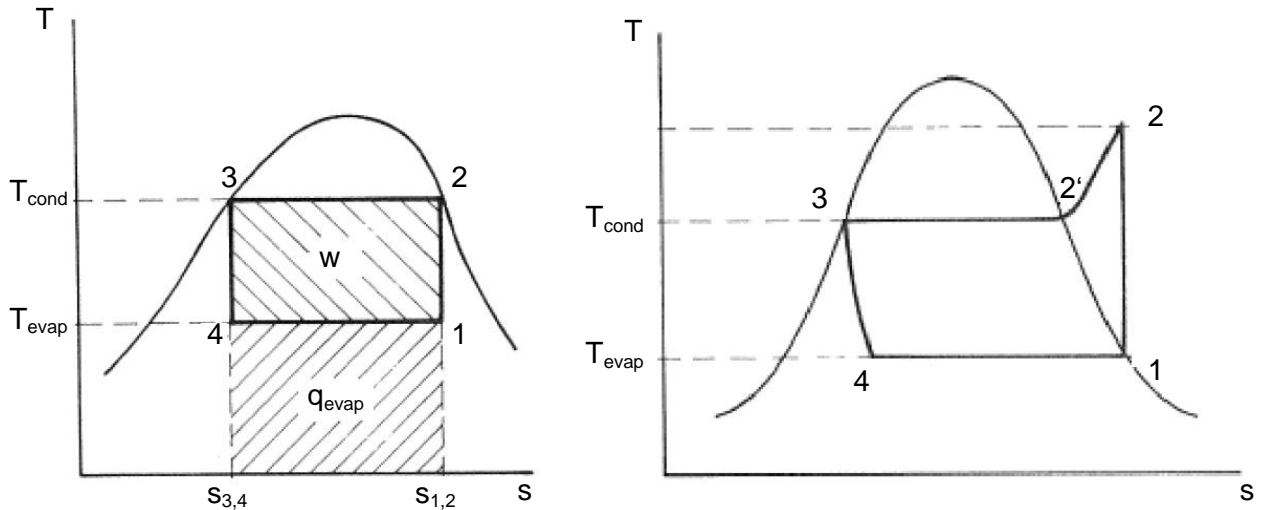


Figure 2-3: Reference cycle for the heat pump process (Rieberer et al., 2009)

In the T/s diagram the converted energies can be seen as areas beneath the state change. For the energy balance it can be written

$$w = q_{cond} - q_{evap} \quad \text{Eq. 2-1}$$

whereby w is the specific work, q_{cond} the specific heat and q_{evap} the specific cold. They can be calculated as

$$q_{cond} = T_{cond} \cdot (s_2 - s_3) \quad \text{Eq. 2-2}$$

$$q_{evap} = T_{evap} \cdot (s_1 - s_4) \quad \text{Eq. 2-3}$$

For the evaluation of the quality of the cycle the Coefficient of Performance (COP) is used which is defined as

$$COP = \frac{\text{usefull energy}}{\text{required energy}} \quad \text{Eq. 2-4}$$

For a heat pump the specific heat is the used energy. If equations 2-2 and 2-3 are inserted in equation 2-4, it can be shown that the maximum possible efficiency for the cycle is the Carnot efficiency.

$$COP_{Carnot} = \frac{T_{cond}}{T_{cond} - T_{evap}} \quad \text{Eq. 2-5}$$

This already implies the very important information that the COP gets better the smaller the difference between the condensation- and the evaporation temperature is, or the condensation-

and evaporation pressure. As a result the COP is often shown in diagrams as a function of the pressure ratio π , which is defined as

$$\pi = \frac{p_{cond}}{p_{evap}} \quad \text{Eq. 2-6}$$

In reality the Carnot process cannot be reached. The compressors are normally not able to compress wet steam which makes it necessary to evaporate to the saturated steam to ensure, that only dry steam is injected into the compressor. The second limitation for reaching the Carnot process is that for the expansion after the condenser an expansion valve is used instead of an expansion turbine. This leads to an isenthalpic state change instead of an isentropic, whereby no energy is won by the expansion. Furthermore the useable enthalpy difference for the heat transfer on the low pressure side reduces. These changes lead to the used reference cycle for the heat pump process which is the Perkins-Evans-Process. It is shown in the T/s diagram in Figure 2-3 on the right side and consists of a

- Isentropic compression (1-2)
- Isobar desuperheating and condensation (2-3)
- Isenthalpic expansion (3-4)
- Isobar evaporation (4-1)

Because of the limitations that an expansion valve is used instead of a turbine and of the dry injection in the compressor, it is not possible to reach the COP defined for the Carnot process. Apart from these limitations, the COP still depends on the temperatures of the condensation and the evaporation.

2.1.4 Working fluids for compression heat pumps

The refrigerant is used for the transportation of the heat from the low to the high temperature level. The technical characteristics are important for the heat pump process as well as the impact of the refrigerant on the environment. This chapter is again mainly based on the script for heat pump technology at Graz University of Technology (Rieberer et al., 2009).

This paragraph mentions some of the most important technical criterions for the selection of the refrigerant. The most important index for the refrigerant is the COP which is important for the efficiency. This implies a small pressure ratio π , which is different for each refrigerant for a certain condensation- and evaporation temperature. Another important refrigerant property is the volumetric heating or cooling capacity. A high volumetric heating capacity reduces the size of the heat pump and with that the costs. Generally it can be said that refrigerants with a high steam pressure have a relatively high volumetric heating capacity. Furthermore the compressor end temperature is important because a higher temperature means a higher stress for the compressor materials and it also influences the used oil. A good heat transfer coefficient is an advantage for the heat transfer in the heat exchangers, especially for the evaporation and condensation. For the refrigerant it is also essential to show good miscibility with the oil of the compressor which circulates in the cycle.

Apart from the technical criterions for the selection of the refrigerant, toxicity and flammability are important as well as the already mentioned impact on the environment. Two numbers are shown here, which describe the influence of the refrigerant on the environment. The ODP

(Ozone Depletion Potential) describes how much degradation of the ozone layer the refrigerant causes compared to R-11, which has an ODP of 1.0. R-11 has the maximum possible ODP, because it contains three chlorine atoms in the molecule. The second number mentioned is the GWP (Global Warming Potential) of the refrigerant. It shows the global warming potential of 1 kg of refrigerant relative to 1 kg CO₂, whereby it is normally specified for a period of 100 years.

Mainly there are two different types of refrigerants which are used, natural- and artificially produced refrigerants. Natural refrigerants are substances, which occur in our biosphere. The advantage of these substances is that their impact on the environment is well known and that their GWP is negligible compared to the GWP of artificially produced refrigerants. Two examples for natural refrigerants are ammoniac and propane. The impact on the environment caused by artificially produced refrigerants is higher, especially the effect on the global warming. In the last century chlorofluorocarbons (CFC) were used but they were forbidden because they are responsible for destroying the ozone layer and they are greenhouse gases. In the 1990s hydro-fluoro-carbon (HFC) refrigerants were invented, which do not contain any chlorine. Two examples for HFC are R-134a or R-152a. Artificial refrigerants without GWP are under research but till now there are no findings which show a comparable performance.

The used refrigerant in this system is R-410a, which is a mixture of two HFC refrigerants, 50 % R-32 and 50 % R-125. It is nearly azeotropic with a temperature glide of only 0.2 K at 1 bar, which means that the two refrigerants hardly separate during the evaporation and condensation process. R-32 is a high pressure refrigerant, which means that the compressor and the cycle have to be dimensioned for more than the commonly used 30 bar. The refrigerant has a high volumetric cooling capacity (Table 2-1, R410a). Because R-32 is flammable it is mixed with R-125 to make the refrigerant incombustible. As a result the volumetric cooling capacity of R-410a is lower than for R-32 but still high compared to other refrigerants like for example R-134a or R-404a. This makes it possible to build the heat pump in a very compact way. R-410a does not have any ozone depletion potential but it is a greenhouse gas with a GWP of 1720. The following Table 2-1 sums up the main properties of R-410a compared to other refrigerants (Jakobs, 2010). The numbers, which depend on the operating point, starting with the volumetric cooling capacity, are given for a point with -5 °C evaporation temperature and 30 °C condensation temperature.

Table 2-1: Properties of R-410a compared to other refrigerants (Jakobs, 2010)

Refrigerant	R-410a	R-134a	R-404a	R-290	R-717
Composition	R-32/125	-	R143a/ 125/134a	-	-
Formula	CH ₂ F ₂ + CF ₃ CHF ₂	CF ₃ CH ₂ F	CF ₃ CHF ₂ + CF ₃ CH ₃	C ₃ H ₈	NH ₃
Group	HFKW	HFKW	HFKW	Hydrocarb.	Inorganic
ODP	0	0	0	0	0
GWP ₁₀₀	1720	1300	3260	3	0
Evaporation temperature (1 bar)	-51.8	-26.4	-46.1	-42.4	-33.7
Critical temperature [°C]	70.2	101.1	72.1	96.7	132.4
Critical pressure [bar]	47.7	40.7	37.4	42.6	113

Volumetric cooling capacity [kJ/m ³]	4414	1865	3153	2610	3146
Compressor end temperature (isentropic) [°C]	56	44	44	44	92
Evaporation pressure [bar]	6.8	2.4	5.1	4.1	3.6
Condensation pressure [bar]	18.8	7.7	14.3	10.8	11.7
Pressure ratio [-]	2.8	3.2	2.8	2.7	3.3
COP [-]	6.08	6.46	5.93	6.39	6.48

Compared to R-134a R-410a has a lower COP but the advantage of R-410a is a much better heat transfer capability and lower pressure drop, which leads to a better system performance. Compared to R-407c R-410a has the advantage of nearly no temperature glide. One further advantage of R-410a is the system compactness. Challenging is the high discharge temperature for high temperature applications. (Zamana, 2010)

2.1.5 Compressor types

Two different types of compressors are used in heat pumps, displacement- and centrifugal. Displacement compressors compress the refrigerant by reducing a closed working volume. A typical example is the piston compressor. Centrifugal pumps increase the speed of the fluid and convert the speed into pressure, whereby they are only used for a far higher power range than needed for domestic heating. For small input powers <10 kW fully hermetic compressors are used, which means that the compressor, and the motor to drive the compressor, are in one compact shell with only the suction and pressure line as outlets as well as the plug for the motor (Rieberer et al., 2009). This also applies for the used compressor in the considered system with a maximum power input of 4.1 kW.

For the power range used in this system piston compressors with a compressor speed of 3000 rpm are a common solution which are produced in high quantities. A compressor type, well suited for speed control, is the rotary compressor (fixed-vane compressor), which consists of a cylindrical piston which moves eccentrically within a cylinder. This type of compressor is also used for applications up to 4.8 kW.

Scroll compressor

A type of compressor which was already invented in the beginning of the last century is the scroll compressor. Since it was not possible to manufacture it at that time with the needed accuracy it was reinvented in the last 20 years (Rieberer et al., 2009). The scroll compressor is described because it is used in the treated heat pump. Figure 2-4 shows the functional principle of a scroll compressor, which is based on the interaction between a fixed scroll and an orbiting scroll. The movable scroll follows the track, which is given by the stationary scroll attached to the compressor body. Both scrolls intersect by centrifugal forces. Figure 2-4 also shows four different stages in the compression process. In the first picture on the top left the refrigerant is sucked in at inlet 1 and 2. In the next picture on the top right the crescent shaped chamber, which is formed by the movement of the orbiting scroll, can already be seen. In the third picture the chamber at the inlet is already closed and the compression process has begun. From there on the volume of the compression space is continuously reduced which leads to a pressure

increase, whereby the chamber moves towards the center. At the end of the compression process the refrigerant leaves through the outlet in the middle of the fixed scroll.

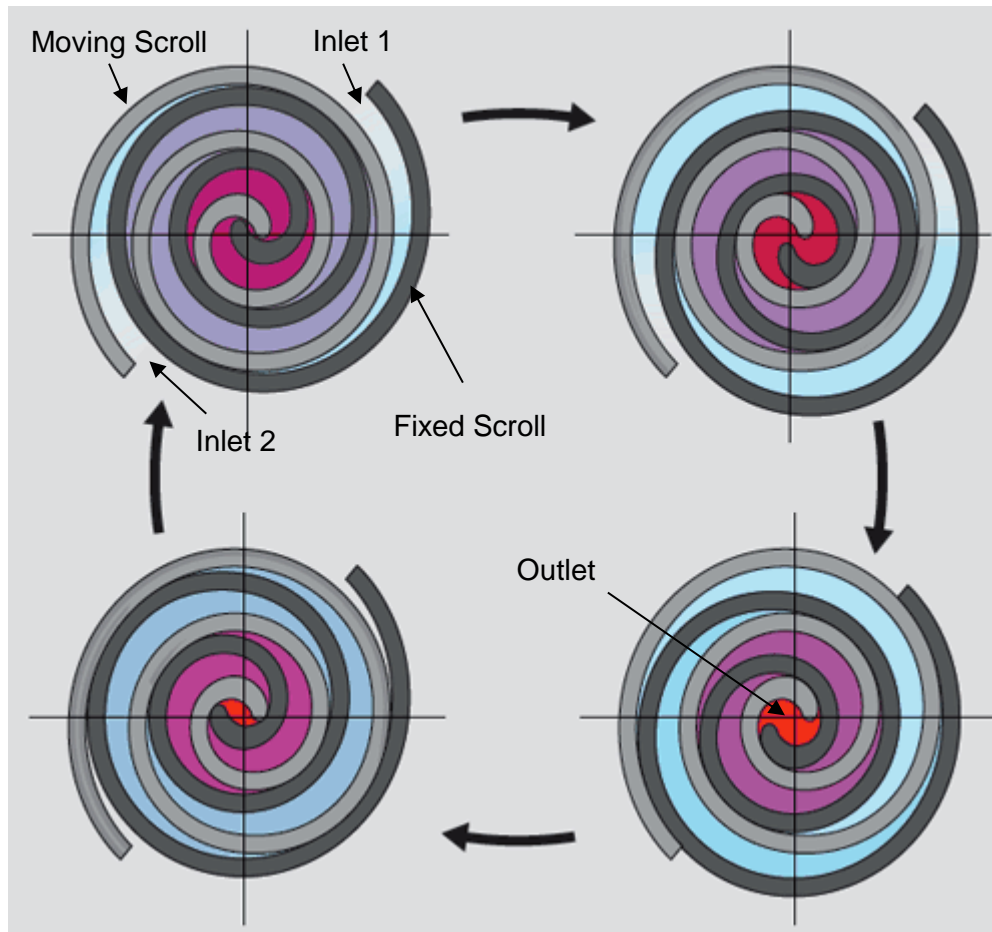


Figure 2-4: Compression process in a scroll compressor
 (<http://www.baulinks.de/webplugin/2012/0001.php4>, 22.04.2014)

The compressor used in the system described in this thesis is a scroll compressor from Copeland, Emerson Climate Technologies. According to the manufacturer the reliability is unmatched with any other state of the art compressor type because it contains 70 % fewer moving parts as well as no inlet and outlet valves. Additionally a scroll compressor can stand a certain amount of liquid refrigerant at the compressor inlet without getting damaged. Furthermore a scroll compressor has up to 50 % less weight and is quieter than other compressor types. (http://www.emersonclimate.com/asia/en-AP/products/compressors/scroll_compressors/Pages, 22.04.2014)

Because it is a rotating compressor it is perfectly suited for speed control, which is also the application it is used for in this thesis. The advantages of a speed controlled compressor are shown in the next chapter. Furthermore the used compressor contains an inlet port for vapour injection needed for the economiser described in chapter 2.1.7. More specific details about the used compressor can be found in the description of the compressor system in chapter 3.1.1.

2.1.6 Speed control

The treated heat pump system includes a variable speed scroll compressor from Copeland. This means that an inverter is used to vary the input frequency and voltage of the compressor and with that the compressor speed. This replaces a constant speed compressor, which can only adapt to the needed heating power by on- and off switching of the compressor. In a former development period of the MacSheep project a cost effectiveness analysis was performed with the help of a Trnsys simulations. An air source heat pump (ASHP) was simulated with- and without speed controlled compressor. This chapter covers the main findings of these simulations. The report includes other investigations about the influence of breakthroughs in advanced heat pump technology, whereby some of the findings are also mentioned in the next chapter. (Heinz et al., 2013a)

The comparison of the ASHP system with- and without speed control was only done for space heating (SH). The speed was controlled to reach a certain outlet temperature of the condenser to keep the temperature of a buffer store at a certain level. The system configuration can be seen in the report. The simulation was done to meet the heat load for two different buildings for the climate Zürich with a space heating demand of 45 kWh/m²a and 100 kWh/m²a.

Figure 2-5 shows the results of this comparison, whereby the hourly values of the heating capacity provided by the radiator heating (Pheat), the condenser of the HP for space heating (PCondSH) and domestic hot water preparation (PCondDHW) can be seen. Since the comparison was done for space heating only the change in the heating capacity for space heating is discussed (PCondSH).

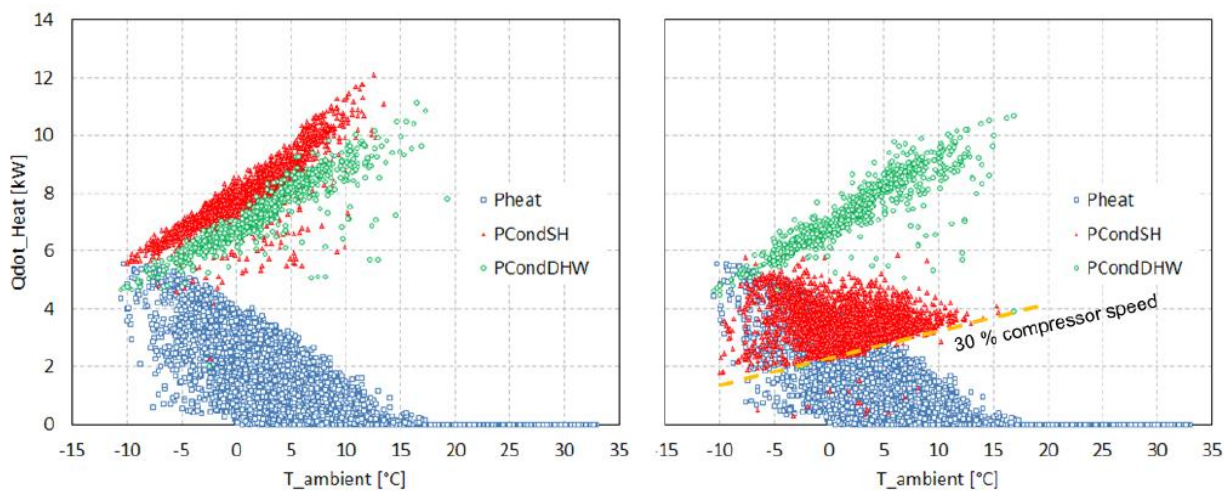


Figure 2-5: Hourly values of the heating capacity: radiator (Pheat), HP in SH mode (PCondSH) and DHW mode (PCondDHW for ASHP Zur45; left: without speed control, right: with speed control. (Heinz et al., 2013a)

In Figure 2-5 on the left side the heating capacity of the constant speed compressor rises with the ambient temperature because of the increasing refrigerant mass flow with the evaporation temperature. The heating capacity of the variable speed compressor on the right side is adapted to the heating demand of the building, which means that the hourly heating capacity, provided by the heat pump, even decreases because of the lower heating demand of the

building with higher ambient temperatures. The 30 % line in the figure shows the minimum compressor speed possible, which is 1800 rpm.

The results show an improvement of the seasonal performance factor (SPF) for both building. Two main causes support the use of a speed controlled compressor, first of all the lower compressor speed leads to lower condenser outlet temperatures. This causes a lower condensation temperature and with that a lower pressure ratio, which leads to a higher COP. Figure 2-6 shows the heat provided by the heat pump condenser with different inlet and outlet water temperatures with- and without speed control. The outlet temperature of the condenser with speed control on the right side is significantly lower.

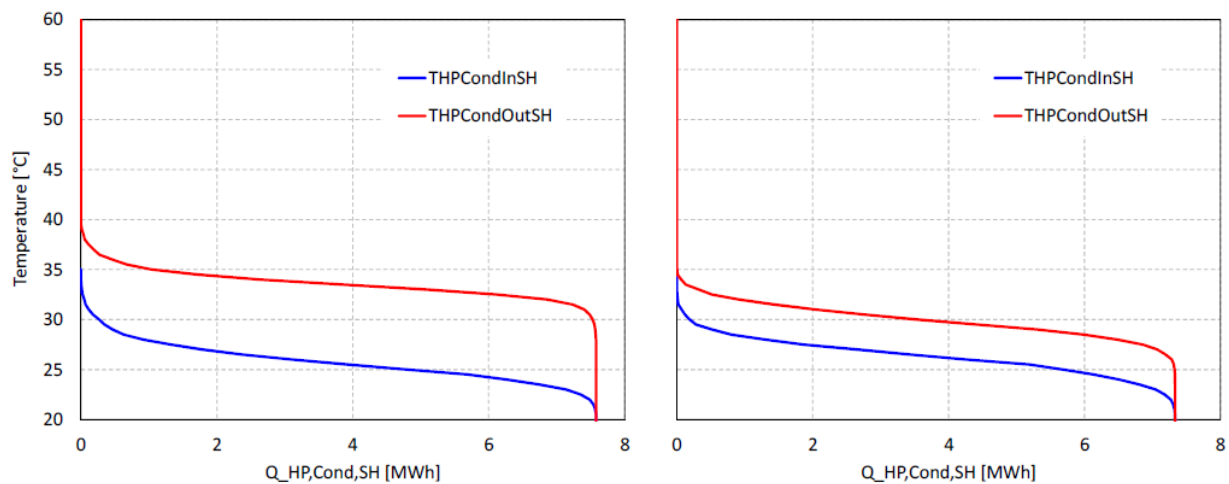


Figure 2-6: Heat provided by the condenser with different inlet and outlet water temperatures; left: without speed control, right: with speed control (Heinz et al., 2013a).

The second advantage of speed control is that the starts and stops are reduced because of the adjustable heating capacity. In the simulation the number of starts was decreased by 55 % from 2344 to 1043 and with that the energy lost for starts and stops decreased by 44 %. This simulation results will be validated in further measurements planned subsequently after this thesis.

It has to be considered that a speed controlled system is more expensive than a constant speed compressor. In the discussed study the energy savings still show the potential of a speed controlled compressor for heat pump systems, especially for applications with small buffer store.

2.1.7 Economiser

An economiser cycle with a vapour injection system is an approach for increasing the efficiency of heat pumps, especially for high pressure ratios. A typical application with an economiser is an ASHP because the efficiency depends on the ambient temperature, which leads to a poor performance (COP) in cold climates. The heating capacity also reduces with decreasing evaporation temperature. Additionally the gas discharge temperature at the compressor outlet rises. With the vapour injection in the compressor at a medium pressure level the gas outlet temperature can be decreased and the heating capacity can be increased for low evaporation temperature, which leads furthermore to a better efficiency. Figure 2-7 shows a comparison of a heat pump cycle without- (left) and with economiser (right).

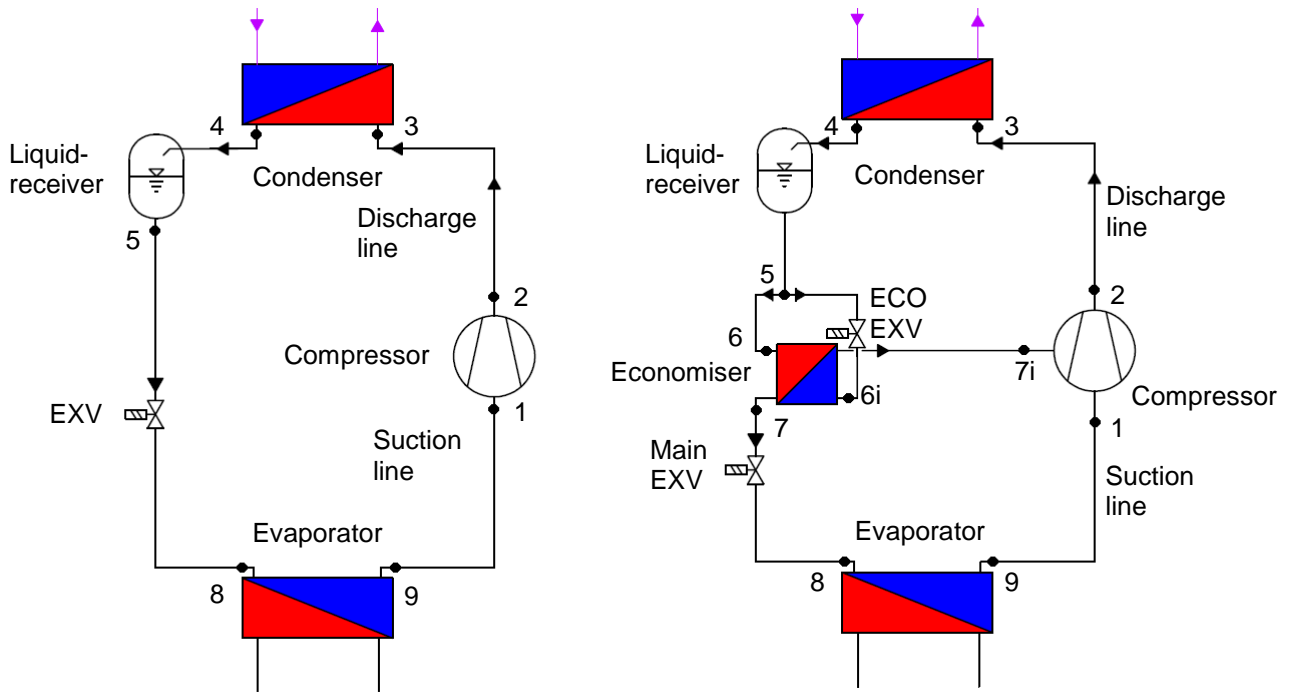


Figure 2-7: Comparison of the schematic view of a heat pump without- (left) and with ECO (right)

Figure 2-8 shows the corresponding temperature-enthalpy diagram for the two different heat pump cycles. The marked points are according to the measured points in the treated heat pump system, which is described in chapter 3.

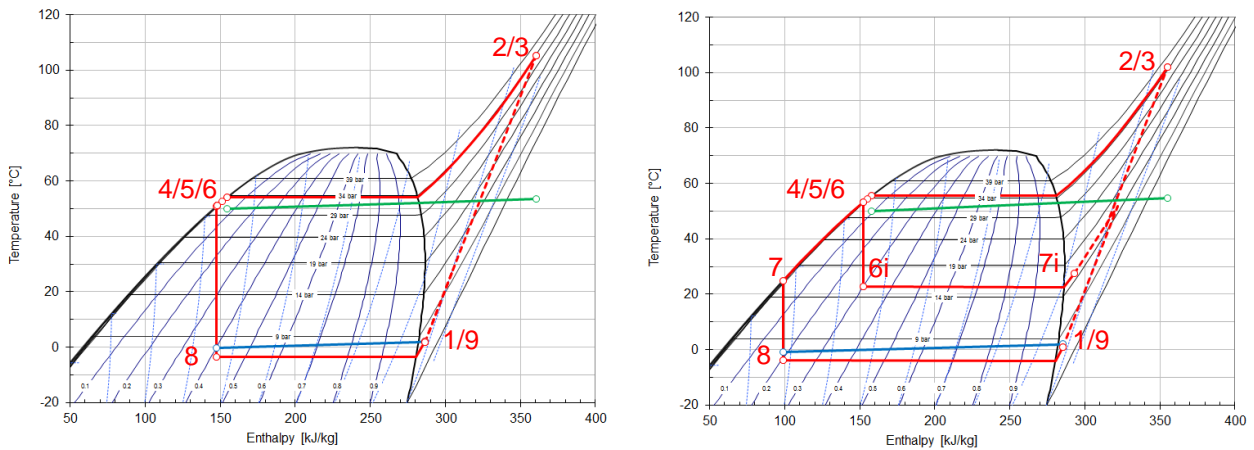


Figure 2-8: Comparison of the heat pump process without (left) and with ECO (right) in a temperature-enthalpy diagram.

In the heat pump cycle with economiser (ECO) the mass flow over the condenser is split up after the high pressure liquid receiver (5). The smaller mass flow is expanded in a second expansion valve (ECO EXV) to a medium pressure level (Figure 2-8) and led to the economiser heat exchanger (HX) (6i). In the economiser the smaller mass flow is fully vaporized by subcooling the main mass flow, which enters the HX in counter flow direction (6). After the subcooling (7) the main mass flow is expanded in the main EXV and led to the evaporator (8), while the superheated injection mass flow enters the compressor at a medium pressure level (7i).

The influence of the economiser was also treated in the simulation of breakthroughs in advanced heat pump technology (Heinz et al., 2013a). The result was a decreased electric demand of 8 % for the mentioned (chapter 2.1.6) 45 kWh/m²a building and 12 % for the 100 kWh/m²a. The influence of the economiser was measured and is discussed in chapter 5.

2.1.8 Desuperheater

A desuperheater is a small heat exchanger, which is implemented in the heat pump cycle between the compressor outlet and the condenser inlet for hot water preparation. The positioning can be seen in the schematic view of the heat pump test rig in Figure 3-1. It uses the superheated refrigerant from the discharge line of the compressor to heat a smaller mass flow of water to a higher temperature level than the temperature at the water outlet of the condenser. Figure 2-9 shows the temperature-enthalpy diagram of the heat pump cycle with desuperheater.

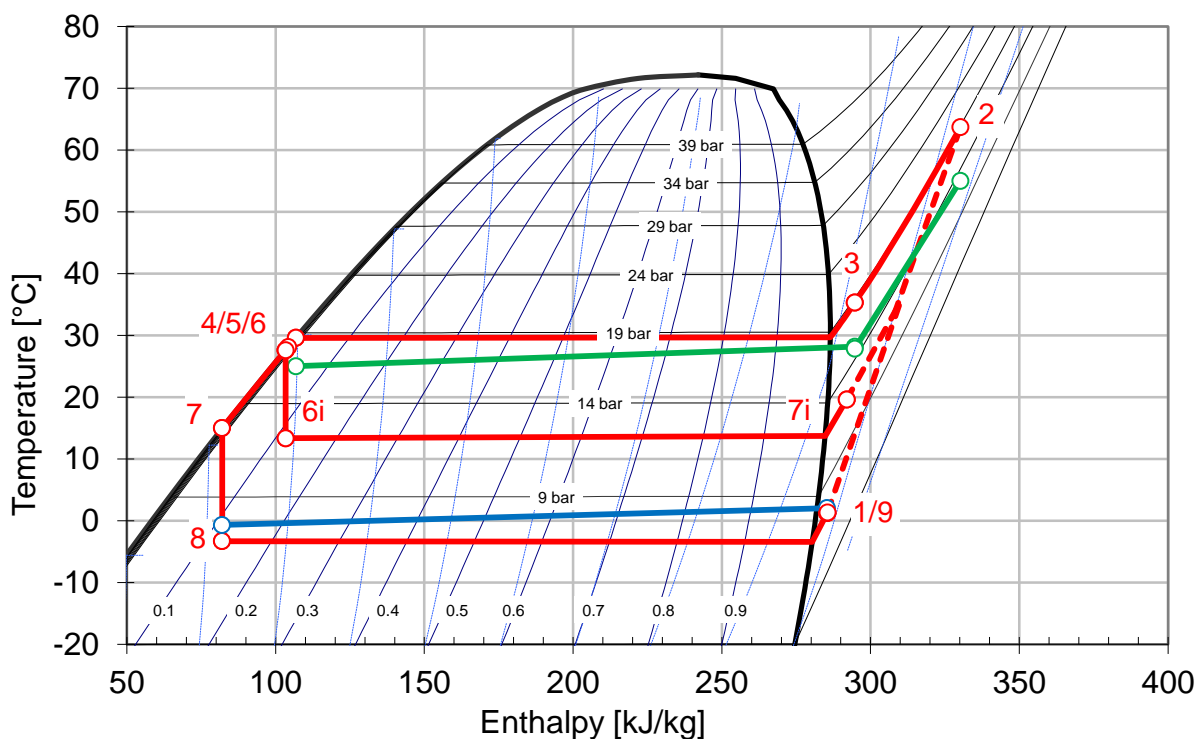


Figure 2-9: Temperature-enthalpy diagram of the heat pump cycle with desuperheater

The main water mass flow over the condenser is split up at the outlet, whereby the bigger part goes to the space heating system (if used) and the smaller part is led over the desuperheater for domestic hot water preparation. This means that the high compressor outlet temperature of the refrigerant can be used to provide a small amount of hot water without increasing the condensation temperature. The water outlet temperature of the desuperheater is controlled by the water mass flow over the desuperheater. The influence of the desuperheater on the COP and its use for domestic hot water (DHW) preparation are discussed in chapter 5.2.4.

2.2 Control

Different control circuits are implemented in the test rig and the periphery, which are discussed in chapter 3.6. This chapter provides the basics needed for the implementation of the controller including the parameter setting. It is mainly based on a script of the University of Applied Science of Pinkafeld (Görtler, 2010a).

2.2.1 Principles

The goal of a control is to develop a system with certain behaviour, for example to keep the temperature on a specified level. The control of a variable can be shown as a control circuit (Figure 2-10), whereby the notations are the following

- w.. reference variable (setpoint which y should reach)
- e .. control error (difference of w and y)
- u .. controlled input (generated by the controller with the controlling algorithm)
- y .. controlled output (process value e.g. mass flow or temperature)
- z .. disturbance variable (influences the process value y)
- e .. as standard signal (for instance 4 – 20 mA)

The control circuit consists mainly of the controller, the controlled system and the measuring device. Normally the setpoint generator changes the reference variable w into an electric standard signal w_E , which is compared to the standard signal of the controlled output y_E . The controlled output is subtracted from the reference variable, which results in the control error e_E . The controlling algorithm calculates the controlled input u_E for the controlled system. In this test rig the LabVIEW program directly compares the controlled output y with the reference variable w to calculate the control error e , which is converted to the controlled input u_E by the control algorithm. The controlled system is the considered process, which can be for example a pump which controls the mass flow. It has the controlled input u_E as input variable and the controlled physical output y , which is measured and changed into an electrical signal and led back to the controller

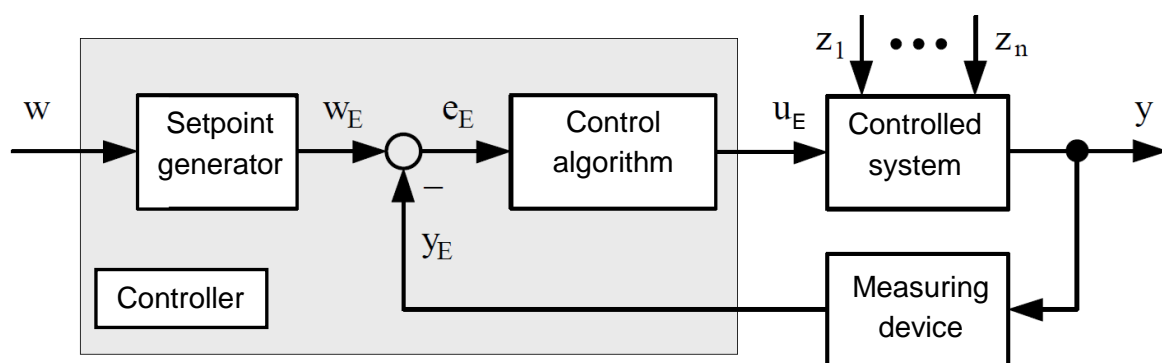


Figure 2-10: Block diagram of a control circuit (Görtler, 2010a)

The control algorithm varies regarding its response characteristics. That means that the step response caused by a change in the control error e on the input, provides a different signal at the output of the control algorithm for a different type of control algorithm. The response characteristics can be classified by three different behaviours which are P-, I-, and D and can be seen in Figure 2-11. If the controller has P-behaviour the response to a change in the control error Δe causes a proportional change in the output of the controller u . For I-behaviour the

response to a change in the control error causes a theoretically infinite change in the output of the controller, which is caused by a constant slope of u . D-behaviour causes the output u to go back to the initial position after a certain time T , whereby the time constant T is the time after the value u is reduced by 66.7%.

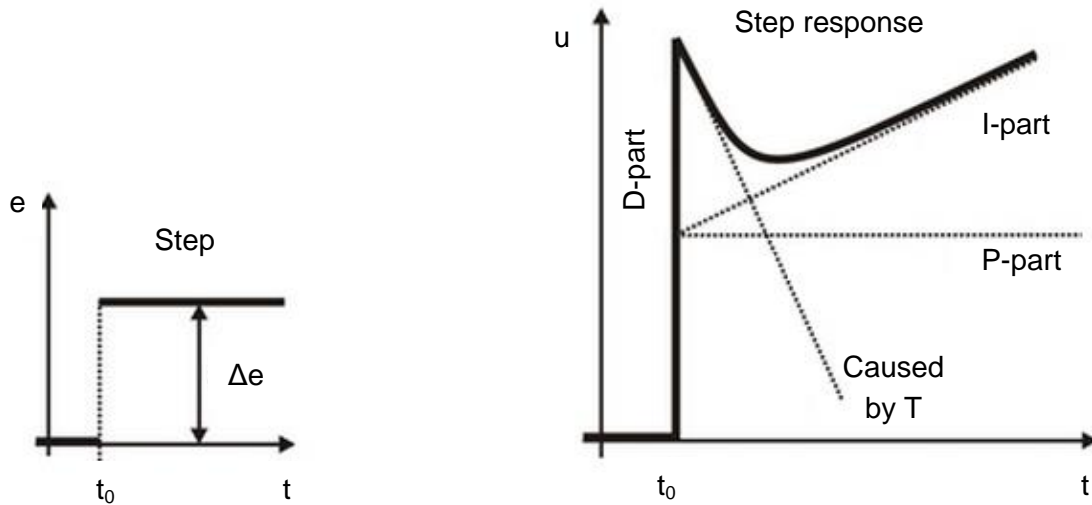


Figure 2-11: Response characteristic of a PID controller (<http://www.geltec.de>, 26.03.2014)

The control algorithm calculates from the controlling difference $e(t)$ the controlled input $u(t)$, whereby each kind of controller can be described with a controller equation. The transmission behaviour of the P-part can be described with

$$u(t) = K_P \cdot e(t) \quad \text{Eq. 2-7}$$

The P-part ensures a fast compensation of the control difference with a proportional change in the control variable u with the controller gain K_P . The I-part makes sure that the setpoint is really reached in a stationary operating point by integration of the control error till it gets to zero. The control variable u is proportional to the integrated control error over time and described with

$$u(t) = K_I \cdot \int e(t) \cdot dt \quad \text{Eq. 2-8}$$

The D-part is used for a fast reaction of the controller to a change in the control error $e(t)$. The control variable $u(t)$ is proportional to the deviation of the control error

$$u(t) = K_D \cdot \frac{de(t)}{dt} \quad \text{Eq. 2-9}$$

For an ideal PID controller the transmission behaviour can be described by summing up the individual parts

$$u(t) = K_P \cdot e(t) + K_I \cdot \int e(t) \cdot dt + K_D \cdot \frac{de(t)}{dt} \quad \text{Eq. 2-10}$$

Depending on DIN 19226 two further control parameters are used for describing the transmission behaviour of controllers, which are the integral time T_N and the derivation time T_V .

$$T_N = \frac{K_P}{K_I} \quad \text{Eq. 2-11}$$

$$T_V = \frac{K_D}{K_P} \quad \text{Eq. 2-12}$$

The transmission behaviour of the ideal PID controller can then be described with

$$u(t) = K_P \left(e(t) + \frac{1}{T_N} \int e(t) \cdot dt + T_V \frac{de(t)}{dt} \right) \quad \text{Eq. 2-13}$$

P controllers are used if a remaining difference of the reference variable w and the controlled output y does not matter. The advantage of this type of controller is that it is fast and easy to parameterise. PI controllers are widely used and have good characteristics concerning response time and accuracy. PID controllers are well suited for control systems of higher orders because of the stabilising D-part, although three variable parameters make it more complicated to parameterize. Furthermore the D- part can cause instability, if there is noise on the controlled output y .

2.2.2 Controller parameter setting by Chien Hornes Reswick

For the parameter setting of the used controllers in the system an experimental method is used. This means that this method does not need a mathematical model of the controlled system, instead an experiment is used. The Chien Hornes Reswick scheme uses the step response of the controlled system for the parameter determination. The transmission behaviour of dynamic systems can be divided into systems with (global P-behaviour) and without (global I-behaviour) compensation which can be seen in Figure 2-12.

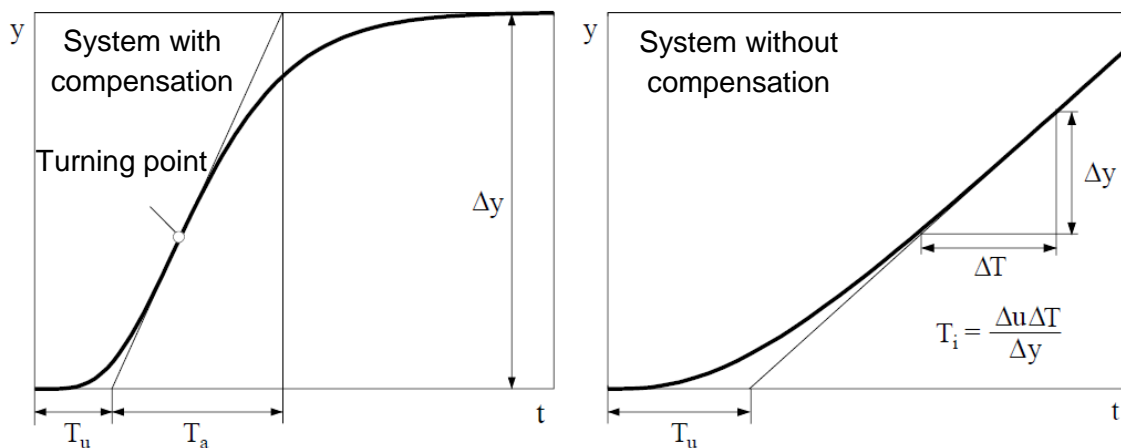


Figure 2-12: Step response of control systems with and without compensation (Görtler, 2007)

For a system with compensation there are two models described to determine the transmission function which are the Wendetangentenmodell (WT) and the Summenzeitkonstantenmodell (SZK). Both are first order models. The WT can be seen in Figure 2-12 on the left. A tangent is

laid into the turning point of the step response and cut with two horizontal lines $y = 0$ and $y = 0 + \Delta y$. The dead time T_u and the compensation time T_a can be read from the step response. The dead time is the time from the beginning of the input signal till the cutting point of the tangent with the starting value of y . The compensation time is the time which passes from the cutting point of the tangent with the starting value of y till the cutting point of the tangent with the end value. Furthermore the gain factor K can be read out of the step response, which is defined as $K = \Delta y / \Delta u$ and needed for the Chien Hornes Reswick scheme (Görtler, 2010a). With the Quotient T_u / T_a the difficulty of controlling a system can be determined, which is shown in Table 2-2. The difficulty increases with a rising dead time for a constant compensation time.

Table 2-2: Difficulty of controlling a system (Görtler, 2010a)

Quotient T_u / T_a	Difficulty
< 0,1	Good controllability
0.2 to 0.3	Controllable
> 0.3	Bad controllability

A second possibility for the determination of the parameters T_u , T_a and K is the SZK, which was used for the parameterization of the test rig controllers. Figure 2-13 shows the comparison of the SZK model to the WT, whereby the SZK model is on the right side. The Parameter K is the end value of the step response. The step response is cut with two horizontal lines at 20 % of the end value of y and at 80% of it. The corresponding times t_{20} and t_{80} are read from the diagram (Hengel, 2012). With the times t_{20} and t_{80} the parameters T_u and T_a can be calculated as shown in the following equations

$$T_a = 0.721 \cdot (t_{80} - t_{20}) \tag{Eq. 2-14}$$

$$T_u = 1.161 \cdot t_{20} - 0.161 \cdot t_{80} \tag{Eq. 2-15}$$

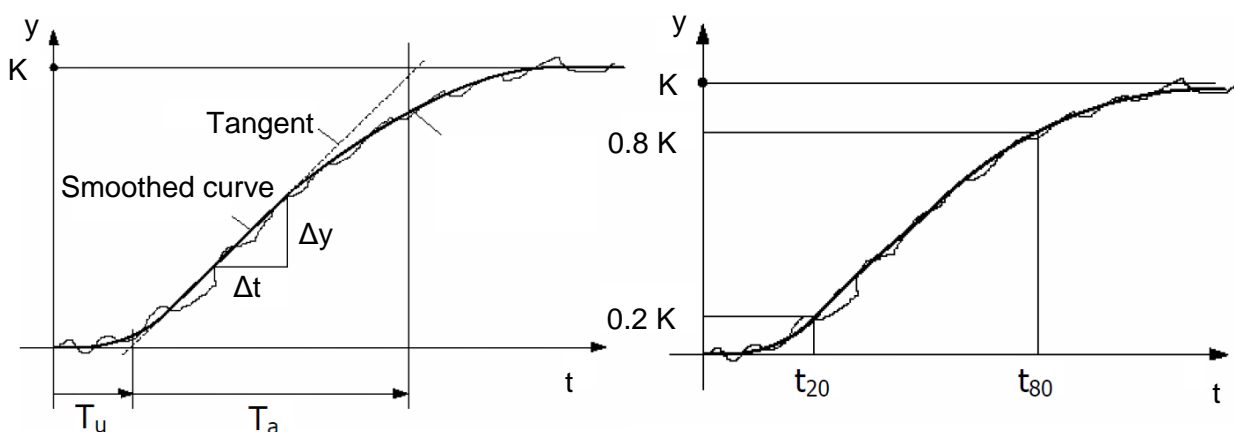


Figure 2-13: WT model compared to the SZK model (Hengel, 2012)

For the parameterization of each controller described in chapter 3.6 the step response is taken twice. One step response of the controlled value y from the lower level to the higher (e.g. step in the static height of the pump from 0 % to 100 %) and one from the higher level to the lower. For both step responses the parameters are taken and averaged. This ensures a similar response of the controller independently from which side the setpoint is reached. With the parameters T_u ,

T_a and K the Chien Hornes Reswick parameterization can be done. Table 2-3 shows the calculation of the controller parameters for different types of controllers. It can be chosen between aperiodic controlling and 20 % overshoot.

Table 2-3: Chien Hornes Reswick parameterization (Görtler 2007)

Control type	Aperiodic controlling		20 % overshoot	
	Leading	Disturbance	Leading	Disturbance
P	$K_p = \frac{0,3T_a}{K_S T_u}$	$K_p = \frac{0,3T_a}{K_S T_u}$	$K_p = \frac{0,7T_a}{K_S T_u}$	$K_p = \frac{0,7T_a}{K_S T_u}$
PI	$K_p = \frac{0,35T_a}{K_S T_u}$ $T_n = 1,2T_a$	$K_p = \frac{0,6T_a}{K_S T_u}$ $T_n = 4T_u$	$K_p = \frac{0,6T_a}{K_S T_u}$ $T_n = T_a$	$K_p = \frac{0,7T_a}{K_S T_u}$ $T_n = 2,3T_u$
PID	$K_p = \frac{0,6T_a}{K_S T_u}$ $T_n = T_a$ $T_v = 0,5T_u$	$K_p = \frac{0,95T_a}{K_S T_u}$ $T_n = 2,4T_u$ $T_v = 0,42T_u$	$K_p = \frac{0,95T_a}{K_S T_u}$ $T_n = 1,35T_a$ $T_v = 0,47T_u$	$K_p = \frac{1,2T_a}{K_S T_u}$ $T_n = 2,3T_u$ $T_v = 0,42T_u$
PD	Average values for disturbance $K_p = \frac{1,8T_a}{K_S T_u}, T_v = 0,5T_u$			

With the aperiodic parameters the controller is slower but does not overshoot compared to the second possibility. For both parameter types it can be chosen between “Leading” and “Disturbance” parameter. If there are any influences from outside the disturbance parameters should be used which are faster than the leading parameters, although this implies that the controller tends more to overshoot.

2.3 Error calculation

To verify the gained results of the cycle evaluation, an error calculation for the COP was performed after the measurements. This chapter gives an introduction about the error of measurement and describes the basics about propagation of uncertainty, which is needed in chapter 4.4. It is mostly based on a script of the University of Applied Science of Pinkafeld (Görtler, 2010b) and a script of Graz University of Technology (Rieberer, 2013).

2.3.1 Error of measurement

The goal of a measurement is to determine the true value x_{true} . Since there is a difference between the measured value x_m and the true value for each measurement, the error estimation is used to determine the range in which the true value lies with a specific certainty. This is why each measurement result x consists of the measured value, which is also the best estimated value, and the measurement error Δx . The measurement error always applies for a confidence interval.

$$x = x_m \pm \Delta x \quad \text{Eq. 2-16}$$

The measurement error is important to determine if two measurements match within their measurement uncertainty and it shows the quality of the measurement.

The measurement error of a single measurement consists of a systematic- and a random part. If it is assumed that the errors are normally distributed the overall error can be calculated as

$$\Delta x = \sqrt{\Delta x_{\text{sys}}^2 + \Delta x_{\text{rand}}^2} \quad \text{Eq. 2-17}$$

Systematic measurement errors have a value and a sign. If a measurement is repeated this error occurs for each measurement. Causes can be for example the influences from outside like a change in the atmospheric pressure or a defect of the measurement device. Systematic errors are still hard to predict because the repetition of a measurement does not help to determine the systematic error. A second measurement with a more accurate measurement device is needed to assess the systematic error. This is done in the calibration process which is described in appendix A-2.3. With the calibration a part of the systematic error can be removed. The remaining deviation is part of the measurement error. Table 3-2 shows the measurement errors for the used measurement devices. For the flow meters, the temperature and the absolute pressure sensors the uncertainty consists of the remaining systematic error after the calibration.

If measurement devices are not calibrated the accuracy specified from the manufacturer has to be used. Most of the time manufacturers give the measurement error as accuracy classes, which are specified in the manual. Accuracy class 1 means that the maximum error is 1 % of the measuring range. This means that 100 % (confidence interval) of all measured values are within that deviation range (It is important to read the manual carefully because some manufacturer also state the error as percentage of the measured value). In this case a rectangular distribution is assumed, which means that each value in this range has the same probability. All systematic errors, which were determined after the calibration process, are

assumed to be rectangular distributed. This distribution can be converted into a normal distribution with

$$\Delta x = \frac{b - a}{\sqrt{12}} \quad \text{Eq. 2-18}$$

whereby $b - a$ is the range in which the measured value has to be. For example a flow meter with 1 % error of measurement of the measured value and a flow of 100 kg/h would have a range of 2 kg/h.

The second part of the measurement error is the random error, which cannot be captured or rectified. Causes are for example not controllable, random interactions with the environment or not controllable impacts of the measurement device. Random errors are not further considered in the calculation of the measurement error but the principles are shown for the sake of completeness. The measured values scatter around the expected value μ . If the system is under steady state condition, random measurement errors can be determined with statistical methods. The arithmetic mean x_0 shows the best approximation to the true value after N measurements x_i

$$x_0 = \frac{1}{N} \cdot \sum_{i=1}^N x_i \sim \mu \quad \text{Eq. 2-19}$$

whereby it corresponds to the expected value, if N goes towards infinity. Additionally to the expected value μ the standard deviation σ is used to describe normally distributed values

$$\sigma = \sqrt{\frac{1}{N} \cdot \sum_{i=1}^N (x_i - \mu)^2} \quad \text{Eq. 2-20}$$

For normally distributed values 68.3 % of all values are in the range $\mu \pm \sigma$, 95.4 % are in the range $\mu \pm 2\sigma$. Because the standard deviation can only be calculated for an infinite amount of measurements the empirical standard deviation s is used.

$$s = \sqrt{\frac{1}{N - 1} \cdot \sum_{i=1}^N (x_i - x_0)^2} \quad \text{Eq. 2-21}$$

It shows the deviation of a single measurement. If a mean lies for example in the confidence interval $x_0 \pm 2s$ ($k = 2$), it also means that about 95 % of all values are in this range. Since for most repeated measurements the deviation of a single measurement is not important the deviation of the arithmetic mean is given with

$$s_{x_0} = \frac{1}{\sqrt{N}} \cdot s = \sqrt{\frac{1}{N \cdot (N - 1)} \cdot \sum_{i=1}^N (x_i - x_0)^2} \quad \text{Eq. 2-22}$$

which shows how far the mean is away from the true mean with a certain confidence. This means that to halve the deviation of the arithmetic mean, four times as much measurements are necessary.

2.3.2 Propagation of uncertainty

Often physical quantities are not directly measured, instead they are calculated from one or more measured values. The influence of the measurement error on the calculated result has to be determined. Figure 2-14 shows how the linear derived error can be calculated if the result, which should be determined, only depends on one measured value

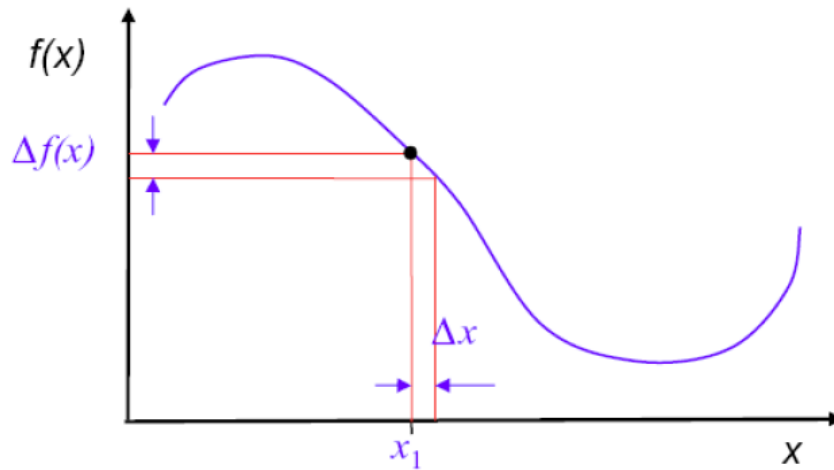


Figure 2-14: Linear propagation of uncertainty (Rieberer, 2013)

$$\Delta f(x) = \frac{\partial f}{\partial x}(x_1) \cdot \Delta x \quad \text{Eq. 2-23}$$

Equation 2-23 gives a good approximation for the change in the function $f(x)$ for small changes because of the measurement error Δx .

If the result of the measurement consists of more than one measured value x_1, x_2, \dots, x_n , the influence of the measurement errors $\Delta x_1, \Delta x_2, \dots, \Delta x_n$ on the result $\Delta f(x_1, x_2, \dots, x_n)$ can also be determined by considering the measurement error of each measured value on the result individually and adding them up.

$$\Delta f(x_1, x_2, \dots, x_n) = \left| \frac{\partial f}{\partial x_1} \right| \cdot \Delta x_1 + \left| \frac{\partial f}{\partial x_2} \right| \cdot \Delta x_2 + \dots + \left| \frac{\partial f}{\partial x_n} \right| \cdot \Delta x_n \quad \text{Eq. 2-24}$$

This equation calculates the maximum possible error for the result if all individual errors reach the maximum value. Normally measurement errors are determined as if they are normally distributed for a certain confidence interval (for example one standard deviation: $k = 1$), because

it is unlikely that all individual measurement errors reach the maximum. This leads to the Gaussian propagation of uncertainty which sums up the individual normally distributed errors geometrically

$$\Delta f(x_1, x_2, \dots, x_n) = \sqrt{\left(\frac{\partial f}{\partial x_1} \cdot \Delta x_1\right)^2 + \left(\frac{\partial f}{\partial x_2} \cdot \Delta x_2\right)^2 \dots \left(\frac{\partial f}{\partial x_n} \cdot \Delta x_n\right)^2} \quad \text{Eq. 2-25}$$

One problem of this measurement error calculation is that the systematic errors are generally not normally distributed, which can lead to an underestimation of the error. For the evaluation of the measurement error in the cycle, the Gaussian error estimation is used. For this error estimation all systematic errors from the calibration process are converted from rectangular distribution into a Gaussian normal distribution with equation 2-18.

3 HEAT PUMP TEST RIG

This chapter deals with the architecture of the test rig and the equipment for measurement and control. After the simulation of different concepts for improving the efficiency of the heat pump process, the most promising ones were realized in a test rig, which was built in the summer of 2013 at the Institute of Thermal Engineering at Graz University of Technology. Most of the construction work was done by Daniel Treichl with supervisors Andreas Heinz and Franz Hengel. In this chapter the layout of the test rig is explained and also the main components. Two mobile devices with water or brine storage and heating rods are used as source and sink for the heat pump prototype. The structure of the source and sink is also described. Furthermore the implemented measurement equipment is discussed, first the placement of the sensors and then the different types. For data acquisition and the control of the test rig a National Instrument (NI) system is used, which is also described in this chapter.

3.1 Refrigerant cycle

To get an overview of the refrigerant cycle Figure 3-1 shows the schematic plan of the heat pump prototype.

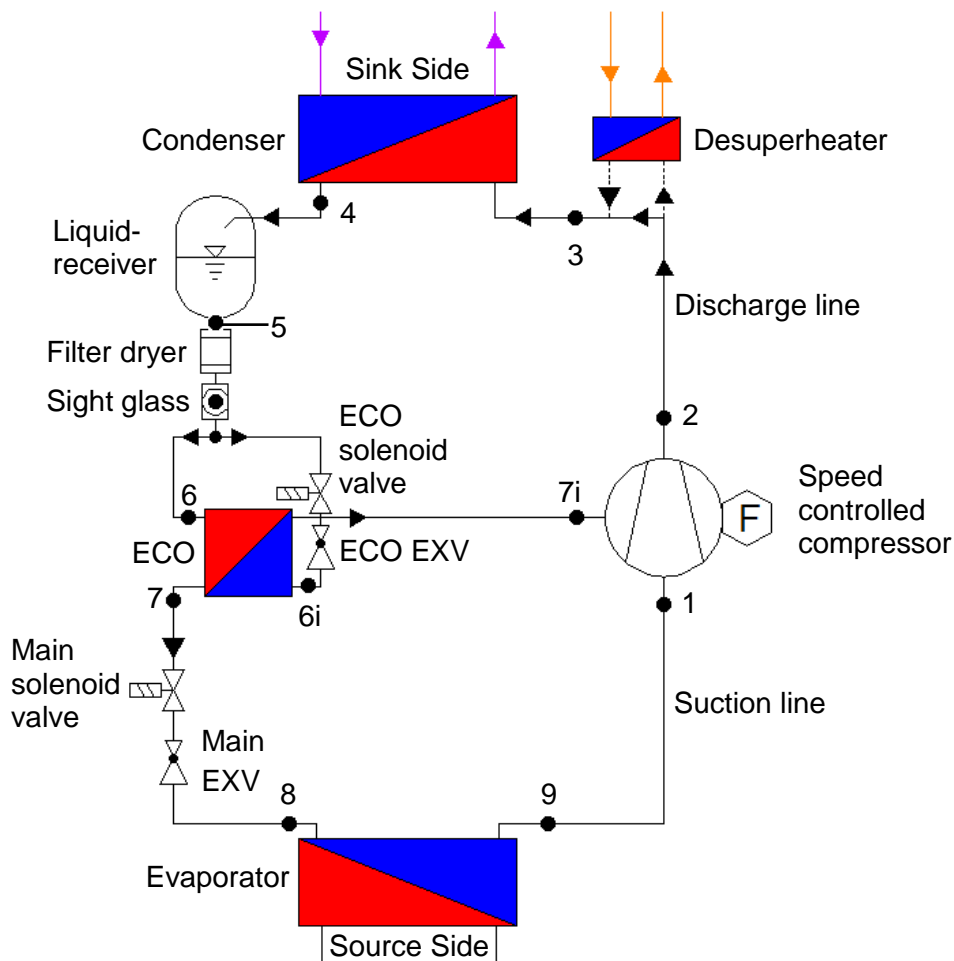


Figure 3-1: Schematic view of the working fluid cycle of the heat pump (Heinz et al., 2013b)

Beginning at the compressor inlet (1) the gaseous refrigerant from the suction line is compressed and then discharged at the outlet port of the compressor (2). Then it passes the discharge line and enters the desuperheater and then the condenser (3). Two ball valves can be used to switch on and off the desuperheater depending on whether hot water should be produced or not. If the desuperheater is switched off, the working fluid enters directly the condenser. After the condenser (4) the liquid receiver is installed to ensure that the refrigerant has a defined liquid state. Furthermore it operates as buffer since it contains most of the refrigerant in the cycle. After the liquid receiver (5) a filter dryer is used to clean dirt and humidity out of the system, followed by a sight glass. It contains an indicator for the humidity in the system and shows bubbles in the working fluid under certain conditions. After the sight glass the refrigerant flow is split up into the main cycle, which enters directly the economiser (6) and into the secondary cycle, which enters the ECO expansion valve, where the refrigerant is expanded to a medium pressure level (6i). In the economiser the refrigerant of the secondary cycle is vaporized again before entering the injection port of the compressor (7i), while the refrigerant on the main cycle is subcooled. After the economiser the working fluid of the main cycle is expanded and enters the evaporator (8). Solenoid valves are placed before each of the two expansion valves to close the circle in addition to the expansion valves. In the evaporator the refrigerant is evaporated and superheated (9) before entering the suction port of the compressor. The whole heat pump cycle layout can be seen in an exemplary temperature-enthalpy diagram in Figure 2-8 / Figure 4-1.

Figure 3-2 shows the test rig after the construction phase including all important parts of the working fluid cycle as well as the connections for the source and sink.

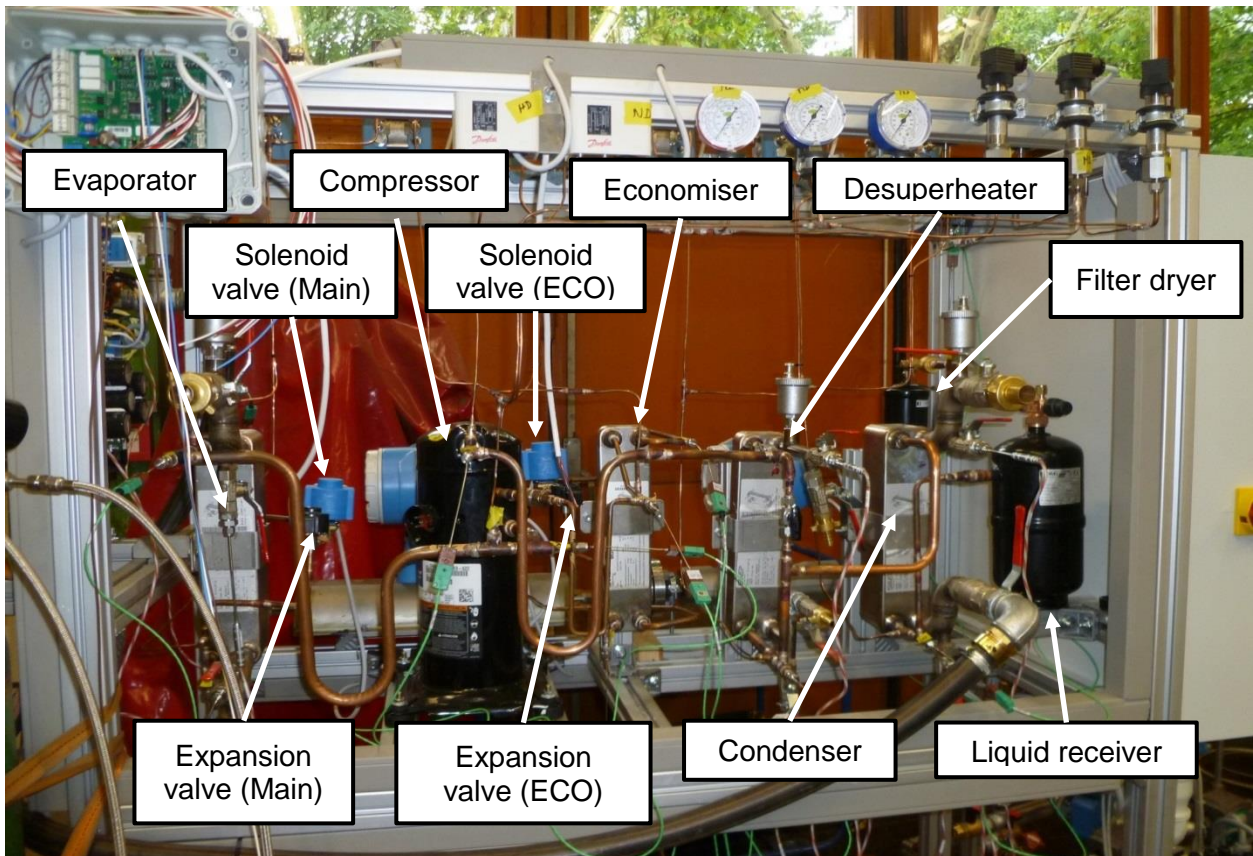


Figure 3-2: Front view of the heat pump prototype (Treichl, 2013)

The components of the heat pump test rig are mounted on a frame which consists of aluminium profiles. The evaporator plate heat exchanger (HX) is fixed on the left side of the test rig, followed by the compressor, which is to the right of the evaporator. The further order of the plate heat exchangers from the left to the right is the economiser, the desuperheater and finally the condenser, whereby the different components are all marked and indicated. Before the inlet of the evaporator the main solenoid- and expansion valves are installed as well as the EVI solenoid- and expansion valve before the inlet of the economiser as described in the schematic view of the heat pump. The liquid receiver and the filter dryer are mounted on the right side of the test rig after the condenser outlet.

3.1.1 Compressor system

The compressor system consists basically of the compressor itself and the motor control drive, which consists of the Superheat and Envelope Controller (SEC), for controlling the refrigerant cycle, and the drive to convert the 50 Hz AC 230 V input into a variable frequency, variable voltage output to power the variable speed compressor. The heat pump system controller controls the SEC board and all further periphery and sensors, which is in this case the computer with the LabVIEW software. Figure 3-3 shows the system with the embedded Copeland compressor.

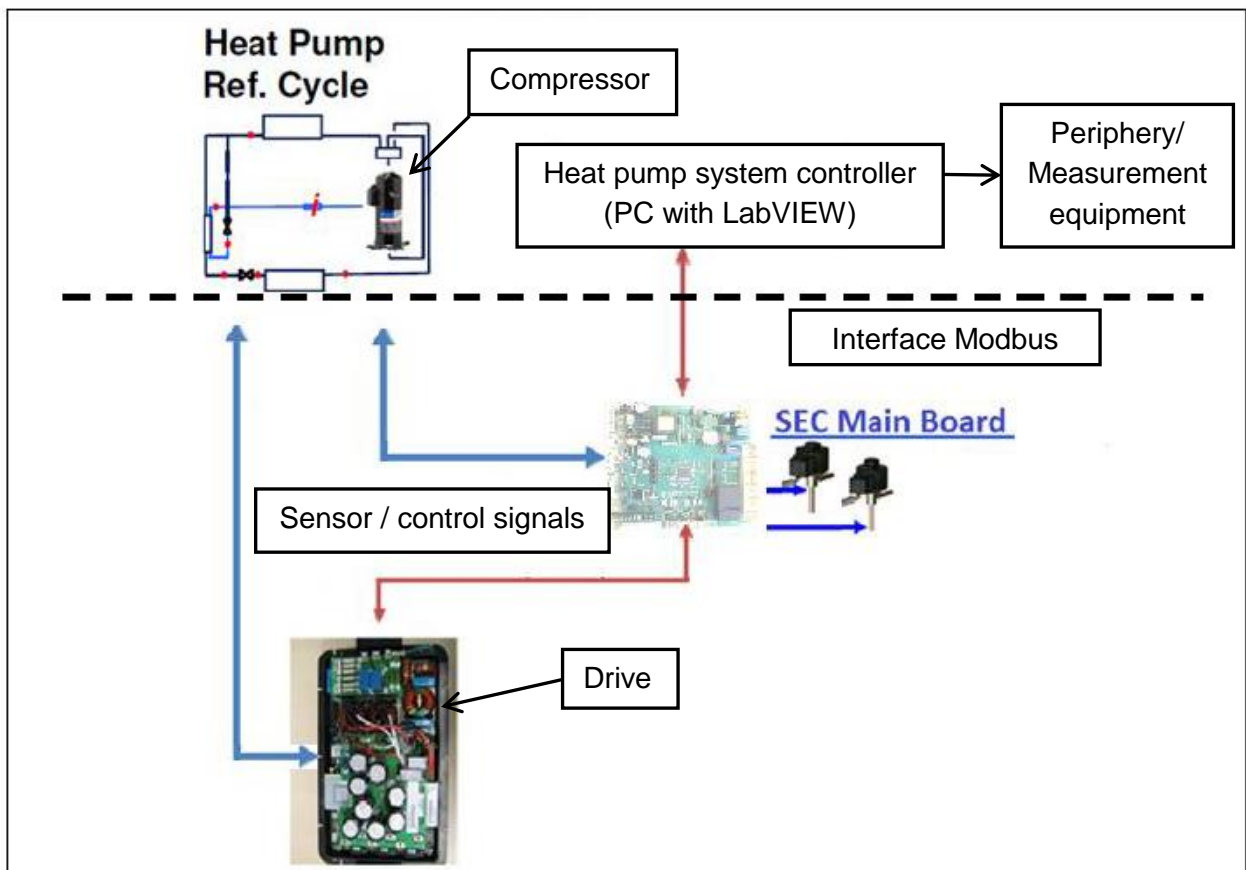


Figure 3-3: Copeland system configuration with system controller (Copeland, 2013d)

Scroll Compressor ZHW08

For the compression of the refrigerant the variable speed scroll compressor ZHW08 K1P 1E9 VS from Copeland is used (Figure 3-4). This compressor contains a second

inlet for vapour injection. This compressor has an operating range from 30 to 117 Hz which equals 1800 to 7020 rounds per minute (rpm). The working principle of a scroll compressor was explained in chapter 2.1.5. The maximum allowable pressure for which the compressor is designed is given with 28 bar for the low-pressure side and with 46 bar for the high-pressure side. The acceptable ambient temperature is -40°C to 50°C and the ambient humidity 30% to 95% for both, the compressor and the drive. For a stable performance the suction gas and injection superheating are specified with 5 K.

The compressor manufacturer Copeland also provides an envelope for the evaporating and condensing temperature, within the compressor can be operated. This envelope depends on the compressor speed, whereby data for this operating areas is listed in the compressor manual (Copeland, 2011) and in the software Select 7.7, which is also provided by the compressor manufacturer (Copeland, 2013a). The control drive, which is described in the next paragraph, measures the torque of the compressor and reduces the speed, if the maximum torque, which is related to the maximum condensing temperature, is exceeded. If this speed reduction is not sufficient, the compressor is shut down.

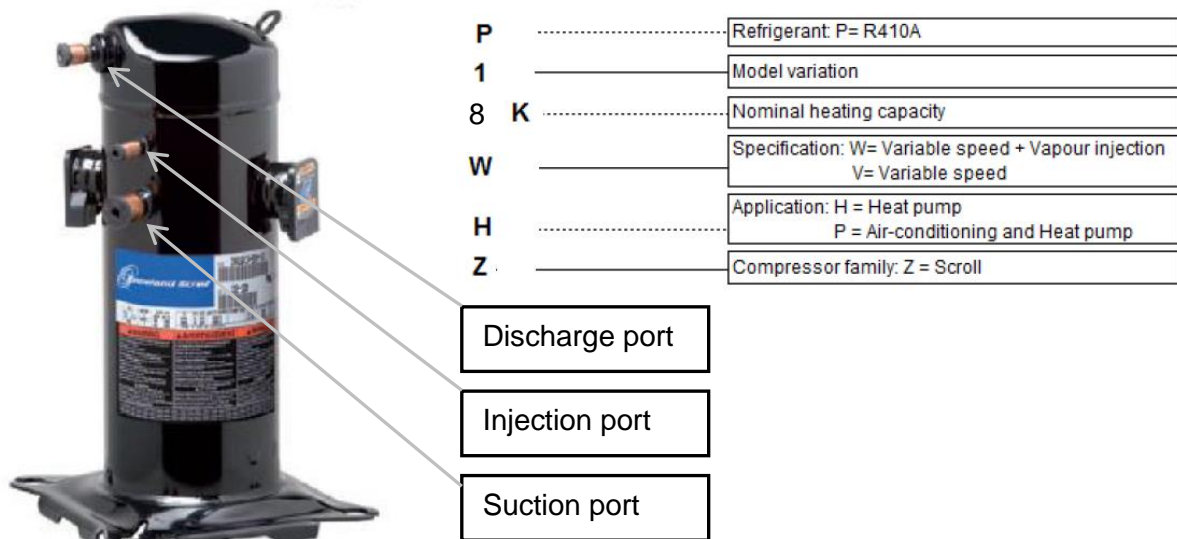


Figure 3-4: Copeland compressor with nomenclature (Copeland, 2011)

Figure 3-5 shows the cross section of the ZHW compressor. The bottom of the compressor is filled with 1.18 litre of oil. The lubricant is transported to the higher parts by means of a centrifugal pump. The oil pump ensures enough oil delivery for the whole speed range from 1800 to 7020 rpm. The compressor is driven by a brushless permanent magnet (BPM) motor, which is controlled by the motor control drive.

The functional principle of the scroll compressor was described in chapter 2.1.5. Here it is partly explained in context with the used type of scroll compressor and the vapour injection. The refrigerant vapour enters through the suction port and fills the whole part beneath the suction inlet. The refrigerant interacts with the compressor motor and the heat from the motor goes to the refrigerant. Then the refrigerant comes to the intake of the compressor where the compression begins (Figure 3-6).

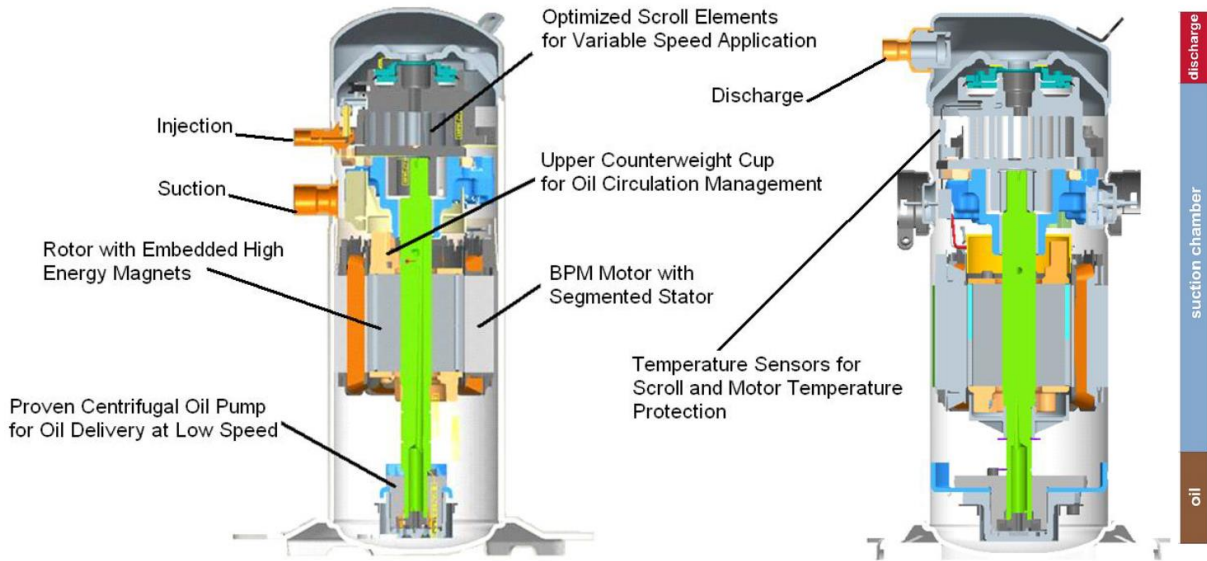


Figure 3-5: Cross section ZHW08 (Copeland, 2011)

During the compression process (chapter 2.1.5) refrigerant vapour from the injection port is injected directly into the spirals from above at a medium pressure level (Figure 3-6; left). After finished compression the refrigerant leaves the scroll through the outlet in the middle (Figure 3-6; right). The outlet contains a discharge valve, which prevents back pressure from the discharge or condenser when the compressor shuts down. The compressor can also handle small amounts of liquid refrigerant with its scroll design. The scroll forms can be separated from each other in the presence of liquid refrigerant and the liquid passes the scroll without damaging it.

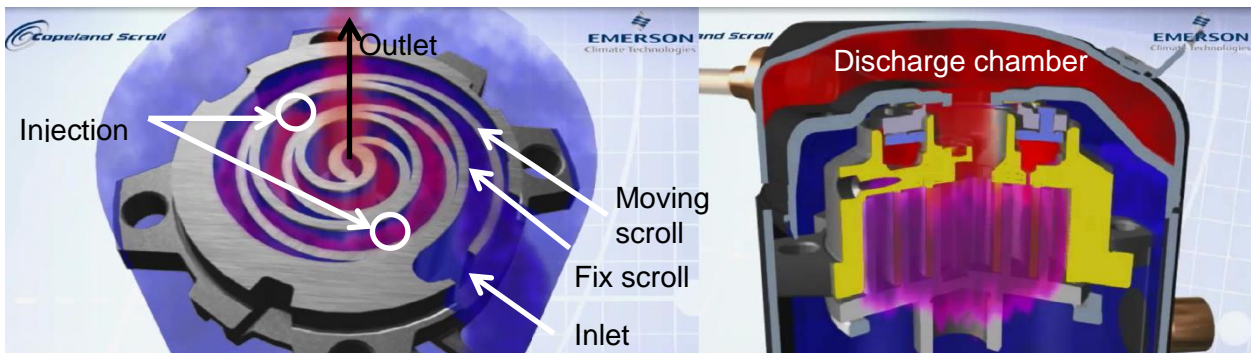


Figure 3-6: Simulation of the compression process in the scroll compressor
(<http://www.youtube.com/watch?v=dsabYhhOko0>, 16.04.2014)

Superheat and Envelope Control (SEC) board

The main functionalities of the SEC board are to manage the compressor speed, the control of the main and EVI superheating via the electronic expansion valves, to manage the defrosting, energy metering functions and the alarm management and safety functions. The SEC controller is not a main system controller, it only controls the refrigerant cycle which includes the scroll compressor, the drive, the electronic expansion valves and the Copeland pressure and temperature sensors. In the considered system the heat pump system controller and the SEC communicate via Modbus. The heat pump system controller is the computer with the LabVIEW program, which controls the whole periphery, which includes all measurement sensors as well

as the sink and the source system, and the heat pump cycle with the SEC system. A more detailed description about the communication between the SEC board and the heat pump control system is provided in chapter 3.5. (Copeland, 2013d)

Drive

The drive is used to convert the frequency from the 50 Hz alternating input voltage into a variable frequency, variable voltage output. This is needed to power the variable speed compressor. The alternating 230 V input voltage is converted into direct voltage. Then the variable frequency and variable output voltage is produced by pulse-width modulation to generate the sinusoidal current (Inverter). The drive can perform controlled and hard shutdowns. Hard shutdowns are performed when a major fault or a loss of power occurs during operation. The drive includes an over current protection and a temperature protection against high internal temperatures. Furthermore it performs a shutdown in case of too high or too low discharge temperature. The drive has to be cooled to keep it in its designed temperature range from -25°C to 65°C. Copeland suggests an air – cooling but in the test rig the cooling of the drive is implemented as a water cooler (Figure 3-7). (Copeland, 2013b)

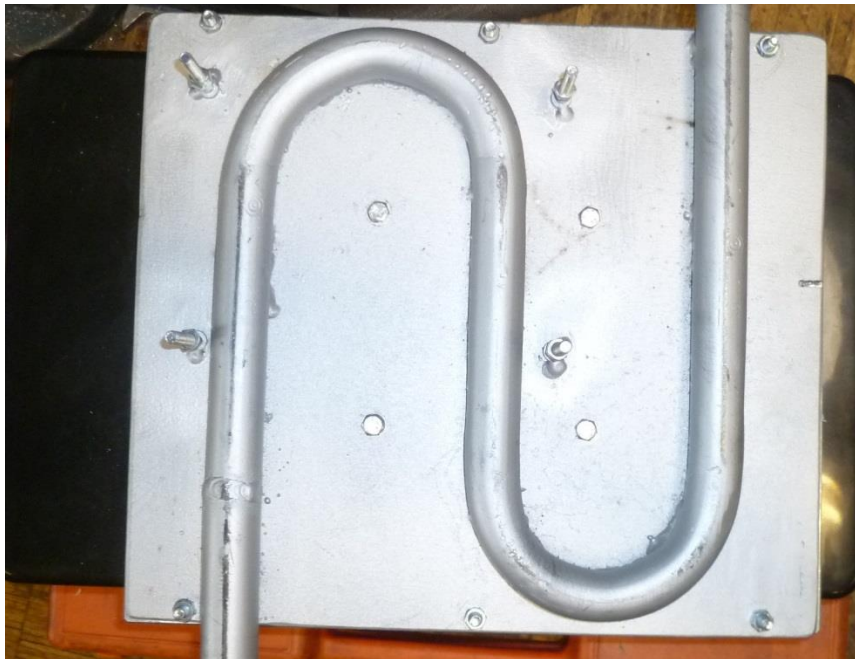


Figure 3-7: Inverter cooling

Heat pump system controller

The system controller, which is in this case the computer with the LabVIEW program, needs to provide the operating mode, which can be “Off”, “Heating”, “Cooling”, “Stand by” or “Manual”. For heating or cooling for example a defined capacity can be set or a specific compressor speed. In the manual mode the expansion valves can be controlled by hand. The SEC also delivers different alarm conditions whereby alarms and warnings do not lead to a shutdown of the compressor. In comparison “Alarm State” forces the compressor to shut down immediately. More information about the SEC board can be found in the SEC – User Guideline (Copeland, 2013d) and the technical information (Copeland, 2013c), which come along with the compressor. These manuals also contain all different alarm states and more information about the operating modes.

3.1.2 Heat exchangers

The used plate heat exchangers are manufactured by SWEP, a leading supplier for brazed plate heat exchangers. Each of the heat exchangers was dimensioned with the SWEP software (<http://www.sponline.swep.net/>, 05.05.2014), which is also provided by the manufacturer. Different parameters have to be given, in this case the working fluid, the temperatures at each inlet and outlet and the mass flow on each side. SWEP calculates the needed power and suggests a type of heat exchanger with a specified number of plates (NoP), surface and pressure losses at each side. The dimensioning was done for the point B-10W35 which means $-10\text{ }^{\circ}\text{C}$ brine inlet temperature in the evaporator at the source side and $35\text{ }^{\circ}\text{C}$ water outlet temperature of the condenser at the sink side. The following Table 3-1 gives an overview of the dimensioning of each heat exchanger with the SWEP software, whereby NoC stands for number of channels. (SWEP, 2013)

Table 3-1: Specifications of the used brazed plate heat exchangers (SWEP, 2013)

	Power [kW]	Sur-face [m ²]	NoP [-]	Fluid [-]	T _{inlet} [°C]	T _{outlet} [°C]	T _{cond} /evap [°C]	Mass flow [kg/h]	P _{loss} [kPa]	NoC [-]
Evaporator	3.51	0.644	30	R410a	-17.02	-12.10	-17.1	62	2.58	14
Side 1				Brine	-10.00	-12.90	-	1261	11.70	15
Condenser	5.07	0.644	30	R410a	91.11	37.90	40.0	82	0	14
Side 1				Water	30.00	35.10	-	857	3,63	15
Desup.	1.25	0.184	10	R410a	91.11	45.14	-	77	2.04	4
Side 1				Water	35.00	55.00	-	54	0.23	5
ECO	0.76	0.092	6	R410a	7.01	11.94	-	17	4.36	2
Side 1				R410a	35.88	8.50	-	60	0.331	3
Side 2										

For each heat exchanger the type B8T (HxNoP/1P-SC-M 4*3/4''&16) with a different number of plates was taken. Each operates as counterflow heat exchanger as it can be seen in Figure 3-8.

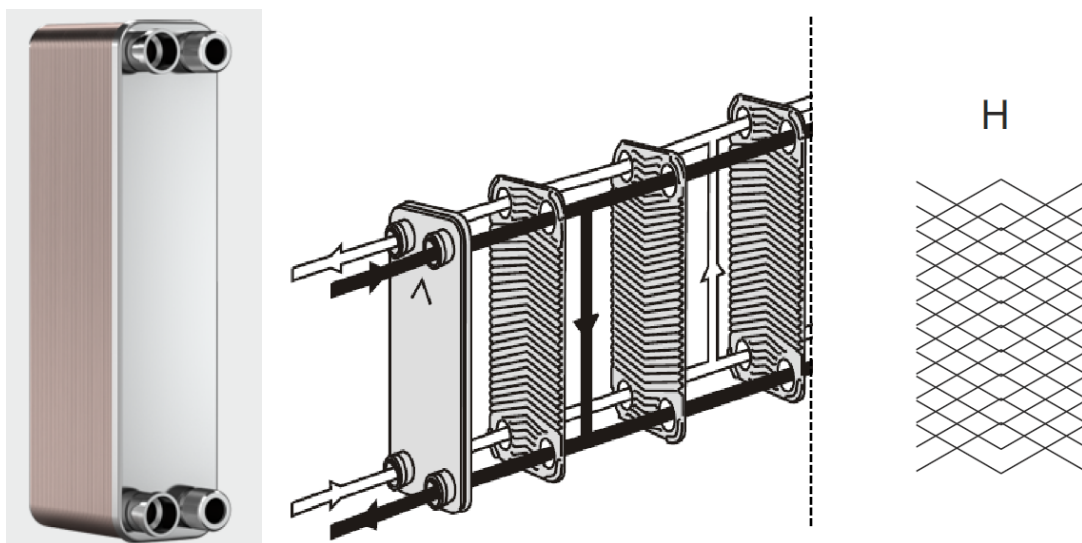


Figure 3-8: SWEP plate heat exchanger counterflow (SWEP, 2010)

The B8T-HX has a width of 76 mm, a height of 317 mm and the depth depends on the number of plates and is given with $4 + 2.24 \text{ mm} \cdot \text{NoP}$. H stands for the layout of the channels which can also be seen in Figure 3-8. 1P states that the fluid runs through the HX only once, S stands for the material of the plates which is stainless steel 316. C means that the brazing material is copper; M indicates that the HX is used for medium pressure applications. For the fitting dimensions it is referred to the user's manual whereby all used in- and outlets have a $\frac{3}{4}$ " outside thread (SWEF, 2010). The B8T can be used for one- and two phase applications and is specially designed for pressures up to 45 bar, which is enough for both the high- and low pressure side of the heat pump cycle. The small arrow on the front plate marks how the heat exchanger has to be connected. For assembling, the installation and maintenance manual has to be considered (SWEF, 2010).

Changes in the Configuration during the measurements

For the improvement of the efficiency of the heat pump cycle two changes at the condenser and the evaporator were made between the measurement series. The measurements of the performance map of the compressor were performed before these changes and the measurements for the evaluation of the heat pump cycle after these changes.

The condenser was replaced with exactly the same model but with 40 plates instead of 30. This was done with the aim to reduce the spread between the condensing temperature and the water temperature at the sink side, after the original HX did not show the expected performance. In chapter 5.2.1 the effect of the HX replacement is discussed.

Before the modifications a distribution pipe with one borehole for each refrigerant plate was installed at the inlet of the evaporator to ensure an equally distributed flow of refrigerant in all channels. The pipe had an inner diameter of 6 mm equal to the incoming pipe and 14 boreholes with a diameter of 1.6 mm to sum up the same area as the incoming pipe. After high pressure losses with higher mass flows this distribution pipe was removed because according to the manufacturer it is not necessary. Test runs without the distribution pipe showed a worse performance of the evaporator than before furthermore the superheating after the evaporator was less stable. As a result another distribution pipe was mounted at the inlet of the evaporator, similar to the one used before, with the same dimensions but three 1.6 mm boreholes for each refrigerant plate instead of one. The outlet temperature of the evaporator got more stable again but the evaporator HX performance (UA) could not reach the values which were reached with the first distribution pipe. The distribution pipes are shown in Figure 3-9, on the left side the one used for the measurement of the compressor performance map after the disassembling and on the right side the new pipe, which was used for the measurements to evaluate the cycle performance.

To sum up the described changes it can be said that the distribution pipe with one borehole for each refrigerant plate, whereby the sum of all areas gives the inlet area of the distribution pipe, showed the best performance of the evaporator, although it caused a pressure loss of 0.05 to 0.7 bar during the measurements for the compressor performance map. To evaluate the influence of the different distribution pipes further test runs would have to be made. The influences of both changes in the cycle are evaluated in chapter 5.2.1.



Figure 3-9: Distribution pipe at the evaporator inlet before (left) and after the modifications (right)

3.1.3 Liquid receiver

After the condenser a high pressure liquid receiver from the manufacturer Klimal is installed, to ensure the liquid state after the condenser. It is also used as a buffer and for cushion of irregularities in the refrigerant flow. Furthermore it can be a reserve for small leakages although this should be prevented. It is important to have magnetic valves, which close the cycle so that the refrigerant cannot pass from the liquid receiver to the low pressure side after the shut off of the compressor. It is also used to compensate changes in the operation conditions on the high pressure side. (Rieberer et al., 2009) In this system this could be the activation or the switch off of the desuperheater. The receiver has a volume of 2.3 litres, which enables it to store nearly the whole refrigerant in the cycle (2.5 litres are filled in the cycle). The maximum allowed pressure is stated with 45 bar, which is enough for the maximum system pressure of 42 bar (Schiessl, 2013).

3.1.4 Filter dryer and sight glass

The filter dryer Danfoss DML083s is integrated in the system. Before the filling of the heat pump the system has to be evacuated to remove all the humidity. During operation the filter dryer has the purpose to filter the dirt and the humidity out of the system. Furthermore it should avoid the risk of acid formation. Figure 3-10 shows the composition of the filter dryer.

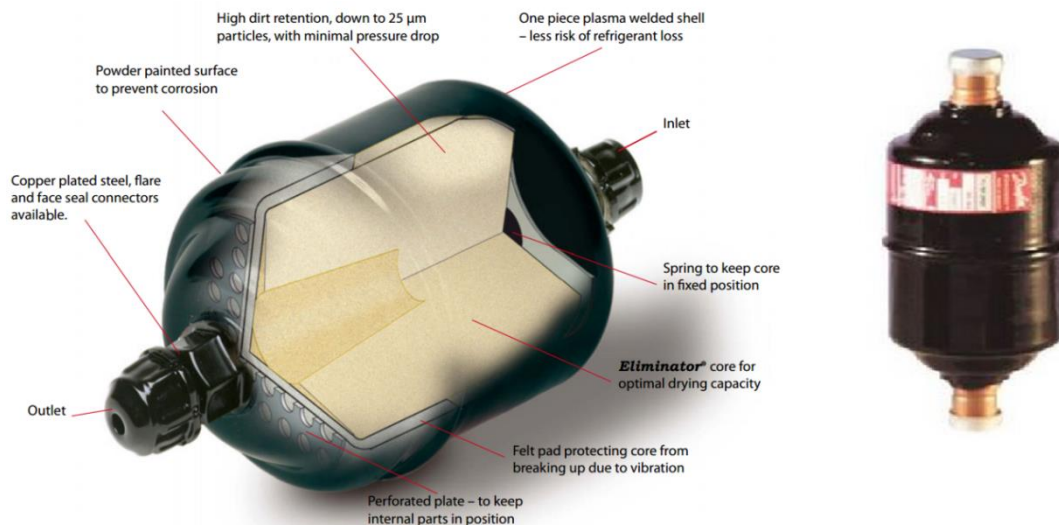


Figure 3-10: Filter dryer Danfoss DML083 structure

The main part is a solid block, which is comparable to a sponge, which absorbs water. Additional aluminium oxide in the block can absorb acids. In combination with a polyester board the filter can also remove dirt particles. For the selection there are two important parameters, the drying capacity and the liquid capacity.

The drying capacity indicates how much water the dryer can remove at 24 °C, for example 1050 ppm to 60 ppm for a certain amount of refrigerant in the system. The liquid capacity shows how much flow rate the dryer can handle, that means the amount of refrigerant which leads to a pressure loss of 0.07 bar in the filter. Danfoss converts this volumetric flow into the liquid capacity (R410a: 0.32 l/min = 1 kW). The used filter dryer DML083s has a liquid capacity of 21 kW which equals 6.72 l/min (Danfoss, 2005).

In combination with the filter dryer a sight glass is installed. It is placed after a coriolis mass flow meter, which is installed after the filter dryer. The sight glass has an indicator which can change the colour. Green means that there is no or a negligible amount of humidity in the system, yellow means that the humidity before the expansion valve is too high. Furthermore it is possible to determine the state of the refrigerant. If bubbles can be seen, the refrigerant is not completely liquid, which could refer to a too high pressure loss in the filter or a refrigerant undercharge in the system. Further causes for a high pressure loss in the filter can be found in the instruction (Danfoss, 2005).

3.1.5 Electronic expansion valves

The purpose of the expansion valves (EXV) is to expand the refrigerant from a high- to a lower pressure level. This is done by reducing the cross section of the EXV. The control variable of the valves is the superheating after the evaporator for the main valve and the superheat at the injection port if a compressor with vapour injection is used. If the superheat is too high, the expansion valve opens and the mass flow increases, if the superheat is too low, the expansion valve closes and the mass flow decreases. Figure 3-11 shows the used electronic expansion valve

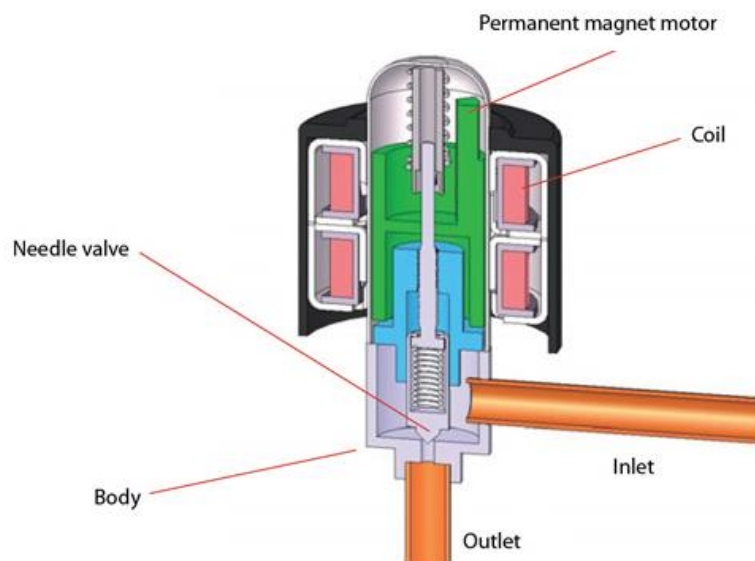


Figure 3-11: Electronic expansion valve (<http://www.danfoss.com>, 12.03.2014)

It uses a small motor to open and close the valve. The SEC board controls the motor of the electronic expansion valve with the help of temperature contact sensors on the evaporator outlet for the main expansion valve and on the economiser outlet for the injection. For the opening of the valve a step motor is used, which does not rotate continuously, it rotates only a small angle for each signal change. This makes a very precise control and a fast adaption for changes in the cycle possible.

In this system two different expansion valves are used, recommended by Copeland. They were delivered with the compressor and the drive. The EXM BOE is used as main expansion valve and the EXM BOD as expansion valve for the injection cycle. Further information about the operating range of these valves can be found in the manual. (Copeland, 2014a)

3.1.6 Solenoid Valves

Two solenoid valves Danfoss EVR3 are placed before each expansion valve. They open when the compressor starts and close when the compressor shuts down. The solenoid valves prevent the refrigerant to flow from the high pressure side to the low pressure side, after the compressor shutdown, which is mandatory in combination with the high pressure liquid receiver. The valves were implemented for safety reasons because depending on Copeland the expansion valves can also close the cycle with the same low leakage as the solenoid valves.

3.1.7 Pipes

For connection of the parts of the cycle copper pipes are used with inner diameters between 4 and 10 mm and one millimeter wall thickness. Two boundary conditions determined the diameters of the pipes. For making the pressure drop as small as possible and therefore being highly efficient the diameter has to be big, but for the circulation of the oil in the cycle a specific flow velocity of the refrigerant with the oil has to be assured. The minimum speed for oil return is 4 m/s for horizontal pipes and 8 m/s for rising pipes (Pohlmann, 2010). The pressure drop can be determined with differential pressure sensors but it has to be considered that a big part of the pressure losses comes from the mounted measurement equipment. Figure 3-12 shows the inner diameter (mm) for each connection pipe in the refrigerant cycle. Changes in the diameter for the mounting of valves and the mass flow meters are not considered.

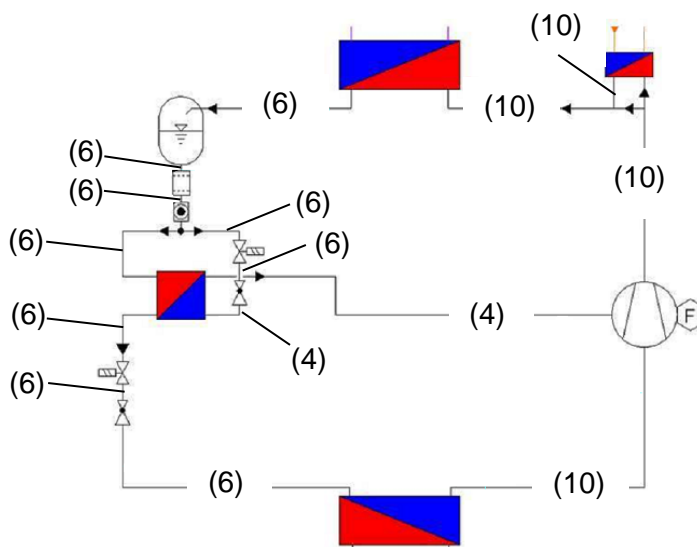


Figure 3-12: Diameter of the connection (copper) pipes in the refrigerant cycle (mm)

3.2 Source cycle

For the source a mobile construction with an integrated electrical heater and a storage of 35 liter, which can be seen in Figure 3-13, is used. This mobile construction is called “Mobile Heat Source” (MHSo). It was built up in a former project. The frame with the indication “Test rig” shows parts which are mounted in a frame under the working fluid cycle, which is pictured in Figure 3-2. It consists of a speed controlled pump (type WILO Stratos 25/1-8) to control the mass flow of the brine, a control valve (type stated in each figure with opening for all measurements, e.g. 4.3/4.3 means that it is completely open) to change the pressure losses and four ball valves to decouple the cycle from the MHSo, which is connected to the test rig via hoses and to disconnect the brine side of the evaporator.

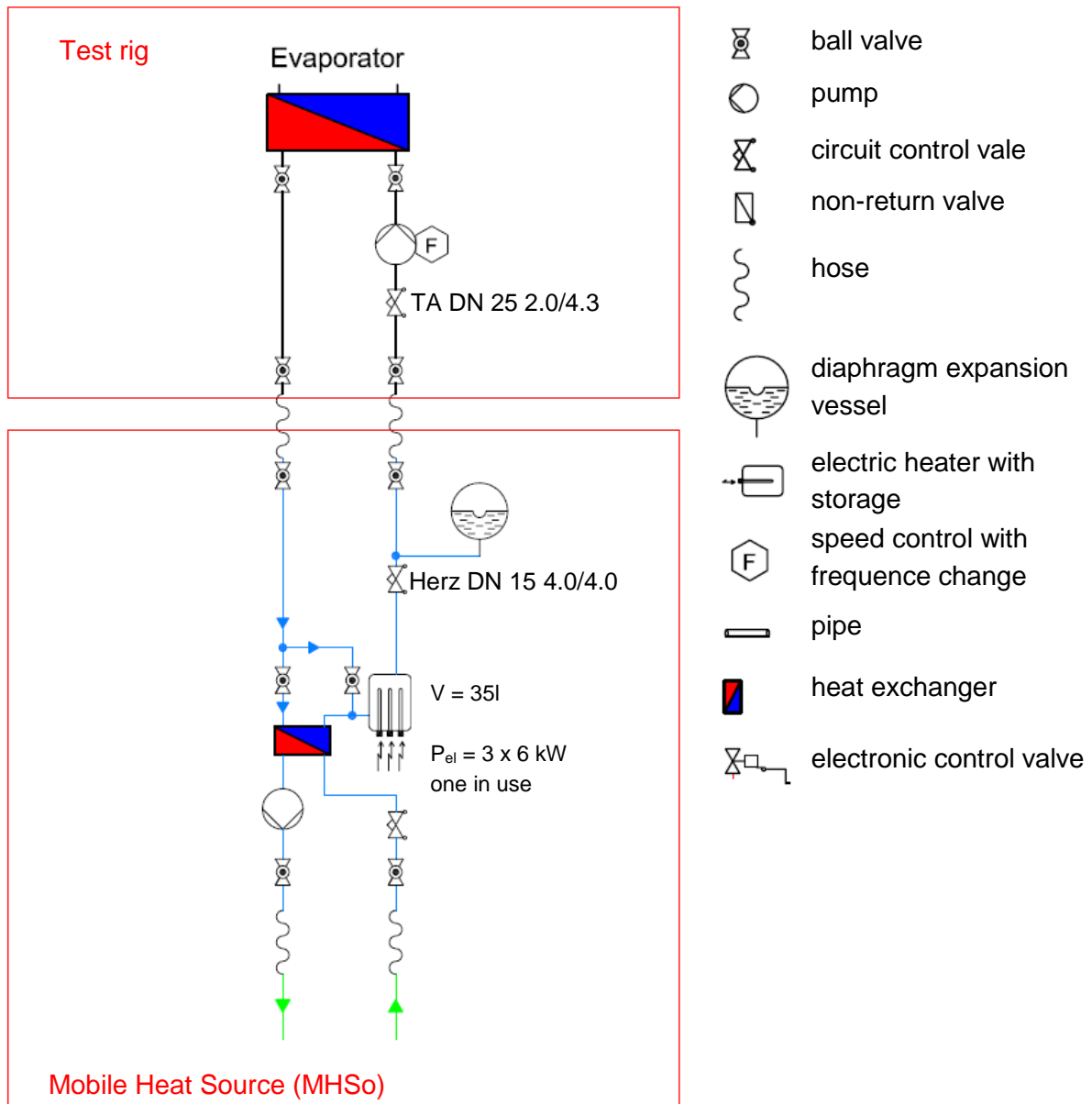


Figure 3-13: Schematic layout of the mobile heating moped used as brine source

In the MHSo the heat exchanger is bypassed with ball valves and the brine goes directly to the 35 liter storage vessel, which contains three heating rods with 6 kW heating power each. For

most measured points only one of them is in use. For operating points with high heating power and low pressure ratios a second one has to be added. The control of the heating rods is described in chapter 3.6. After the electric heater the brine goes through a completely opened control valve to the connection to the test rig.

3.3 Sink cycle

Figure 3-14 shows the schematic view of the sink side. The water cycle is, equal to the source, partly mounted on the test rig under the refrigerant cycle and partly on a mobile construction called “Mobile Heat Sink” (MHSi).

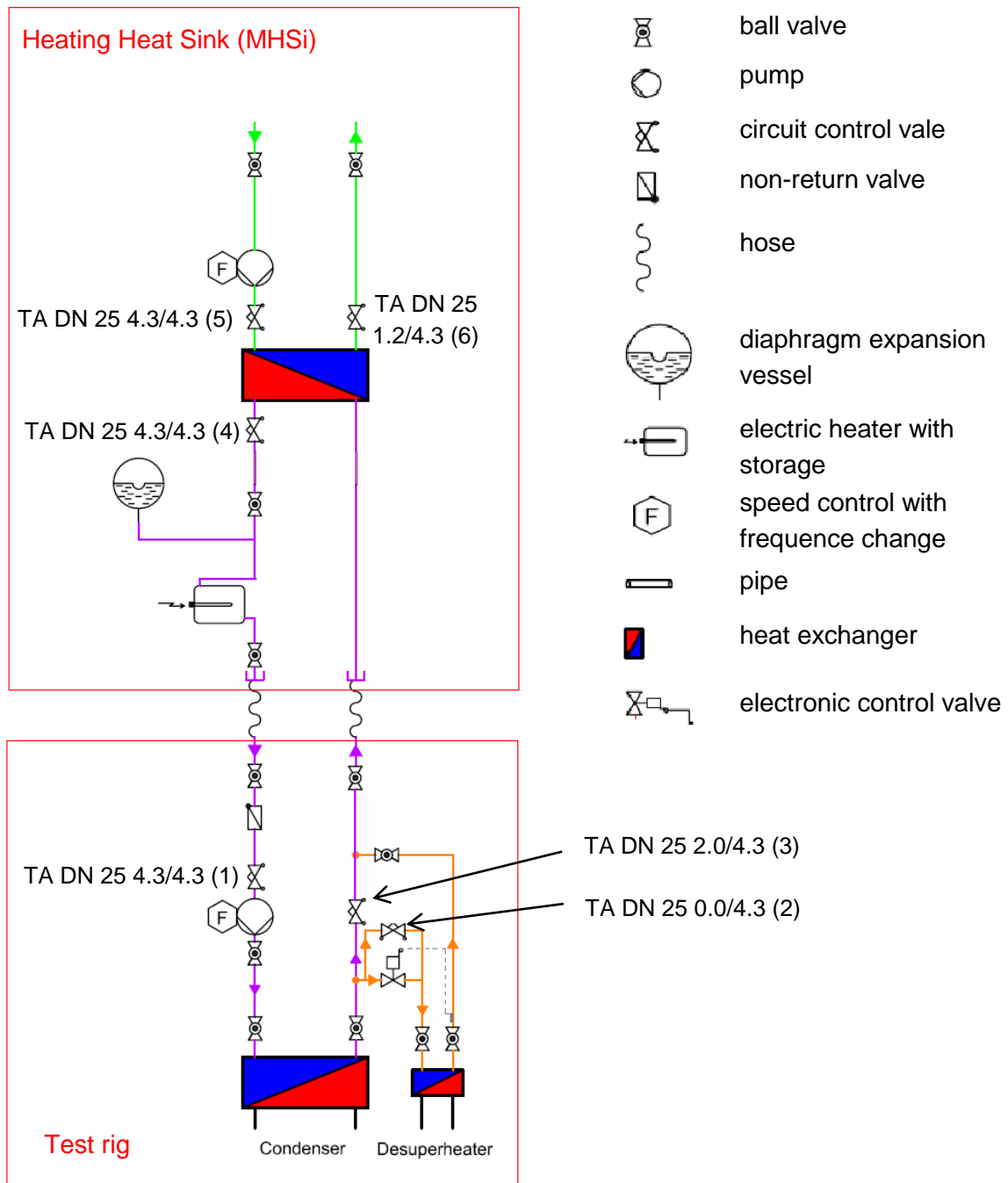


Figure 3-14: Schematic view of the sink side with water cycle and secondary heat exchanger

The heat exchanger mounted on the MHSi is used to reject heat, which is produced by the heat pump, to a secondary brine cycle, which is connected to a cooling machine. The description also includes the position of the control valves to reproduce the measured points.

Starting with the parts mounted on the test rig the cooled water comes from the MHSi and goes through a control valve (1) to a speed controlled pump (type WILO Stratos 25/1-8), which drives the water cycle. Through further ball valves the water flows to the condenser. After the condenser the water can be split up and led over the desuperheater depending on whether hot water should be produced or only warm water for space heating. The circuit control valve (2), which is parallel to the thermostatic valve, was completely closed during all the test runs, the mass flow over the desuperheater is controlled with the thermostatic valve TA TBV-CM 15LF and the electrical linear actuator MC15/24-C. Further information about the thermostatic valve and the electrical actuator can be read in the manuals (TA, 2011, TA, 2013). If the thermostatic valve is closed, all the water flows only over the condenser. One further control valve (3) is in the cycle, which was on position 2.0/4.3 during the test runs. From here the water flows back to the MHSi.

The schematic layout of the MHSi only includes parts which are along the cycle of the fluids, for simplification it does not include components which did not have any influence on the cycle during the measurements. The water from the test rig flows directly in the heat exchanger where the produced heat is rejected. After the heat exchanger the water passes a fully opened control valve (4). The tank with the included heating rods was only used as storage tank. After the storage tank hoses build the connection back to the test rig.

The second side of the heat exchanger is connected to a brine storage tank, which can be cooled with a R507 cooling system to supply the connected systems with brine of a certain temperature. Because the brine distributor after the storage works without differential pressure a speed controlled pump (type WILO Stratos 30/1-8) is used to ensure a certain brine mass flow. This system was already described in an early diploma thesis by Patrick Hauser (Hauser, 2009). The pump is also used to control the temperature at the condenser inlet by changing the mass flow of the brine over the heat exchanger. At the brine inlet and outlet of the heat exchanger control valves are mounted, whereby the valve at the inlet (5) is completely open and the valve on the outlet (6) has position 1.2. This is important because for this position the control parameters for controlling the water inlet temperature of condenser were determined. More detailed information about the control circuits can be found in chapter 3.6.

3.4 Measurement equipment

For the experimental analysis of the heat pump many different measurement instruments are installed on the test rig. The next pages describe where these sensors are mounted and which ones are used. For evaluation of the whole cycle, sensors for temperature (T), absolute pressure (P), differential pressure (PD), flow rate (F) and power (EQ) are installed. The position of these sensors can be seen in Figure 3-15. The sensors are named according to DIN 19227 (DIN19227, 1993). Table 3-2 includes all measuring points, defines in which fluid the sensors are measuring and the category and type of each sensor.

Table 3-2: Measuring points and sensor properties on the test rig (Heinz et al., 2013b)

Measuring point	Fluid	Category	Type	Measuring range	Accuracy
TEr01..9	R410a	Temperature	TC type K	-40 to 1100°C	±0.2 K
FE_r5	R410a	Mass flow	Coriolis	0 to 2000 kg/h	±0.3 %
FE_r7	R410a	Mass flow	Coriolis	0 to 450 kg/h	±0.3 %
PE_r1	R410a	Abs. pressure	DMS	0 to 20 bar	±0.02 %
PE_r2	R410a	Abs. pressure	DMS	0 to 50 bar	±0.01 %
PE_r7i	R410a	Abs. pressure	DMS	0 to 30 bar	±0.02 %
PDE_r01..9	R410a	Diff. pressure	Capacitive	0 to 1000 mbar	±0.1 % FSO
EQEP_r1	-	Elec. energy	Pulse counter	230 V / 25 A	±1 %
TE_w1..2	Water	Temperature	Pt100	-200 to 850 °C	±0.02 K
TE_d1..c2	Water	Temperature	Pt100	-200 to 850 °C	±0.02 K
FE_w4..5	Water	Vol. flow	Magnetic inductive	0.24 to 6 m ³ /h	±0.2%
TE_b1..2	Brine	Temperature	Pt100	-200 to 850 °C	±0.02 K
FE_b1	Brine	Vol. flow	Magnetic inductive	0.24 to 6 m ³ /h	±0.2%

For the calculation of the error of measurement later on it will be referred to this table. The accuracy of the temperature sensors applies to the calibrated range from -20 to 90°C. The accuracy for the mass and volumetric flow meters also applies to the maximum deviation from the reference balance after the calibration. At both inlets and the outlet of the compressor absolute pressure sensors are mounted. The error is set for the calibrated sensors, whereby the accuracy for the non-calibrated sensor would be 0.2 % FSO. The absolute pressure in all other measuring points in the system is calculated by adding or subtracting the measured differential pressures from the three absolute pressure sensors. The calibration process is documented in the Appendix A-2.3.

Heat pump Test Rig

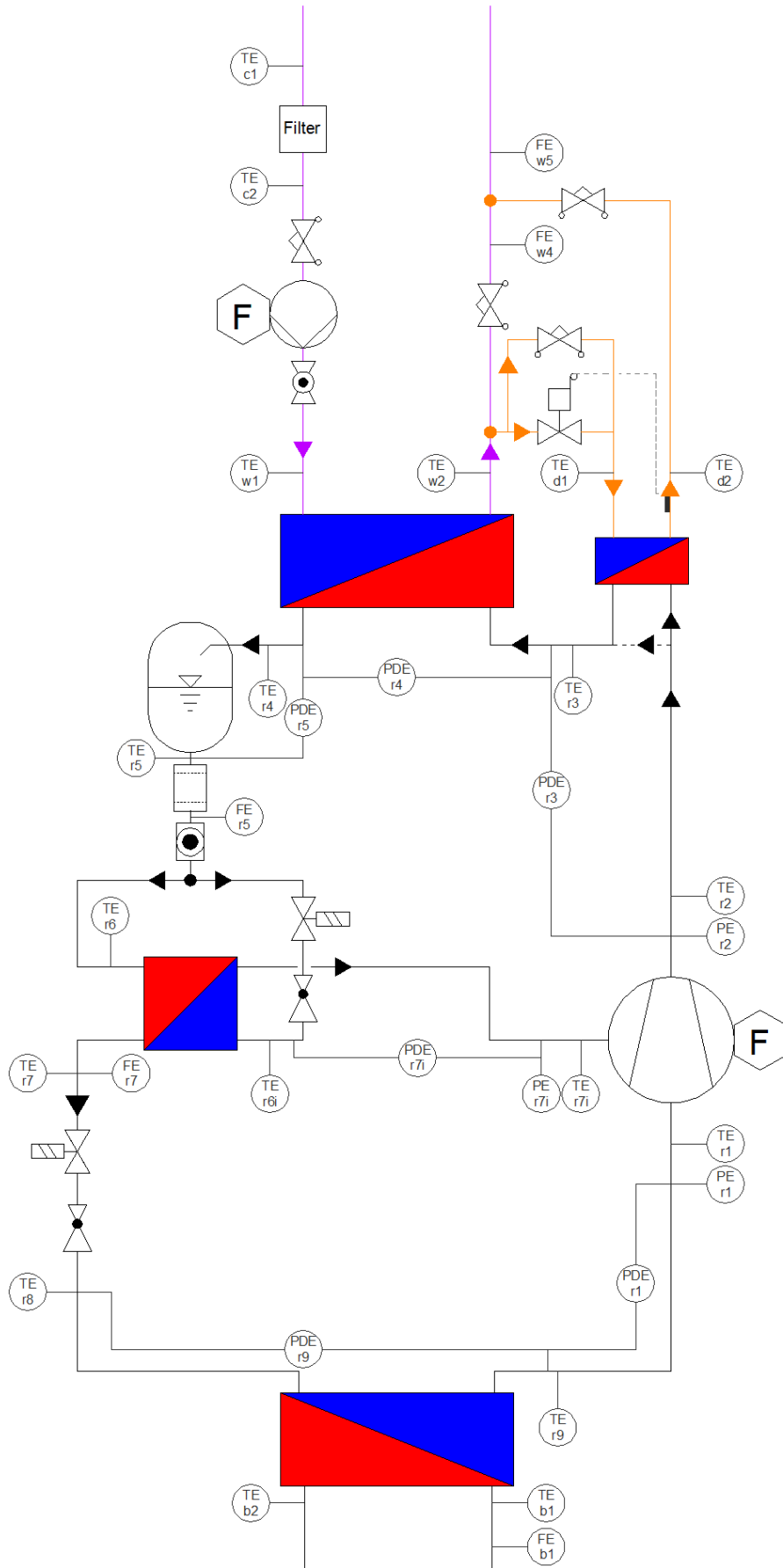


Figure 3-15: Test rig layout with points of measurement (Heinz et al., 2013b)

3.4.1 Temperature

Two different temperature sensors are used for the test rig, Pt100 resistance thermometers in the water and brine cycle and thermocouples (TC) in the working fluid cycle. A short description of the working principle of these sensors is included in this chapter. Resistance thermometers are more accurate than thermocouples, calibrated they can reach accuracies up to ± 0.01 K, whereby after the calibration the biggest deviation from the reference sensor was ± 0.02 K. The thermocouples showed a deviation of ± 0.2 K, although most of them only had a difference of a few hundredths K to the reference sensor. The reason why they are used in the refrigerant cycle instead of the more accurate resistance thermometers is their lower price, especially for small diameters and that they are also much more compact. The sensors in the test rig are mounted into the cycle of the fluid and not mounted on the surface. Common resistance thermometers are available with 3 and 6 mm diameter while the used thermocouples have a diameter of 1 - 1.5 mm. The smallest inner diameter of the copper pipes is 4 mm in the liquid line. To insert a 3 mm resistance thermometer in these pipes would affect the flow too much and would cause a high pressure loss. Subsequently these two measuring principles are described. For the control of the expansion valves Copeland uses NTC temperature sensors which are directly connected to the SEC board. They are surface contact temperature sensors with an accuracy of ± 0.2 K compared to the reference sensor (Treichel, 2013).

Thermocouples

Thermocouples use a thermoelectric effect, the so called "Seebeck" effect, for measuring temperature. If two different metals are joined at both ends and there is a temperature difference at both connection points, electric current starts to flow (Figure 3-16a). If the circuit is not closed, a voltage difference can be measured (Figure 3-16b). For determining the temperature at a specific point (t_1) the temperature at the point of comparison (t_0) has to be known. Then the voltage difference can be measured, which is proportionate to the temperature difference. One possibility to get an accurate t_0 is to put the connection of comparison into iced water. Nowadays this point of comparison is already included in the input modules for the data acquisition, like in this case the analogue input module NI 9213, which is described in 3.5.

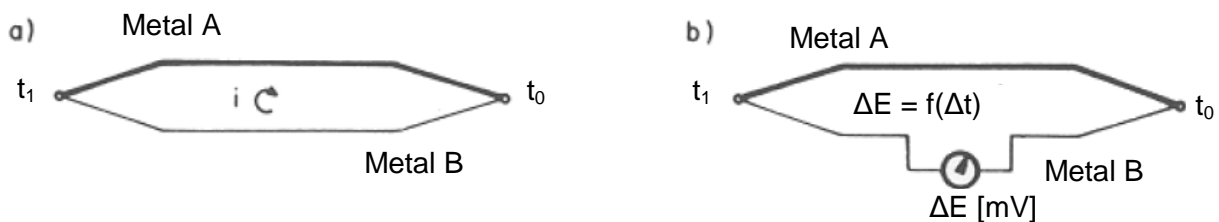


Figure 3-16 "Seebeck" effect used in thermocouples (Rieberer, 2013)

Depending on the used metal combination there are different types of thermocouples which have different differential voltage for a thermal gradient. In this test rig thermocouples of type K are used, which do have a Seebeck coefficient of about $40 \mu\text{V/K}$ at 20°C (Rieberer, 2013). TC measure the temperature only at the small point where the metals are joined and not as average of a certain length. It is important not to use plugs or balancing lines from different types because this leads to wrong results. On the test rig thermocouples with plugs were used but this led to problems because the vibrations of the test rig caused the brazed wires in the plug to break.

Resistance thermometers Pt100

The principle of this measurement is the fact that the resistance of a material varies with the temperature. All resistance thermometers used in the test rig are Pt100 platinum sensors. That means that the resistance of these sensors is $100\ \Omega$ at $0\ ^\circ\text{C}$. Figure 3-17 shows the structure of a resistance thermometer on the right and the two possibilities for the wiring of a resistance thermometer on the left. If high accuracy is not necessary the 2-wire configuration may be used. The resistance in the wires is also measured, which leads to errors in the measurement. If high accuracy is needed the 4-wire configuration is chosen. The current I_R with its wires is used to power the resistor while the wire with I is used for the measurement. The inner resistance of the voltage measurement U is high so only I_R flows over the resistance R . This method compensates all changes in the wire resistance and is used for all Pt100 elements in the cycle. Compared to the TC the Pt100 does not measure in a small point, it measures over a length, which can be some millimetres or more. LEMO couplings are used for connecting the resistance thermometer from PMR to the wire.

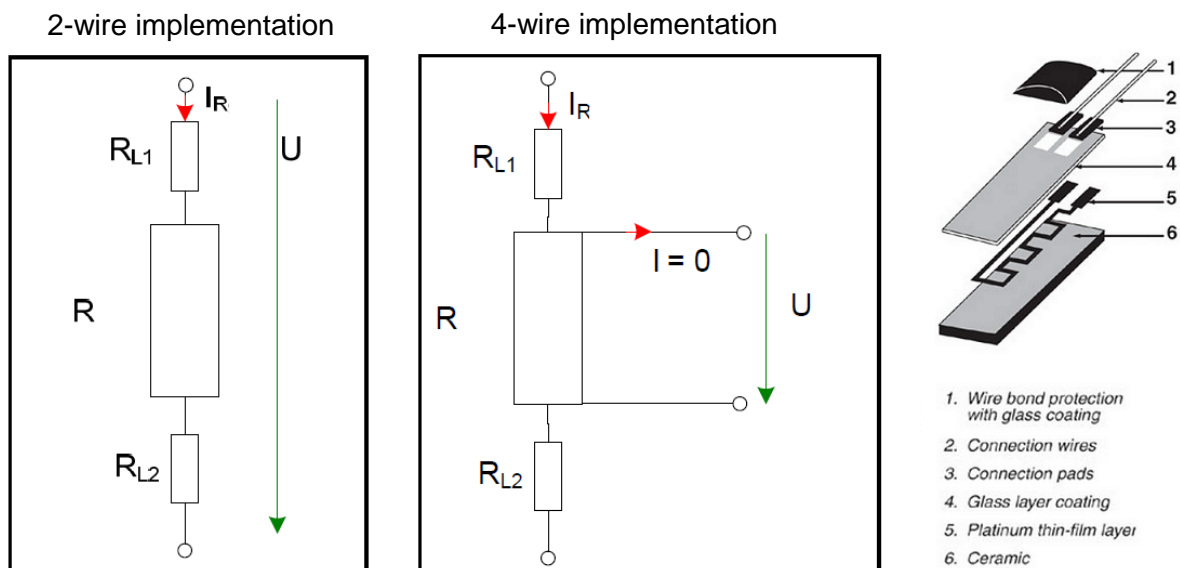


Figure 3-17: Resistance thermometer structure and wiring (Rieberer, 2013) and (http://www.omega.com/pptst/F_Series.html, 16.04.2014)

The resistance thermometers are “class A” which refers to the admissible tolerance of the Pt100 which is $0.15\ ^\circ\text{C} + 0.002 \cdot |t|$. The temperature range of a Pt100 is from -200 to $650\ ^\circ\text{C}$ (http://www.pmr.at/_lccms/_/00089/, 16.04.2014). The relationship between resistance and temperature can be read in the literature and is normally described with a second order function for the temperature range 0 to $650\ ^\circ\text{C}$ and a third order function for the temperature range -200 to $0\ ^\circ\text{C}$. (Rieberer, 2013)

NTC resistance thermometers

For the controlling of the expansion valve Copeland uses NTC resistors, which were delivered with the compressor and the SEC board. NTC stands for Negative Temperature Coefficient and means that the resistance falls when the temperature rises. The correlation between resistance and temperature is not linear and given in the SEC manual (Copeland, 2014b). Because of the high resistance of the NTC the voltage drop in the wires does not have to be considered. The

sensors are directly connected to the SEC board of the compressor and are mounted on the pipes as surface contact sensors. The sensors show a good accuracy, compared to the reference sensor used for the calibration of the Pt100 and TC, of less than ± 0.2 K for each calibration point.

3.4.2 Pressure

Two different types of sensors are used for the pressure measurements, absolute pressure sensors at the out- and inlets of the compressor and differential pressure sensors to determine the pressure in all points of the cycle. Figure 3-15 shows the position of each sensor. For safety reasons two pressure switches are included in the system to shut down the heat pump in case of too high condensation pressure or too low evaporation pressure. The measuring range is listed in Table 3-2 as well as the measuring accuracy, which applies for the calibrated sensor.

Absolute Pressure

Three absolute pressure sensors are installed, which are connected to the measuring positions with capillary tubes. The measuring points are around the compressor, one at the inlet (low pressure level), one at the injection port (medium pressure level) and one at the outlet of the compressor (high pressure level). The pressure sensors are of type PMR GmbH type PITC-1.2.4.1 and can be seen in Figure 3-18 on the left. The accuracy for the not calibrated sensor is given with 0.2 % FSO. The sensor consists of a stainless steel diaphragm, which is directly connected with a thin film strain gauge (DMS), which measures the deformation of the diaphragm. Further specifications can be read in the manual. (PMR, 2013)



Figure 3-18: Absolut pressure sensor from PMR on the left, Copeland pressure sensor in the middle and differential pressure sensor from XMD on the right

Three additional relative pressure sensors were delivered by Copeland (Figure 3-18 middle) along with the compressor and the SEC board. They are of type PT5 with pressure maximums of 18, 30 and 50 bar. They are connected to the same capillary tubes as the system pressure sensors. These sensors are only used by the SEC board for the compressor and system control with a guaranteed accuracy of ± 1 % of the measured value (Emerson, 2013).

Differential pressure

For the determination of the absolute pressure in significant points of the cycle differential pressure sensors from XMD of type 340-1001 are used. This sensor consists of a two chamber aluminium die cast case with a stainless steel diaphragm. The deformation of the diaphragm is measured by capacitive means. The sensors can stand a permissible static pressure of up to 130 bar. These sensors are also important to determine the pressure loss in every part of the working fluid cycle like the heat exchangers, different valves or the pipes. This was important for the modifications, which were made to improve the cycle efficiency. The sensor is shown in Figure 3-18 on the right. More detailed specifications can be read in the manual (IMPRESS, 2013).

Pressure switch

For safety reasons a high- and a low pressure switch from Danfoss type KP1 and KP6W (Danfoss, 2013) are installed to shut down the system in case of a wrong operating point (condensation temperature too high / evaporation temperature too low). If the pressure is undercut on the low pressure side or exceeded on the high pressure side the compressor is turned off. For that a spring at the inlet gets compressed and if the pressure gets too high (or too low for the low pressure switch) the electric circuit is interrupted. These pressure switches provide a mechanical safety device in addition to all safety measures, which are included in the software for the controlling of the heat pump cycle.

3.4.3 Flow rate

Two different systems are used to measure the flow rate in the system. Two Coriolis mass flow measurement devices are used for the heat pump cycle with the working fluid R410a and three magnetic inductive volumetric flow measurement devices are used for the water and brine cycle. The description of the used devices also includes a short explanation of the working principle of these two kinds of measurement devices.

Coriolis mass flow rate measurement in the refrigerant cycle

Two Coriolis mass flow meters are used for measuring the mass flow of the refrigerant, the Promass 83A DN04 (Endress+Hauser, 2013b) with a maximum mass flow of 450 kg/h for the low pressure cycle through the evaporator and the Promass 83F DN08 (Endress+Hauser, 2013c) with a maximum mass flow of 2000 kg/h for the high pressure cycle through the condenser, which consists of the mass flow through the evaporator plus the mass flow through the injection port of the compressor because of the economiser circuit.

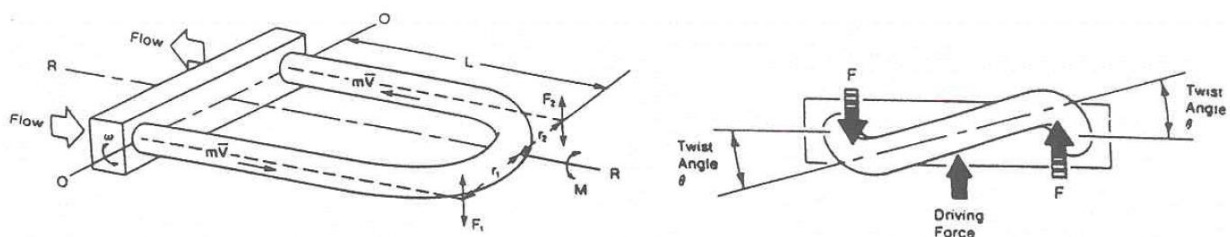


Figure 3-19: Functional principle of a coriolis mass flow meter (Rieberer, 2013)

The principle of this measurement method is the Coriolis force, which exists in a rotating reference system with a moving mass on it. The direction of the force is vertical to the moving direction of the mass and vertical to the rotational axis of the reference system. Figure 3-19 shows the working principle of a Coriolis mass flow meter. The medium passes through a pipe loop, which is fixed at the inlet and outlet of the fluid. The pipe is brought to oscillation around the O-O axis by the help of an electromagnet. This oscillation leads to a Coriolis force on the moving fluid in the pipe. Since the fluid goes in different directions in the inlet- and outlet pipe the Coriolis force goes in different directions, which can be seen in Figure 3-19 on the right. This Coriolis force leads to a torque around the R-R axis and hence to a twisting of the pipe. The twisting angle is measured, which is proportional to the mass flow. (Rieberer, 2013) One of the main advantages of the Coriolis principle is that it measures the mass flow directly, which is needed for most applications. It is very accurate with the only drawback of its high price.

MID volumetric flow rate measurement in the water and brine cycle

For the measurement of the flow rate of the brine and water cycle the volumetric flow meter Promag 50P DN15 (Endress+Hauser, 2013a) is used. With the density of the water the mass flow can be calculated. The density is a function of the temperature. Figure 3-20 shows the working principle of a MID volumetric flow meter as well as the device used in the test rig.

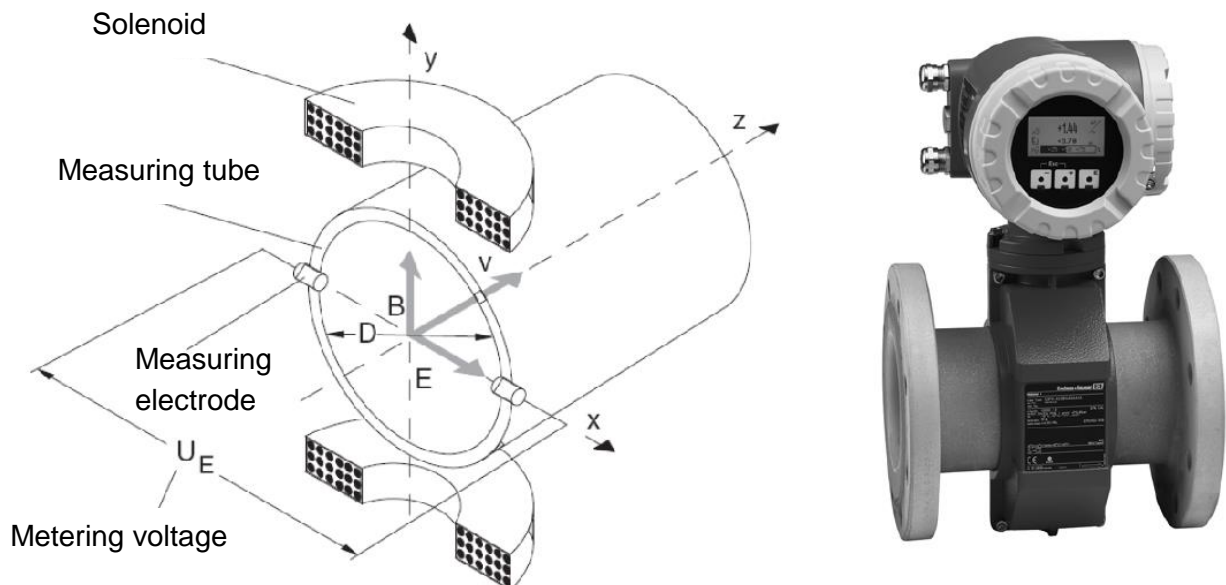


Figure 3-20: Measurement principle of a MID volumetric flow meter left (Rieberer, 2013) and Promag 50P right (Endress+Hauser, 2013a)

The measuring principle is the separation of moving electronic charges in a magnetic field. Electronic charges get distracted by the magnetic field according to Faraday's induction law, the positive charges to one side and the negative charges to the other. The tube, which consists of non-magnetic material, is placed between solenoids. Two electrodes are inserted in the tube, which are in contact with the fluid. A magnetic field with the induction B is applied by the solenoids vertically to the flow direction of the fluid which flows with the speed v . The magnetic field passes through the tube and through the fluid and because of the separation of the charges a voltage U_E is applied to the two electrodes which are inserted in the tube. The voltage U_E is proportional to the magnetic induction B , the inner diameter D of the tube and the speed of the fluid v .

$$U_E \sim B \cdot D \cdot v$$

For the MID it is a basic requirement that the fluid is electrically conducting.

3.4.4 Electric meter

For the measurement of the electric power consumption of the compressor including the SEC board and the drive, the electric meter AAD1 D5E from Saia-Burgess is used. It is a one-phase electric meter with a maximum current of 25 A, which is sufficient for all measurements. The maximum power consumption of the compressor drive is 4 kW, which means an input current of approximately 17 A with a voltage of 230 V. The electric meter emits 1000 impulses per kWh, which are counted with the LabVIEW software. For the stationary measurement points it has to be considered to run each point for a certain time to reach a certain accuracy. The accuracy is listed in Table 3-2.

3.5 Data acquisition and visualisation

For data acquisition and visualisation a National Instruments (NI) system is installed. In addition to the hardware the main part of this package is the software LabVIEW. It is also used for the control of the periphery. Figure 3-21 shows the NI system configuration for the communication.

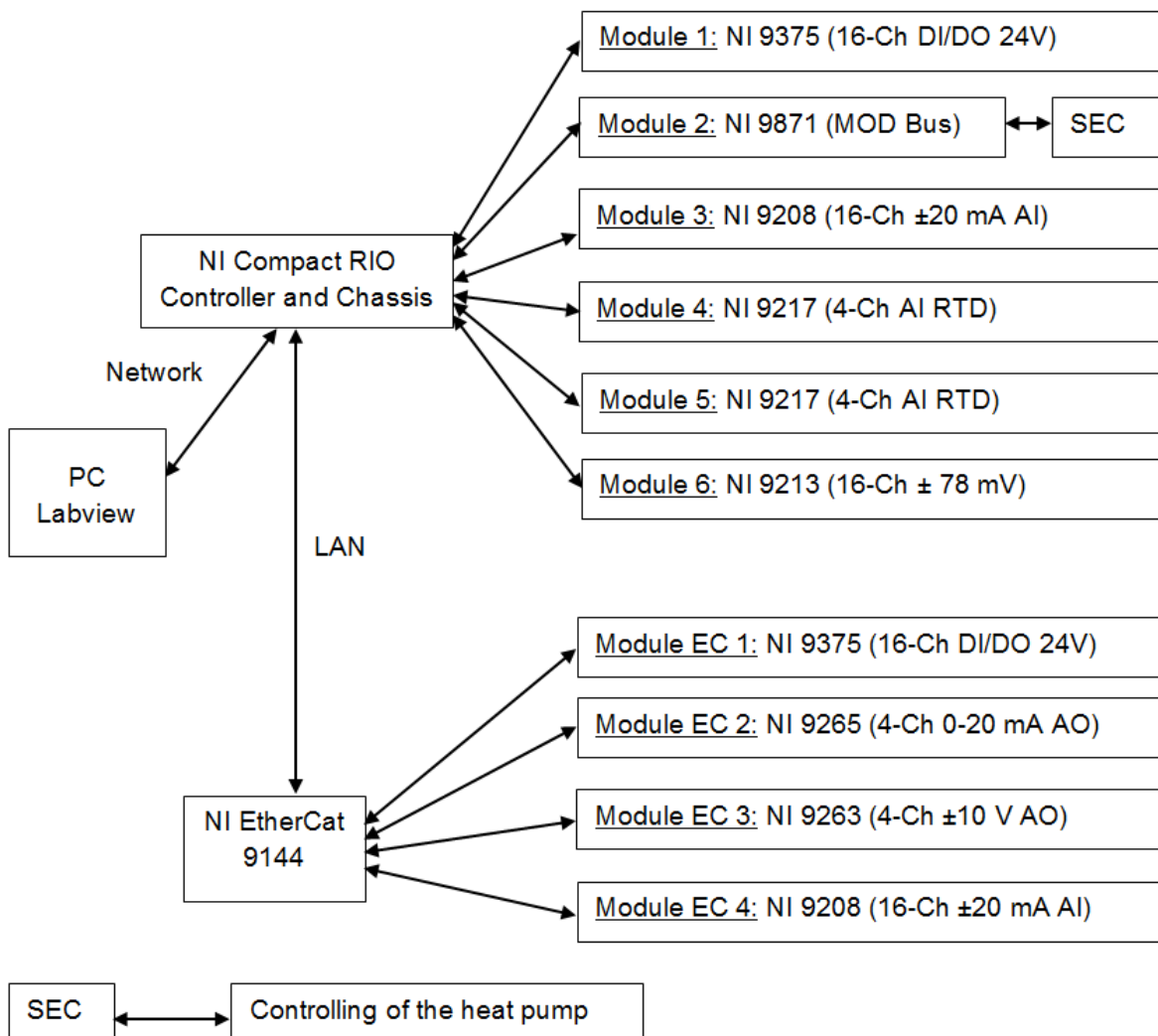


Figure 3-21: NI system configuration for communication

The NI CompactRIO system consists of a controller, the chassis, which can be mounted with different input and output modules, and the I/O modules itself. Furthermore the system can be expanded with one or more further expansion chassis to add more I/O modules which, are also controlled by the NI CompactRIO controller. For the controlling the software LabVIEW is running on a windows computer, which is connected to the controller via network connection.

3.5.1 Compact RIO hardware

The most important hardware part of the CompactRIO system is the controller NI cRIO-9024, which can be used for stand-alone execution of LabVIEW real-time applications and for windows applications. All applications for the controlling of the heat pump test rig are programmed on the windows computer, except the recording of the counter for the measurement of the electric energy consumption, which is programmed as a real-time application. The controller has a CPU with 800 MHz, 512 MB RAM and 4 GB Storage for logging data and for storing programs. It also includes a USB board for connecting storage drives. The CompactRio controller is embedded in an eight-slot reconfigurable FPGA chassis whereby reconfigurable means that I/O modules can be changed depending on the needs of the system. FPGA means that the chassis contains a core with an integrated circuit, which is programmed to use elemental I/O functions to read and write signal information from each module (<http://www.ni.com/compactrio/whatis>, 24.03.2014). It contains six modules for the communication with the periphery. The system can be extended with expansion chassis if more I/O modules are needed. The controller is connected to the expansion chassis NI EtherCAT 9144, which has eight further slots for I/O modules and does not need any additional software, whereby four slots are occupied with further modules. Figure 3-21 shows the configuration of the main chassis and the EtherCAT chassis and Table 3-3 depicts a short description of the different modules. The configuration of the different modules can be seen in the Appendix A-3.

Table 3-3: Description of the different I/O Modules

Name	Type	Description
NI 9208	16-Channel, ± 20 mA AI Module, 24-Bit	Input of all mass- and volumetric flow meters and all pressure transmitters
NI 9213	16-Channel, I TC Input Module ± 78 mV, 24-Bit	Input of all TC
NI 9217	4-Channel, 100 Ω RTD AI Module 24-Bit	Input of all Pt100
NI 9263	4-Channel, ± 10 V AO Module, 16-Bit	Control of all pumps in the periphery cycle and desuperheater control valve
NI 9265	4-Channel, 0 to 20 mA AO Module, 16-Bit	Control of the heating rod in the brine cycle
NI 9375	16-Channel, 24V DI- and 24V 16-Channel DO Module,	Reading of the electric meters (DI), SEC alarms and status (DI), for the controlling of the solenoid valves (DO) and for the activation of all pumps and heating rods (DO)
NI 9871	4-Port, RS485/RS422 Serial Interface Module for CompactRIO	Reading and writing to the SEC board, the Copeland control device for the compressor and the expansion valves.

3.5.2 LabVIEW

The whole data acquisition, visualisation of the measured data and the controlling is done with the NI software LabVIEW which is a part of the CompactRIO package. It can be used on different platforms, whereby a windows computer is used here. LabVIEW is a graphical programming language, which uses symbols to connect and develop various measurement and control systems. Programs are called Virtual Instruments (VIs) in LabVIEW because the instruments in the front panel look like real world devices, for example an oscilloscope. A VI consists of a front panel, which is the user interface and a block diagram, which contains the graphical source code. All objects placed in the front panel also appear in the block diagram with terminals for wiring. For example a control element can be wired with an indicator element in the block diagram, whereby the value of the control element can then be seen on the indicator element in the front panel. Compared to text based programming languages, where commands are used for program execution, in LabVIEW symbols are used for programming. The order of execution is determined by the dataflow between the functions in the block diagram. The block diagram contains different functions, which can be chosen from function palettes for the programming. A VI can always be used as independent program with its front panel or it can be used as SubVI, which means that it is called from another VI. If it is used as SubVI, the inputs and outputs have to be defined and it appears as a block with these inputs and outputs in the block diagram of the main VI. This makes it possible to generate a structured program with many layers. Furthermore it includes the advantage that each VI can be tested individually and then integrated into the main program.

One advantage of LabVIEW is that it is used by a large user group, which implies a large community. It contains a vast number of applications and functions for acquiring and analysing measured data, for the control of instruments and for the monitoring of applications.

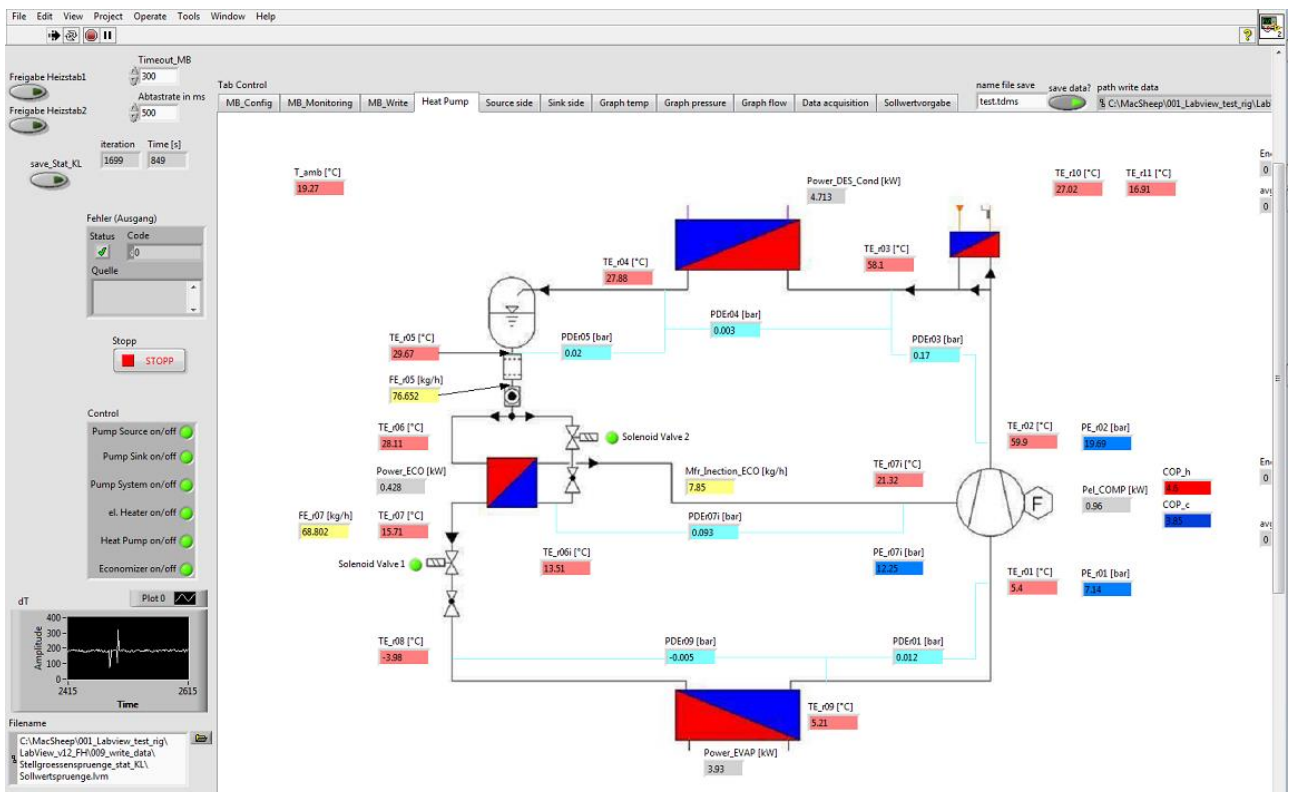


Figure 3-22: User interface for controlling the heat pump test rig

Figure 3-22 shows a small part of the user interface used for the control of the heat pump prototype and the periphery. The user interface can be adapted to the user's needs and preferences. LabVIEW is used for the reading of the whole measurement data and writing it into Log-files (chapter 3.4), for the visualisation of the heat pump cycle as well as the periphery to monitor the process and for the control of the periphery cycles. The control circuits are described in chapter 3.6

With the Modbus communication, shown in Figure 3-3 and Figure 3-21, the LabVIEW user interface is also used for setting the parameters for the heat pump control and providing the operating mode (Heating, Cooling..). Many different diagrams are included in the user interface to monitor the measured values, which are temperature, pressure, and mass flow diagrams over time and an envelope diagram, which has the evaporation temperature on the horizontal-axis and the condensing temperature on the vertical axis. This can be used to see the operating point of the heat pump immediately.

3.6 Control circuits in the system

For the operation of the test rig a reliable control of the periphery system is necessary. On the source side the mass flow of the brine cycle and the power of the heating rod have to be controlled, on the sink side one pump for the mass flow in the cycle and one pump for the mass flow over the heat exchanger for heat rejection are necessary. The mass flow over the desuperheater is also controlled. The principles needed for the implementation and the parameter setting of the controllers are described in chapter 2.2. This chapter describes more specific the implemented control circuits in the system and shows the results of the parameter setting by CHR.

Five controllers are implemented into the LabVIEW software for the controlling of the heat pump prototype and the periphery, two on the source side, which are circuit Nr. 1 & 2 in

Circuit Nr. 1 is the controlling of the heating rod in the MHS_o, which is shown in Figure 3-13. This heating rod has to compensate the cooling power of the heat pump. The test rig is dimensioned for a cooling power of 3.5 kW, although this value varies a lot in the different operating points. The controlled variable is the temperature at the evaporator inlet TE_{b1}. A PI controller is used, whereby the disturbance parameters show the best performance (Table 3-5). Since the parameters are taken for a special operating point (cooling capacity of 2.65 kW), this values are only adequate for this point. The modification of these parameters for different cooling capacities is described at the end of this chapter.

Table 3-4 and three on the sink side, which are Nr. 3 to 5 in the table. The table contains the controlled device for each circuit and the variable value. Furthermore it includes the controlled variable and the measurement device, whereby the placement of the device can be seen in Figure 3-15. All controlled devices can be controlled in the range from 0 to 100 %. The parameters needed for the CHR are summarized in Table 3-5. With the formulas shown in Table 2-3 the parameters for the controller can be calculated. A more specific description of the control cycles is given after Table 3-4.

Circuit Nr. 1 is the controlling of the heating rod in the MHS_o, which is shown in Figure 3-13. This heating rod has to compensate the cooling power of the heat pump. The test rig is dimensioned for a cooling power of 3.5 kW, although this value varies a lot in the different operating points. The controlled variable is the temperature at the evaporator inlet TE_{b1}. A PI controller is used, whereby the disturbance parameters show the best performance (Table 3-5). Since the parameters are taken for a special operating point (cooling capacity of 2.65 kW), this values are only adequate for this point. The modification of these parameters for different cooling capacities is described at the end of this chapter.

Table 3-4: Control circuit overview

Circuit Nr.	Controlled device	Variable value	Controlled Variable	Measurement device
1	Heating rod	Heating power (100 % = 6kW)	Temperature	TE _{b1} [°C]
2	Pump source (brine)	Static height (100 % = 7 m)	Volumetric flow	FE _{b1} [kg/h]
3	Pump sink (water)	Static height (100 % = 7 m)	Volumetric flow	FE _{w4} [kg/h]
4	Pump MHS _i HX (water)	Static height (100 % = 7 m)	Temperature	TE _{w1} [°C]
5	Control valve desuperheater	Opening (0 - 100 %)	Temperature	TE _{d2} [°C]

Circuit Nr. 2 & 3 are used to control the volumetric flow in the source and sink cycle. Circuit Nr. 2 is the control of the speed controlled pump in the brine cycle. The placement of the pump can be seen in Figure 3-13. The measurement device is the MID volumetric flow meter, which measures the value FE_{b1}, which is the evaporator inlet mass flow (Figure 3-15). For all operating points the dimensioning volumetric flow of 1078 l/h is taken. Circuit Nr. 3 is similar because a speed controlled pump with the same static height is used to control the volumetric flow of the sink cycle. The placement of the pump can be seen in Figure 3-14 as well as the placement of the measuring sensor FE_{w4}, which is shown in Figure 3-15. For both pumps a PI controller was chosen with the leading parameters, which can be seen in Table 3-5. To increase the stability, the integral time T_N was adjusted experimentally compared to the CHR value.

Control circuit Nr. 4 also includes a speed controlled pump, which controls the flow rate over the heat exchanger, which is used to reject heat from the sink side of the test rig. The pump is installed on the MHS_i, which can be seen in Figure 3-14. The controlled variable is the water inlet temperature to the condenser TE_{w1}. The parameters only work for the pressure loss in the cycle, which is caused by the control valves at the inlet and outlet of the heat exchanger, whereby the position was described in chapter 3.3. For the controlling of this circuit a PI controller is used with the parameters for disturbance (Table 3-5). The parameters are taken for a heating capacity of 5 kW and the same as for control circuit Nr. 1 the parameters are only adequate for this operating point.

It has to be mentioned that it is not possible to set every temperature at the inlet of the condenser for every heat flow. The temperature, which enters the heat exchanger from the

brine storage (chapter 3.3), can only be adjusted to a certain level, which means that for a temperature at the condenser inlet of 20 °C a lower temperature from the global brine storage is used than if a condenser inlet temperature of 50 °C is needed. So the control circuit Nr. 4 can only control the temperature of the condenser inlet in a certain range, which also depends on the heating power.

Control circuit Nr. 5 controls the mass flow over the desuperheater on the sink side. This is done by opening and closing the electronic control valve, which can be seen in Figure 3-14. The controlled variable is the temperature TE_d2 at the desuperheater outlet (Figure 3-15). The mass flow is controlled in a range from 0 to 63 kg/h, whereby this can be changed. For the controlling a PI controller is used with disturbance parameters.

Table 3-5: Final parameters calculated by CHR

Circuit Nr.	K [-]	T _a [s]	T _u [s]	K _p [-]	T _N [s]	T _V [s]
1	0.665	1750	47.5	33.24	190.2	0.0
2	0.208	5.3	7.3	1.22	9.0	0.0
3	0.165	5.0	6.3	1.70	9.0	0.0
4	0.183	1089	42.3	84.72	169.2	0.0
5	0.430	70.0	15.0	3.51	120.0	0.0

Adjustable K_p for control circuit 1 & 4

Both, the heating capacity and the cooling capacity vary with the operating point. This makes it very complicated to parameterize the controllers for the inlet temperature of the condenser and evaporator because each operating point needs different parameters. For a higher capacity the temperature changes faster and for a lower capacity slower. If the temperature changes faster, the controller needs a smaller proportional gain K_p to compensate this change in the same way as for a slower reaction. The controller parameterized for a heating capacity of 5 kW is too slow for a lower heating capacity and too fast for a higher one. This problem is solved by changing the proportional gain K_p linearly with the heating and cooling capacity compared to the point, for which the parameters are determined. If for example the heating capacity reduces from 5 kW to 2.5 kW the proportional gain doubles to adjust the controller to the slower reaction of the system. This simple variation of the proportional gain shows satisfying performance for the control of the condenser and evaporator inlet temperature. The linear algorithm for the variable K_p is implemented in the LabVIEW program for these two control circuits.

4 DATA EVALUATION

This chapter shows how the data is evaluated, especially for determining the compressor- and cycle performance. Furthermore it includes the calculation of the heat transfer coefficient U for the evaporator and condenser HX, which is done to verify the dimensioning. The Gaussian error propagation is used to determine the influence of the error of measurement on the results of the cycle evaluation.

4.1 Compressor efficiency

The performance of the compressor is mainly determined by two efficiencies, the overall isentropic efficiency and the volumetric efficiency. The overall isentropic efficiency compares the actual needed power of the compressor, for a certain pressure ratio and mass flow, to the power the compressor would need, if the compression would be isentropic, which means reversible without any heat exchange with the environment. For the calculation of the overall isentropic efficiency the compressor losses are needed. The volumetric efficiency describes the actual volumetric flow through the compressor compared to the theoretical possible flow resulting from the swept volume. Figure 4-1 shows the heat pump cycle with the points of measurement needed for the calculation of the different efficiencies. These points can also be seen in the schematic view of the heat pump cycle in chapter 3.1. Figure 4-3 includes also all theoretical points of the compression process needed for the calculation of the overall isentropic efficiency.

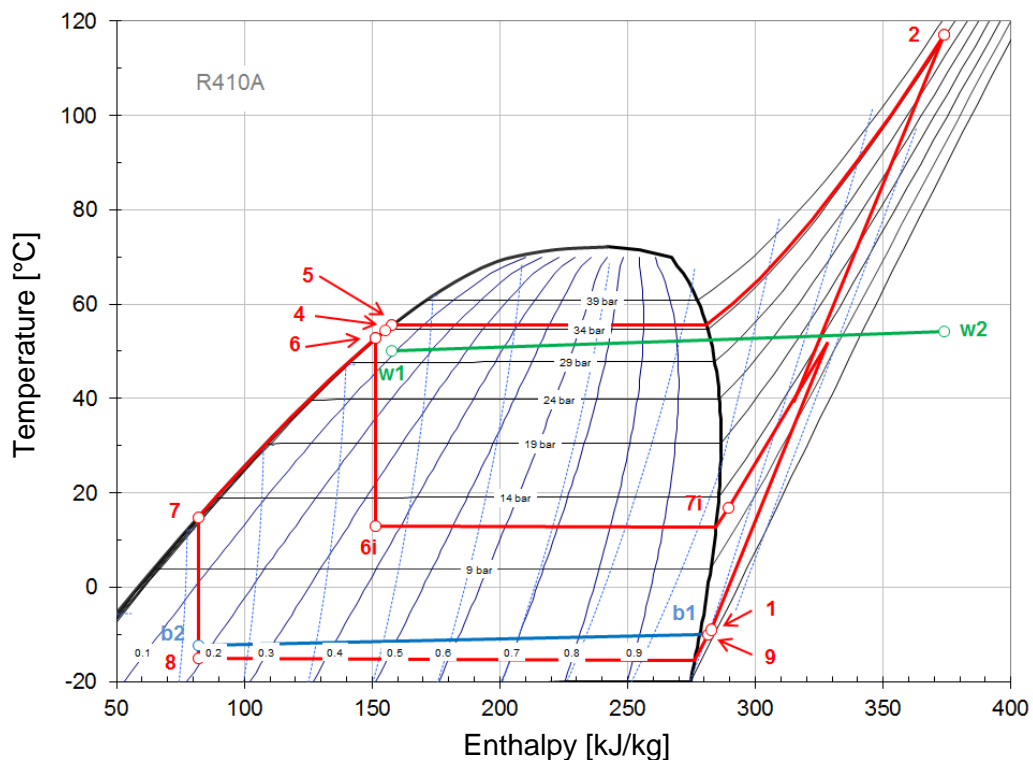


Figure 4-1: Temperature-enthalpy diagram of the working fluid cycle with high pressure ratio

4.1.1 Compressor losses

For the calculation of the overall isentropic efficiency the compressor losses are needed, which describe the heat losses of the compressor system to the ambient. This includes the heating losses of the compressor with the motor, the inverter and the SEC board. Compressor losses are calculated via the energy balance over the compressor, which is shown schematically in Figure 4-2. The main mass flow over the evaporator ($\dot{m}_{r, \text{evap}}$) with the enthalpy h_{r1} and the injection mass flow over the injection port ($\dot{m}_{r, \text{inj}}$) with the enthalpy h_{r7i} are the input values as well as the electric power (P_{el}) to drive the compressor. All these inputs have to sum up to the output mass flow ($\dot{m}_{r, \text{cond}}$) with the output enthalpy h_{r2} . The difference are the compressor losses $\dot{Q}_{\text{comp, loss}}$, which can be calculated as

$$\dot{Q}_{\text{comp, loss}} = \dot{m}_{r, \text{evap}} \cdot h_{r1} + \dot{m}_{r, \text{inj}} \cdot h_{r7i} + P_{el} - \dot{m}_{r, \text{cond}} \cdot h_{r2} \quad \text{Eq. 4-1}$$

With this calculation the compressor losses have a positive sign. To quantify the compressor losses independently from the input power the relative losses can be stated as percentage of P_{el}

$$f_{\text{comp, loss}} = \frac{\dot{Q}_{\text{comp, loss}}}{P_{el}} \quad \text{Eq. 4-2}$$

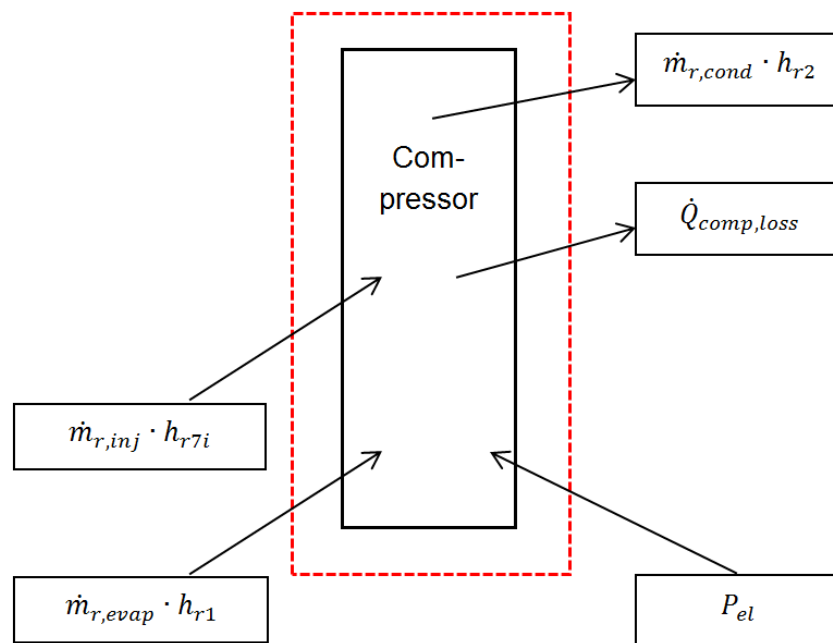


Figure 4-2: Energy balance over the compressor

4.1.2 Overall isentropic efficiency

The overall isentropic efficiency is calculated by comparing the needed input power for a reversible compression to the power really needed for the compression. There is a difference in the calculation of the isentropic efficiency depending if refrigerant is injected at the medium pressure level or not. The calculation is first shown for the compression with vapour injection and then the simplifications for the compression without vapour injection are given.

With Vapour injection

Figure 4-3 shows the compression process with vapour injection in the temperature-enthalpy diagram. The points 1, 7i and 2 are measured points which can also be seen in Figure 4-1, all other points are calculated values, which are needed for the determination of the overall isentropic efficiency. For the calculation of the efficiency, it is assumed that two compressors are used, the first compression stage is from the low level pressure to the medium pressure level and the second compression is from the medium pressure level to the high pressure level. The isentropic efficiency is calculated for both stages individually. For the first stage the isentropic compression is from 1 to 2'is, whereby the point 2' is reached because the compressor does not work reversible. The point 2'wo loss would be reached, if all heat losses from the compressor would go into the refrigerant and nothing into the ambient air. The same applies for the second compression stage.

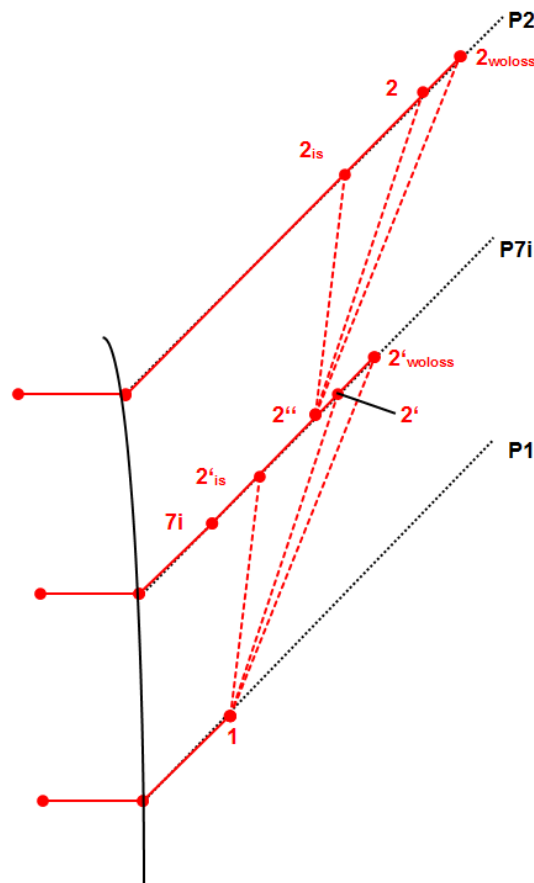


Figure 4-3: Theoretical points for the calculation of the isentropic efficiency in the temperature-enthalpy diagram

The overall isentropic efficiency for the low pressure (LP) stage is defined as

$$\eta_{is,over,LP} = \frac{h_{2'is} - h_1}{h_{2'wo loss} - h_1} \quad \text{Eq. 4-3}$$

For the high pressure stage (HP) the overall isentropic efficiency can be calculated as

$$\eta_{is,over,HP} = \frac{h_{2is} - h_{2''}}{h_{2woloss} - h_{2''}} \quad \text{Eq. 4-4}$$

which leads to two equations with four unknown. One more equation is obtained by using the compressor losses calculated in 4.1.1 to calculate $h_{2woloss}$ with

$$(h_{2woloss} - h_{2''}) \cdot (1 - f_{comp,loss}) = h_2 - h_{2''}$$

which is transformed to

$$h_{2woloss} = \frac{h_2 - f_{comp,loss} \cdot h_{2''}}{1 - f_{comp,loss}} \quad \text{Eq. 4-5}$$

The point $h_{2'}$ losses can be calculated in the same way for the first pressure stage

$$h_{2'woloss} = \frac{h_{2'} - f_{comp,loss} \cdot h_1}{1 - f_{comp,loss}} \quad \text{Eq. 4-6}$$

The two new variables $h_{2'}$ and $h_{2''}$ can be linked by forming the enthalpy flow balance at the medium pressure level

$$h_{2''} = \frac{\dot{m}_{r,evap} \cdot h_{2'} + \dot{m}_{r,inj} \cdot h_{7i}}{\dot{m}_{r,evap} + \dot{m}_{r,inj}} \quad \text{Eq. 4-7}$$

The last equation to solve the equation system is given by the assumption that the overall isentropic efficiency is the same for both pressure stages

$$\eta_{is,over,LP} = \eta_{is,over,HP} \quad \text{Eq. 4-8}$$

Now the equation system consists of six independent equations for the four unknown points in the compression process and the two efficiencies for the two stages. The equation system has to be solved for each operating point.

Without Vapour injection

Without vapour injection there is no mass flow over the second inlet port of the compressor. The isentropic efficiency is calculated in the following way

$$\eta_{is,over} = \frac{h_{2is} - h_1}{h_{2woloss} - h_1} \quad \text{Eq. 4-9}$$

whereby

$$h_{2woloss} = \frac{h_2 - f_{comp,loss} \cdot h_1}{1 - f_{comp,loss}} \quad \text{Eq. 4-10}$$

Instead of six equations only two are needed for the calculation of the isentropic efficiency.

4.1.3 Volumetric efficiency

The volumetric efficiency describes the actual volumetric flow rate compared to the theoretical possible flow rate generated by the compressor. It describes valve losses as well as leakage and reexpansion between the two scroll spirals (Rieberer et al., 2009). The theoretical possible flow rate is given by the swept volume (V_{swept}) of the compressor and the compressor speed

$$\dot{V}_{swept} = V_{swept} \cdot n \quad \text{Eq. 4-11}$$

The theoretical possible flow rate is stated by the manufacturer with 2.8 m³/h for a speed of 3000 rounds per minute (n) for the first stage, and the same flow rate multiplied by the factor 0.71 for the second stage. With equation 4-11 the swept volume can be calculated from the compressor manufacturer's data. The volumetric efficiency has to be calculated individually for both pressure stages. For the first stage it is defined as

$$\eta_{vol,LP} = \frac{\dot{m}_{r,evap} \cdot v_{r,1}}{V_{swept} \cdot n} \quad \text{Eq. 4-12}$$

whereby $v_{r,1}$ is the specific volume of the refrigerant at the inlet of the compressor. It can be determined with the material properties in this point as a function of the pressure and the temperature, which are measured. For the second stage the volumetric efficiency is defined as

$$\eta_{vol,HP} = \frac{\dot{m}_{r,cond} \cdot v_{r,2''}}{V_{swept} \cdot 0.71 \cdot n} \quad \text{Eq. 4-13}$$

whereby the specific volume v in the calculated point 2'' can be again determined with the material properties in this point as a function of the pressure, which is measured, and the enthalpy, which is calculated in chapter 4.1.2. . The volumetric efficiency of the whole scroll compressor is defined as the average of the efficiencies for both compression stages.

$$\eta_{vol} = \frac{\eta_{vol,LP} + \eta_{vol,HP}}{2} \quad \text{Eq. 4-14}$$

4.2 Cycle performance

For the evaluation of the cycle performance the Coefficient of Performance (COP) is used, which is the ratio of the useful energy to the required energy to run the cycle, which was already described in chapter 2.1.3.

$$COP = \frac{\text{usefull energy}}{\text{required energy}}$$

Sometimes the required energy only consists of the input power of the compressor but it can also include further units to run the cycle like pumps or valves. For this heat pump the required energy is determined as the input power to run the compressor and the input power for the SEC board to control the heat pump cycle, whereby the SEC board was added after the measurement of the compressor performance map. This means that for the evaluation of the compressor performance map the input power of the SEC board is not included and for the evaluation of the cycle, the influence of the ECO and the desuperheater it is.

The useful energy can be both, the cooling capacity on the low pressure side of the heat pump (evaporator) or the heating capacity on the high pressure side (condenser). For some applications the heating and the cooling capacity can be used and therefore both capacities are added as useful energy. If the cooling capacity is the used energy the COP is defined as

$$COP_C = \frac{\dot{Q}_{evap}}{P_{el}} \quad \text{Eq. 4-15}$$

whereby the cooling capacity in the evaporator can be calculated for the refrigerant side, which is defined as

$$\dot{Q}_{r,evap} = \dot{m}_{r,evap} \cdot (h_{r9} - h_{r8}) \quad \text{Eq. 4-16}$$

and for the brine side which gives

$$\dot{Q}_{b,evap} = \dot{m}_b \cdot (h_{b1} - h_{b2}) = \dot{m}_b \cdot cp_b \cdot (t_{b1} - t_{b2}) \quad \text{Eq. 4-17}$$

The position of the used enthalpies in the formula can be seen in Figure 4-1, which shows the cycle in the temperature-enthalpy diagram. The heating capacity calculated with the brine cycle needs the temperature of the brine inlet (t_{b1}) and the brine outlet (t_{b2}), whereby the positioning of the sensors can be seen in Figure 3-13. If there is no heat exchange of the evaporator with the ambient both values should result in the same cooling capacity.

Since the test rig is designed for heating the COP_C is not further considered in the evaluation of the heat pump cycle. The focus is on the COP for heating, which is defined as

$$COP_H = \frac{\dot{Q}_{cond} + \dot{Q}_{desup}}{P_{el}} \quad \text{Eq. 4-18}$$

As already shown for the COP for cooling the heating capacity on the high pressure side can also be calculated for the refrigerant cycle and the water cycle, whereby the overall heating capacity for the refrigerant side is calculated as

$$\dot{Q}_{r,cond} + \dot{Q}_{r,desup} = \dot{m}_{r,cond} \cdot (h_{r2} - h_{r5}) \quad \text{Eq. 4-19}$$

If the measurement point 3 in the refrigerant cycle is used (Figure 4-1), it is also possible to calculate the heating capacity individually for the condenser and the desuperheater, which leads to

$$\dot{Q}_{r,cond} = \dot{m}_{r,cond} \cdot (h_{r3} - h_{r5}) \quad \text{Eq. 4-20}$$

for the condenser and to

$$\dot{Q}_{r,desup} = \dot{m}_{r,cond} \cdot (h_{r2} - h_{r3}) \quad \text{Eq. 4-21}$$

for the desuperheater. For the water side the heating capacity is calculated individually for the condenser and the desuperheater with the inlet and outlet temperatures of the heat exchangers and the mass flow. The placement of the sensors can be seen in Figure 3-14. For the condenser the heating capacity is given with

$$\dot{Q}_{w,cond} = \dot{m}_{w,cond} \cdot (h_{w2} - h_{w1}) = \dot{m}_{w,cond} \cdot cp_w \cdot (t_{w2} - t_{w1}) \quad \text{Eq. 4-22}$$

and for the desuperheater with

$$\dot{Q}_{w,desup} = \dot{m}_{w,desup} \cdot (h_{d2} - h_{d1}) = \dot{m}_{w,desup} \cdot cp_w \cdot (t_{d2} - t_{d1}) \quad \text{Eq. 4-23}$$

If the COP is used in the further chapters it is always referred to the COP for heating.

For the evaluation of the cycle the economiser capacity is also of interest, which can be calculated for the high pressure- and the medium pressure level, whereby for the high pressure side the capacity can be calculated as

$$\dot{Q}_{r,ECO,HP} = \dot{m}_{r,evap} \cdot (h_{r6} - h_{r7}) \quad \text{Eq. 4-24}$$

and with

$$\dot{Q}_{r,ECO,MP} = \dot{m}_{r,inj} \cdot (h_{r7i} - h_{r6i}) \quad \text{Eq. 4-25}$$

for the medium pressure side.

4.3 Heat exchanger performance

For the dimensioning of the heat exchangers the software was used, which was provided by the manufacturer SWEP (chapter 3.1.2). After the condenser did not reach the expected performance a UA calculation was performed for the condenser and the evaporator to compare it with the results from the software. The UA shows how much heating capacity the heat exchanger can exchange per Kelvin and has the unit W/K. The larger this value is, the better is the heat transfer and a smaller temperature difference between two fluids is necessary to transfer a certain heating capacity. The relation between the heating capacity and the overall heat transfer coefficient is

$$\dot{Q} = U \cdot A \cdot \Delta T_{log} \quad \text{Eq. 4-26}$$

whereby \dot{Q} is the heat transfer rate, which was calculated in chapter 4.2 for all heat exchangers, U is the heat transfer coefficient, A is the heat exchanger area and ΔT_{log} is the logarithmic mean temperature difference, which is defined as

$$\Delta T_{log} = \frac{\Delta T_{high} - \Delta T_{low}}{\ln\left(\frac{\Delta T_{high}}{\Delta T_{low}}\right)} \quad \text{Eq. 4-27}$$

With the logarithmic temperature difference the average temperature difference between the fluids is calculated. In chapter 5.2.1, which deals with the improvement of the cycle performance, the calculated values and the manufacturer values are compared.

4.3.1 Evaporator

Figure 4-4 shows the temperature-enthalpy diagram of the evaporation process in the heat exchanger, which can also be seen in the temperature-enthalpy diagram of the whole cycle (Figure 4-1).

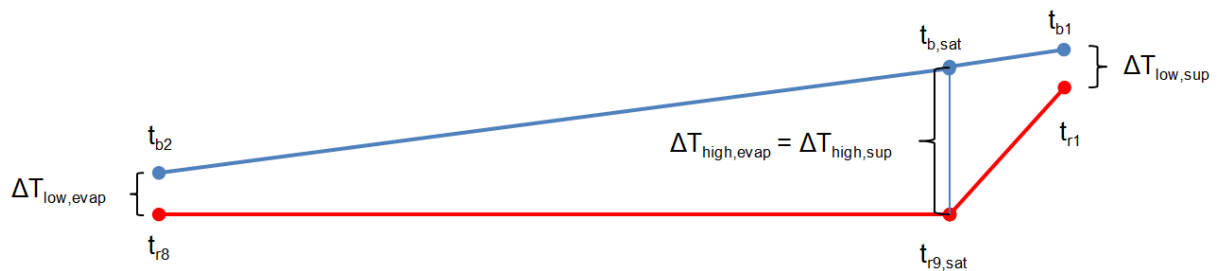


Figure 4-4: Temperature-enthalpy diagram of the evaporation in the heat exchanger

For the calculation of UA the process in the evaporator has to be divided into at least two parts, the evaporation process and the superheating. UA has to be calculated for each part individually and then it can be added. All marked temperatures are measured or determined with the measured pressure except $t_{b,sat}$, which has to be calculated as

$$t_{b,sat} = t_{b2} + (t_{b1} - t_{b2}) \cdot \frac{(h_{r9,sat} - h_{r8})}{(h_{r1} - h_{r8})}$$

All enthalpies are determined with material property tables for the used refrigerant R410a. The temperature differences needed for the calculation are calculated with

$$\Delta T_{low,evap} = t_{b2} - t_{r8}$$

$$\Delta T_{high,evap} = \Delta T_{high,sup} = t_{b,sat} - t_{r,sat}$$

$$\Delta T_{low,sup} = t_{b1} - t_{r1}$$

The calculated temperature differences for the two segments can now be inserted into equation 4-27, which gives the logarithmic temperature differences for the two segments

$$\Delta T_{log,evap} = \frac{\Delta T_{high,evap} - \Delta T_{low,evap}}{\ln\left(\frac{\Delta T_{high,evap}}{\Delta T_{low,evap}}\right)} \quad \text{Eq. 4-28}$$

$$\Delta T_{log,sup} = \frac{\Delta T_{high,sup} - \Delta T_{low,sup}}{\ln\left(\frac{\Delta T_{high,sup}}{\Delta T_{low,sup}}\right)} \quad \text{Eq. 4-29}$$

With the logarithmic temperature difference the UA values for the two segments can be calculated and added

$$UA_{evap} = \frac{\dot{m}_{r,evap} \cdot (h_{r9,sat} - h_{r8})}{\Delta T_{log,evap}} \quad \text{Eq. 4-30}$$

$$UA_{sup} = \frac{\dot{m}_{r,evap} \cdot (h_{r1} - h_{r9,sat})}{\Delta T_{log,sup}} \quad \text{Eq. 4-31}$$

$$UA_{evaporator} = UA_{evap} + UA_{sup} \quad \text{Eq. 4-32}$$

For this calculation it is mentioned that it is only correct if the superheat is not the limiting factor for the heat exchange. That means that $\Delta T_{low,sup}$ which can be seen in Figure 4-4 is > 0 .

4.3.2 Condenser

Figure 4-5 shows the condensing process in the temperature-enthalpy diagram. The whole diagram can be seen in Figure 4-1. The shown calculation of UA is for the case that the desuperheater is not used. If the desuperheater is also used, the calculation has to be adapted because then the Δh of the superheated refrigerant gets less for the condenser or it only condenses the refrigerant. The calculation of UA is similar to the evaporator, the process has to be divided into at least two segments for the desuperheating and the condensing.

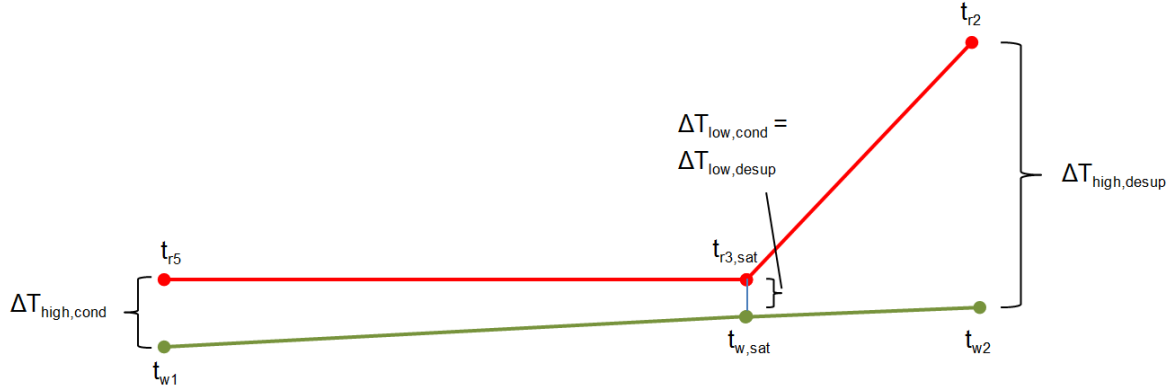


Figure 4-5: Temperature-enthalpy diagram of the condensing process in the heat exchanger

All temperatures are measured or calculated with the measured pressures with refrigerant property values except $t_{w,sat}$, which has to be calculated as

$$t_{w,sat} = t_{w1} + (t_{w2} - t_{w1}) \cdot \frac{(h_{r3,sat} - h_{r5})}{(h_{r2} - h_{r5})}$$

The enthalpies are determined according to refrigerant property data. The temperature differences needed for the logarithmic temperature difference follow as

$$\Delta T_{high,cond} = t_{r5} - t_{w1}$$

$$\Delta T_{low,cond} = \Delta T_{low,desup} = t_{r3,sat} - t_{w,sat}$$

$$\Delta T_{high,desup} = t_{r2} - t_{w2}$$

With the logarithmic temperature differences UA can be calculated.

$$\Delta T_{log,cond} = \frac{\Delta T_{high,cond} - \Delta T_{low,cond}}{\ln\left(\frac{\Delta T_{high,cond}}{\Delta T_{low,cond}}\right)} \quad \text{Eq. 4-33}$$

$$\Delta T_{log,desup} = \frac{\Delta T_{high,desup} - \Delta T_{low,desup}}{\ln\left(\frac{\Delta T_{high,desup}}{\Delta T_{low,desup}}\right)} \quad \text{Eq. 4-34}$$

$$UA_{cond} = \frac{\dot{m}_{r,cond} \cdot (h_{r3,sat} - h_{r5})}{\Delta T_{log,cond}} \quad \text{Eq. 4-35}$$

$$UA_{desup} = \frac{\dot{m}_{r,cond} \cdot (h_{r2} - h_{r3,sat})}{\Delta T_{log,desup}} \quad \text{Eq. 4-36}$$

$$UA_{condenser} = UA_{cond} + UA_{desup} \quad \text{Eq. 4-37}$$

4.4 Error of measurement for the cycle evaluation

For the evaluation of the cycle, especially the COP, an error analysis was performed. This chapter describes the influence of the single measurement errors of different measurements on a calculated result. The needed basics for the error of measurement and the propagation of uncertainty are described in chapter 2.3.

For the calculations of the error of measurement for the heating capacities material property tables for the brine, the water and the refrigerant are used. Because of this it is not always possible to form the first derivation of each equation. In this case an approximation with the finite difference scheme is made, whereby $\Delta x_{1,var}$ is a small variation of x_1 , which leads to a small variation of f .

$$\frac{\partial f}{\partial x_1} \cdot \Delta x_1 \sim \frac{\Delta f}{\Delta x_{1,var}} \cdot \Delta x_1 \quad \text{Eq. 4-38}$$

The equations, which are needed to determine the cycle performance and with that also the error of measurement, are defined in chapter 4.2. The systematic errors after the calibration are listed in Table 3-2.

Evaporator

For the evaporator heating capacity on the brine side the mass flow is directly measured and the flow enthalpies are determined with material property tables with the measured temperatures.

$$\dot{Q}_{b,evap} = f(\dot{m}_b, t_{b1}, t_{b2}) = \dot{m}_b \cdot (h_{b1} - h_{b2}) \quad \text{Eq. 4-39}$$

The error of measurement can be calculated as

$$\Delta \dot{Q}_{b,evap} = \sqrt{\left(\frac{\partial \dot{Q}_{b,evap}}{\partial \dot{m}_b} \cdot \Delta \dot{m}_b\right)^2 + \left(\frac{\Delta \dot{Q}_{b,evap}}{\Delta T_{b1,var}} \cdot \Delta T_{b1}\right)^2 + \left(\frac{\Delta \dot{Q}_{b,evap}}{\Delta T_{b02,var}} \cdot \Delta T_{b2}\right)^2} \quad \text{Eq. 4-40}$$

with the derivative

$$\frac{\partial \dot{Q}_{b,evap}}{\partial \dot{m}_b} = (h_{b1} - h_{b2}) \quad \text{Eq. 4-41}$$

The other errors are calculated with finite differences, whereby this is shown once for the influence of the measurement error Δt_{b1} . All other finite differences are calculated in the same way. The temperature t_{b1} is varied slightly by $\Delta T_{b1,var}$, which causes a change in the heating capacity $\Delta \dot{Q}_{b,evap} \cdot \Delta T_{b1,var}$ can be chosen individually, it can also be set to ΔT_{b1} , which means that exactly the range of the measurement error is linearized. Then the change in the heating capacity is calculated as

$$\Delta \dot{Q}_{b,evap} = \dot{Q}_{b,evap}(t_{b1}, t_{b2}, \dot{m}_b) - \dot{Q}_{b,evap}(t_{b1} - \Delta T_{b1,var}, t_{b2}, \dot{m}_b) \quad \text{Eq. 4-42}$$

The same can be done for ΔT_{b2} whereby it is varied for $\Delta T_{b2,var}$.

Condenser

In the same way as for the evaporator the mass flow is measured directly and the enthalpy flows are determined with property tables for water as a function of the inlet and outlet temperature.

$$\dot{Q}_{w,cond} = f(\dot{m}_{w,cond}, t_{w1}, t_{w2}) = \dot{m}_{w,cond} \cdot (h_{w2} - h_{w1}) \quad \text{Eq. 4-43}$$

The error of measurement follows as

$$\Delta \dot{Q}_{w,cond} = \sqrt{\left(\frac{\partial \dot{Q}_{w,cond}}{\partial \dot{m}_{w,cond}} \cdot \Delta \dot{m}_{w,cond}\right)^2 + \left(\frac{\Delta \dot{Q}_{w,cond}}{\Delta T_{w1,var}} \cdot \Delta T_{w1}\right)^2 + \left(\frac{\Delta \dot{Q}_{w,cond}}{\Delta T_{w2,var}} \cdot \Delta T_{w2}\right)^2} \quad \text{Eq. 4-44}$$

with the derivation for the mass flow

$$\frac{\partial \dot{Q}_{w,cond}}{\partial \dot{m}_{w,cond}} = (h_{w2} - h_{w1}) \quad \text{Eq. 4-45}$$

Desuperheater

For the desuperheater the mass flow on the water side is calculated as difference of the mass flow over the condenser (FE_w4) and the mass flow without the flow over the desuperheater (FE_w5), which can be seen in Figure 3-15. This was done because the used MID flow meters are not accurate for small flows (range 10 to 65 kg/h). The flow FE_w4 is called $\dot{m}_{w,cond}$ for all calculations, the flow FE_w5 is determined as $\dot{m}_{w,wodes}$. The error of measurement for the heating capacity of the desuperheater is calculated in the following way

$$\dot{Q}_{w,desup} = f(\dot{m}_{w,cond}, \dot{m}_{w,wodes}, t_{d1}, t_{d2}) = (\dot{m}_{w,cond} - \dot{m}_{w,wodes}) \cdot (h_{d2} - h_{d1}) \quad \text{Eq. 4-46}$$

$$\Delta \dot{Q}_{w,desup} = \sqrt{\left(\frac{\partial \dot{Q}_{w,desup}}{\partial \dot{m}_{w,cond}} \cdot \Delta \dot{m}_{w,cond}\right)^2 + \left(\frac{\partial \dot{Q}_{w,desup}}{\partial \dot{m}_{w,wodes}} \cdot \Delta \dot{m}_{w,wodes}\right)^2 + \left(\frac{\Delta \dot{Q}_{w,desup}}{\Delta T_{d1,var}} \cdot \Delta T_{d1}\right)^2 + \left(\frac{\Delta \dot{Q}_{w,desup}}{\Delta T_{d2,var}} \cdot \Delta T_{d2}\right)^2} \quad \text{Eq. 4-47}$$

with the derivatives

$$\frac{\partial \dot{Q}_{w,desup}}{\partial \dot{m}_{w,cond}} = (h_{d2} - h_{d1}) \quad \text{Eq. 4-48}$$

$$\frac{\partial \dot{Q}_{w,desup}}{\partial \dot{m}_{w,wodes}} = -(h_{d2} - h_{d1}) \quad \text{Eq. 4-49}$$

Electric Input power

To measure the electric power input of the compressor an electric meter counts for every Wh used. It has a measurement error of 1 % of the measured value according to the manufacturer but it also has to be considered that the measurement result can always be one count wrong, if the measurement is stopped just before or just after the counter counts the next Wh. This possible error is added to the manufacturer's accuracy. The error depends on the number of counts N_{count} , which also means that it gets more accurate the longer an operating point is measured.

$$\Delta N_{count} = \frac{1}{N_{count}} \cdot P_{el} \quad \text{Eq. 4-50}$$

The worst case is assumed, which means that this error sums up with the error of the accuracy class of the electric meter to

$$\Delta P_{el} = (\Delta N_{count} + \Delta P_{el,1\%}) \quad \text{Eq. 4-51}$$

whereby this error has to be transformed into a normally distributed error with equation 2-18.

Coefficient of Performance

Finally all individually calculated errors are used to determine the measurement error of the COP

$$COP = f(\dot{Q}_{w,cond}, \dot{Q}_{w,desup}, P_{el}) = \frac{\dot{Q}_{w,cond} + \dot{Q}_{w,desup}}{P_{el}} \quad \text{Eq. 4-52}$$

$$\Delta COP = \sqrt{\left(\frac{\partial COP}{\partial \dot{Q}_{w,cond}} \cdot \Delta \dot{Q}_{w,cond}\right)^2 + \left(\frac{\partial COP}{\partial \dot{Q}_{w,desup}} \cdot \Delta \dot{Q}_{w,desup}\right)^2 + \left(\frac{\partial COP}{\partial P_{el}} \cdot \Delta P_{el}\right)^2} \quad \text{Eq. 4-53}$$

with the derivatives

$$\frac{\partial COP}{\partial \dot{Q}_{w,cond}} = \frac{1}{P_{el}} \quad \text{Eq. 4-54}$$

$$\frac{\partial COP}{\partial \dot{Q}_{w,desup}} = \frac{1}{P_{el}} \quad \text{Eq. 4-55}$$

$$\frac{\partial COP}{\partial P_{el}} = -\frac{\dot{Q}_{w,cond} + \dot{Q}_{w,desup}}{P_{el}^2} \quad \text{Eq. 4-56}$$

Heating capacity Economiser

In addition to the COP the measurement error is also determined for the economiser load, which is calculated similarly to the heating capacities before.

$$\dot{Q}_{r,ECO,HP} = f(\dot{m}_{r,evap}, t_{r6}, t_{r5}) = \dot{m}_{r,evap} \cdot (h_{r,6} - h_{r,7}) \quad \text{Eq. 4-57}$$

$$\dot{Q}_{r,ECO,HP} = \sqrt{\left(\frac{\partial \dot{Q}_{r,ECO,HP}}{\partial \dot{m}_{r,evap}} \cdot \Delta \dot{m}_{r,evap}\right)^2 + \left(\frac{\Delta \dot{Q}_{r,ECO,HP}}{\Delta T_{r6,var}} \cdot \Delta T_{r6}\right)^2 + \left(\frac{\Delta \dot{Q}_{r,ECO,HP}}{\Delta T_{r7,var}} \cdot \Delta T_{r7}\right)^2} \quad \text{Eq. 4-58}$$

with the derivation

$$\frac{\Delta \dot{Q}_{r,ECO,HP}}{\Delta \dot{m}_{r,evap}} = (h_{r,6} - h_{r,7}) \quad \text{Eq. 4-59}$$

5 RESULTS AND DISCUSSION

This chapter consists of two main parts, the evaluation of the compressor performance and the evaluation of the heat pump cycle. The previous chapter defines how the different compressor efficiencies and the cycle efficiency are calculated. This chapter begins with the analysis of the compressor performance, which includes the compressor losses, the overall isentropic efficiency and the volumetric efficiency. Furthermore the influence of the ECO on the different efficiencies is discussed. The cycle performance is evaluated with the COP, whereby the influence of the desuperheater and the economiser on the cycle performance are also analysed. The measurement matrices for the compressor and cycle evaluation are documented in the Appendix A-4.

5.1 Analysis of the compressor

72 operating points were measured for the compressor performance map, which includes eight different speeds between 2100 and 5400 rpm, three different brine inlet temperatures in the evaporator, which are -10, 2 and 12 °C and three different water inlet temperatures in the condenser, which are 20, 30 and 50 °C. The measurement matrix for the analysis of the compressor can be seen in A-4.1. Special focus in the evaluation is on the overall isentropic and the volumetric efficiency, whereby the compressor losses are also discussed.

5.1.1 Compressor heat losses

The calculation of the compressor losses can be seen in chapter 4.1.1. The absolute losses vary between 44 and 290 W for the whole measurement matrix. Since the absolute losses depend on the power input of the compressor, only the relative compressor losses are evaluated, which are given in % of the compressor input power. Figure 5-1 shows the compressor losses depending on the pressure ratio for five different speeds.

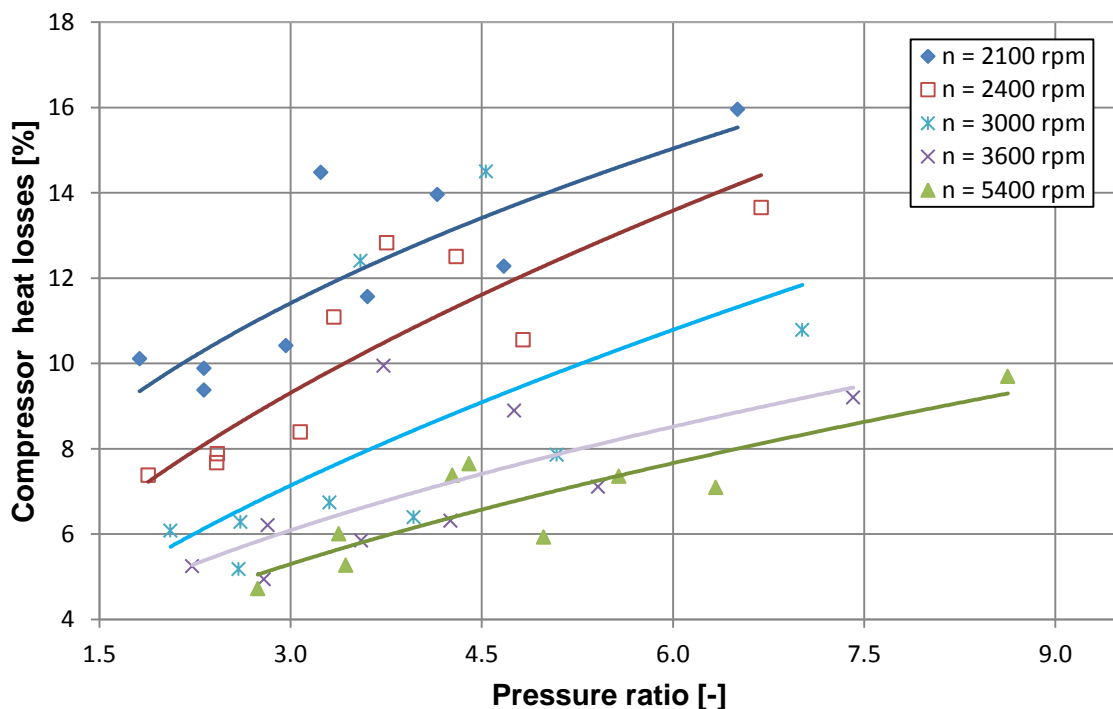


Figure 5-1: Compressor losses for different speeds depending on the pressure ratio

Potential best-fit curves are used to visualize the trend of the compressor losses. The relative compressor losses vary between 4 and 16% for the whole measurement matrix. Figure 5-1 shows that the relative heat losses decrease with a higher compressor speed. One cause is that the compressor emits a certain amount of heat for a certain compressor temperature. Referred to the compressor input power the losses are higher for a low compressor input power and therefore a low speed.

Furthermore the compressor losses include the inverter losses as well as the motor losses, because the power consumption can only be measured for the whole compressor system. The inverter losses can be partly determined by measuring the water inlet – and outlet temperature of the cooling. It results in average inverter losses of 36 W (varying between 17 and 93 W), which is an average percentage of 37 % of the total compressor losses. It shows also the trend that the relative inverter losses decrease with increasing speed. Because of the high water flow rate in the inverter cooling this measurement includes a high error, but it gives an approximate value for the inverter losses. Another cause for the decreasing compressor losses with higher speeds is that the BPM motor, which powers the compressor, has a better efficiency with higher speeds.

Figure 5-1 also shows that the relative heat losses increase with the pressure ratio. A higher pressure ratio implies a higher outlet temperature of the refrigerant from the compressor, which leads to higher heat losses. Figure 5-2 proves this by showing a similar trend of the compressor losses as a function of the compressor outlet temperature.

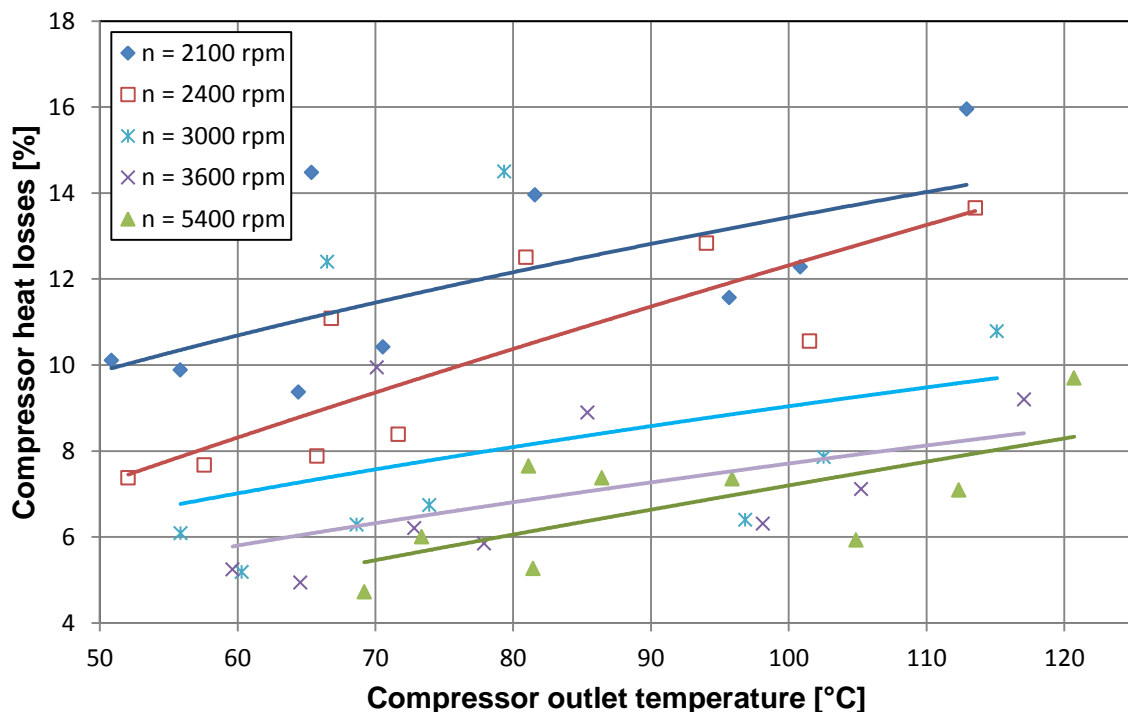


Figure 5-2: Compressor losses for different speeds depending on the compressor outlet temperature

Both figures show some points with far higher losses compared to the best fit curve. For all compressor speeds these are the points with the lowest brine inlet temperature of -10 °C to the

evaporator and with that a low evaporation temperature. Two operating points with 3000 rpm differ from the trend of the others, which cannot be explained without further measurements.

5.1.2 Overall isentropic efficiency

This chapter shows and discusses the overall isentropic efficiency of the compressor in the measured compressor performance map. The evaluation of the overall isentropic efficiency is described in chapter 4.1. Figure 5-3 shows the measured points for five different speeds as a function of the pressure ratio as well as the linear trends.

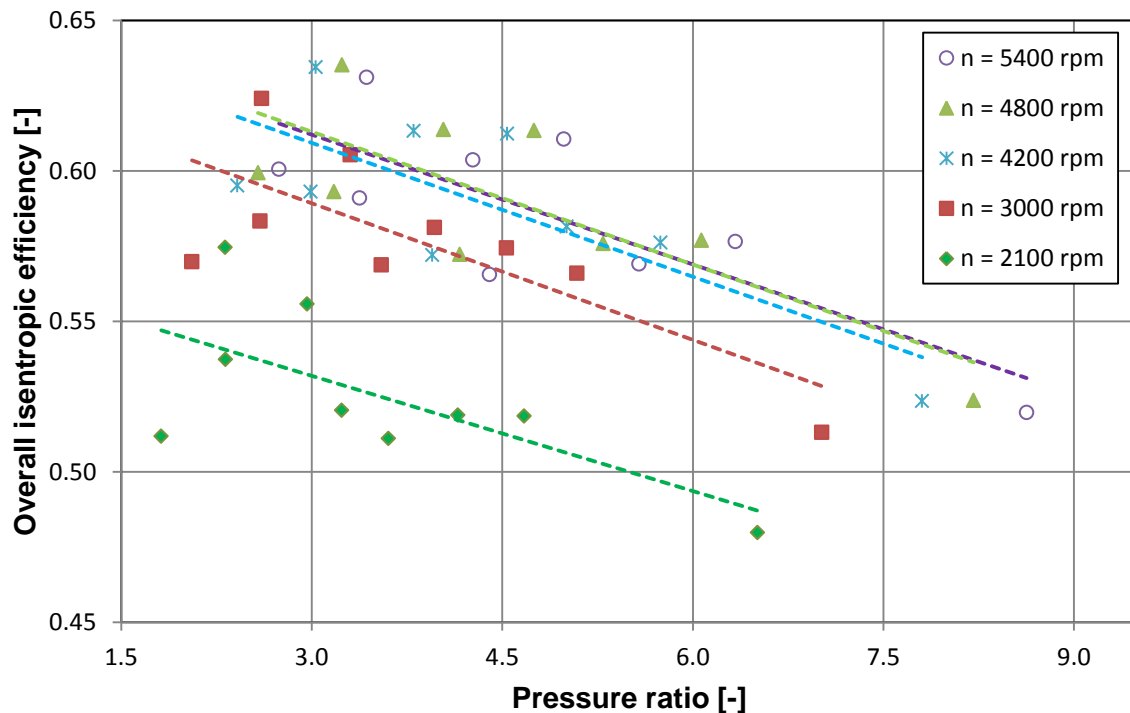


Figure 5-3: Overall isentropic efficiency as a function of the pressure ratio for different compressor speeds

The overall isentropic efficiency varies between 0.48 and 0.64 for the whole performance map. The highest efficiency is reached for a point with a pressure ratio of 3.24 and a speed of 4800 rpm, the lowest efficiency occurs for a measurement point with a pressure ratio of 6.51 and a speed of 2100 rpm. Although the overall trend shows that the isentropic efficiency decreases with the pressure ratio, the highest efficiency is not reached for the lowest pressure ratio. For all four different speeds the highest overall isentropic efficiency is reached for a point with a pressure ratio between 2.32 and 3.43. Apart from that the figure also shows points with the same pressure ratio and much lower overall isentropic efficiency which leads to the assumption that the efficiency does not only depend on the pressure ratio. It also depends on the condensing and evaporation temperature. One more aspect, which can be seen in Figure 5-3, is that the overall isentropic efficiency increases with the compressor speed. The difference between 2100 and 3000 rpm is in average about 0.05. With further increase of the speed the increase in overall isentropic efficiency decreases. The two speeds 4800 and 5400 rpm show nearly the same linear trend line, which means that there is no increase of the isentropic efficiency any more.

Figure 5-4 shows the overall isentropic efficiency for three different operating points with different evaporation- and condensation temperatures with eight different speeds each. The first number in the legend indicates the brine inlet temperature to the evaporator and the second number the water inlet temperature to the condenser. It is obvious that the overall isentropic efficiency rises with the compressor speed and has its minimum at the lowest compressor speed and its optimum between 3500 and 5000 rpm. Again the point with the lowest pressure ratio (12/20) does not have the highest isentropic efficiency, if it is compared to the point with the higher pressure ratio (2/30).

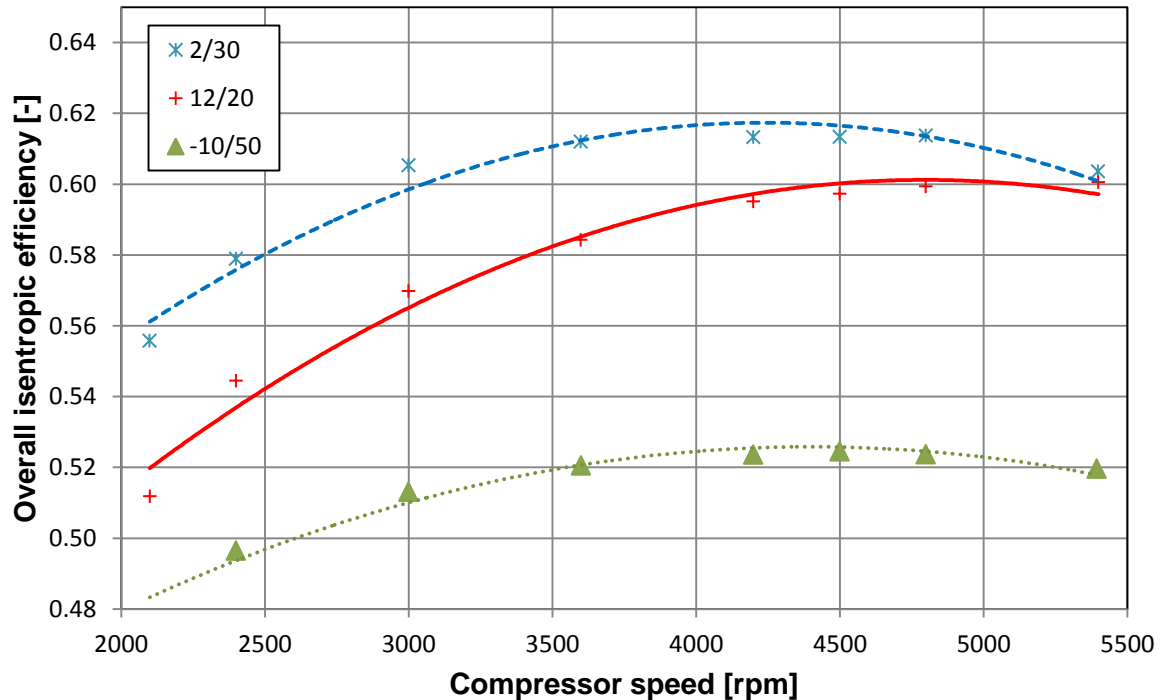


Figure 5-4: Overall isentropic efficiency for different speeds and three different operating points

Figure 5-5 shows all measured points in one diagram. Each line shows an operating point with the same brine inlet temperature of the evaporator and the same water inlet temperature in the condenser. The different points of each line correspond to eight different speeds. Because of the higher temperature differences in the heat exchangers for higher compressor speeds and therefore higher heating capacity, the pressure ratio rises with the compressor speed. Third order polynomial best fit curves are used to show the trend. It can be seen again that for each point the overall isentropic efficiency rises with the compressor speed, which was already discussed before. For a water inlet temperature of 50 °C (full line) the efficiency rises with higher evaporation temperature which also means lower pressure ratio. The same can be said for the water inlet temperature of 30 °C and 20 °C whereby this effect is much lower with lower condensing temperatures. The compressor shows the best performance with 12 °C brine inlet temperature in the evaporator and 30 °C water inlet temperature in the condenser. This corresponds to an evaporation temperature between -0.85 and 6.05 °C and a condensation temperature between 36.81 and 44.10 °C for all speeds.

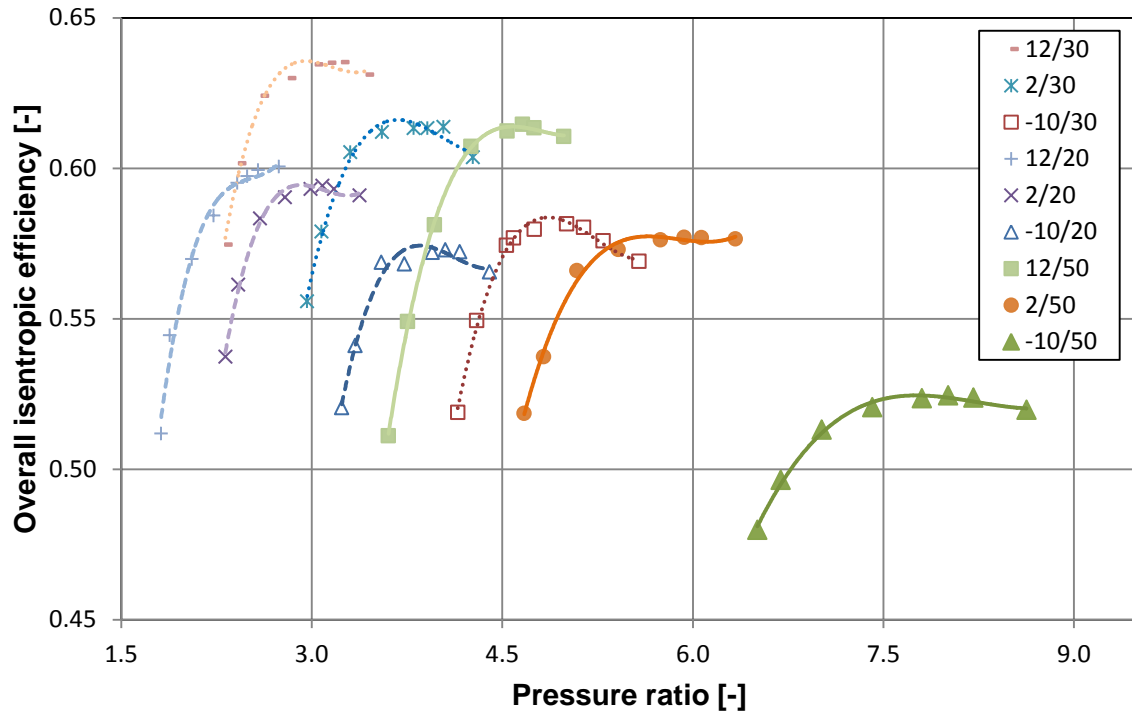


Figure 5-5: Overall isentropic efficiency for the whole compressor performance map

5.1.3 Volumetric efficiency

The volumetric efficiency varies between 0.77 and 0.93 for the whole compressor performance map, whereby the lowest efficiency occurs for a pressure ratio of 6.51 and a speed of 2100 rpm and the highest efficiency for a pressure ratio of 2.06 and a speed of 3000 rpm. Figure 5-6 shows the volumetric efficiency as a function of the pressure ratio for five different speeds.

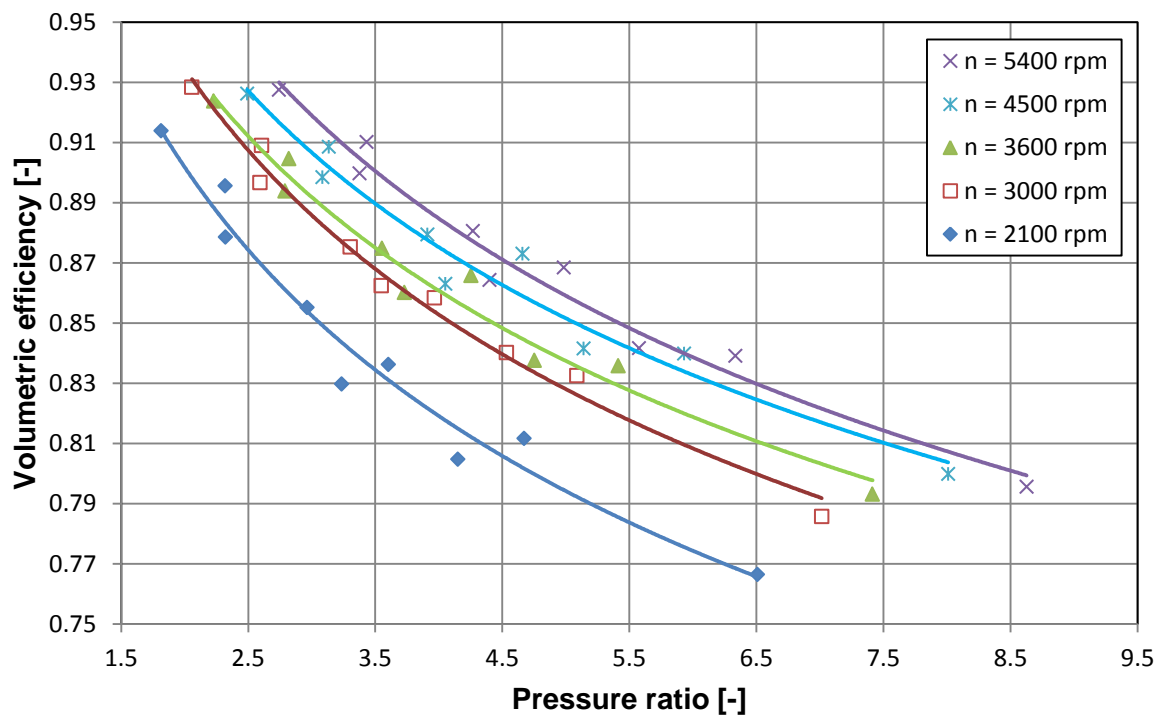


Figure 5-6: Volumetric efficiency for different compressor speeds

Potential best fit curves are used to show the trend. Compared to the overall isentropic efficiency the volumetric efficiency mainly depends on the pressure ratio and not significantly on the evaporation and condensation temperature. The volumetric efficiency decreases with increasing pressure ratio and is influenced by the compressor speed. With higher compressor speed the volumetric efficiency increases.

This can also be seen in Figure 5-7, which shows the volumetric efficiency as a function of the compressor speed for three different operating points, whereby 12/20 refers again to a brine inlet temperature to the evaporator of 12 °C and a water inlet temperature to the condenser of 20 °C. Compared to Figure 5-4, which shows that the operating point with the smallest pressure ratio (12/20) does not have the highest isentropic efficiency, Figure 5-7 states the different for the volumetric efficiency. The point with the smallest pressure ratio also has the highest volumetric efficiency.

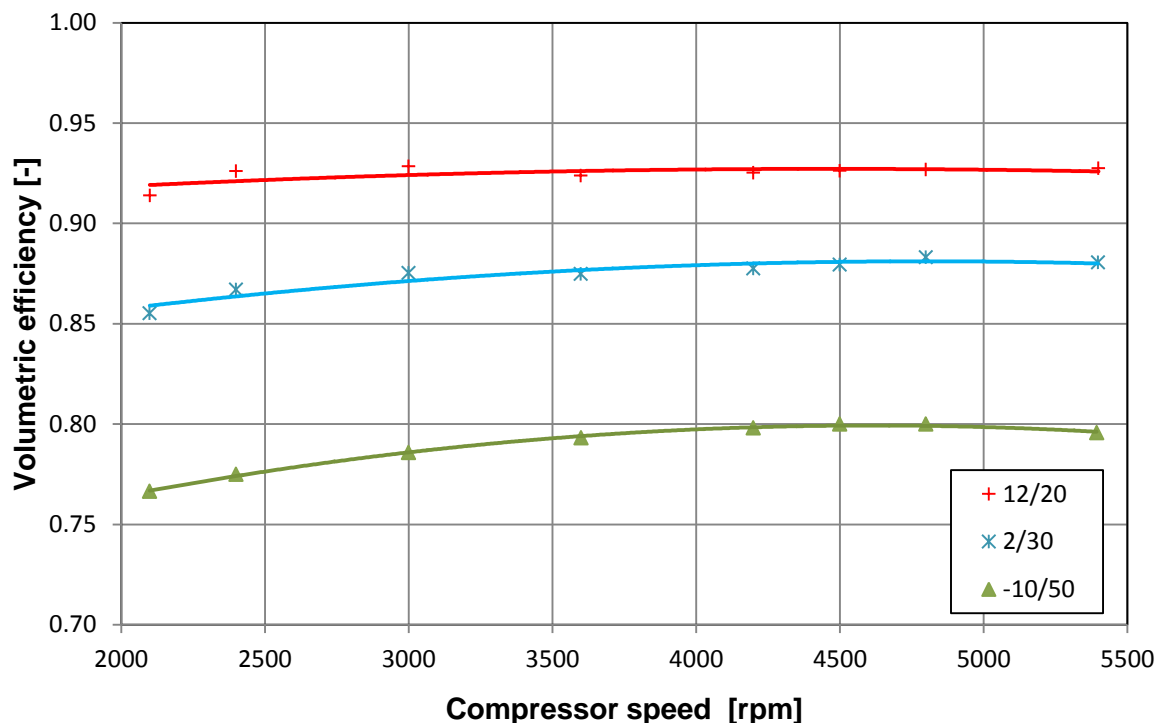


Figure 5-7: Volumetric efficiency for different operating points and pressure ratios

The volumetric efficiency rises with the compressor speed, whereby this trend is more pronounced for the high pressure ratio (-10/50). One cause is that for the point 12/20 the pressure ratio increases more with higher speeds because of the higher heating capacity transferred at the heat exchangers.

Figure 5-8 shows all operating points of the performance map, whereby each line consists again of the eight different speeds from 2100 to 5400 rpm. It shows the already discussed results that the compressor always has the lowest volumetric efficiency at the lowest speed. The volumetric efficiency rises with the compressor speed up to 3000 rpm. For higher speeds the general trend is that the volumetric efficiency still rises but it depends on the operating point. For high pressure ratios (operating point -10/50) the trend continuous up to 4800 rpm, for small pressure ratios (Operating point 12/20) the volumetric efficiency decreases from 3000 to 3600 rpm and

then rises again. In general the points with the lowest pressure ratio show the best performance.

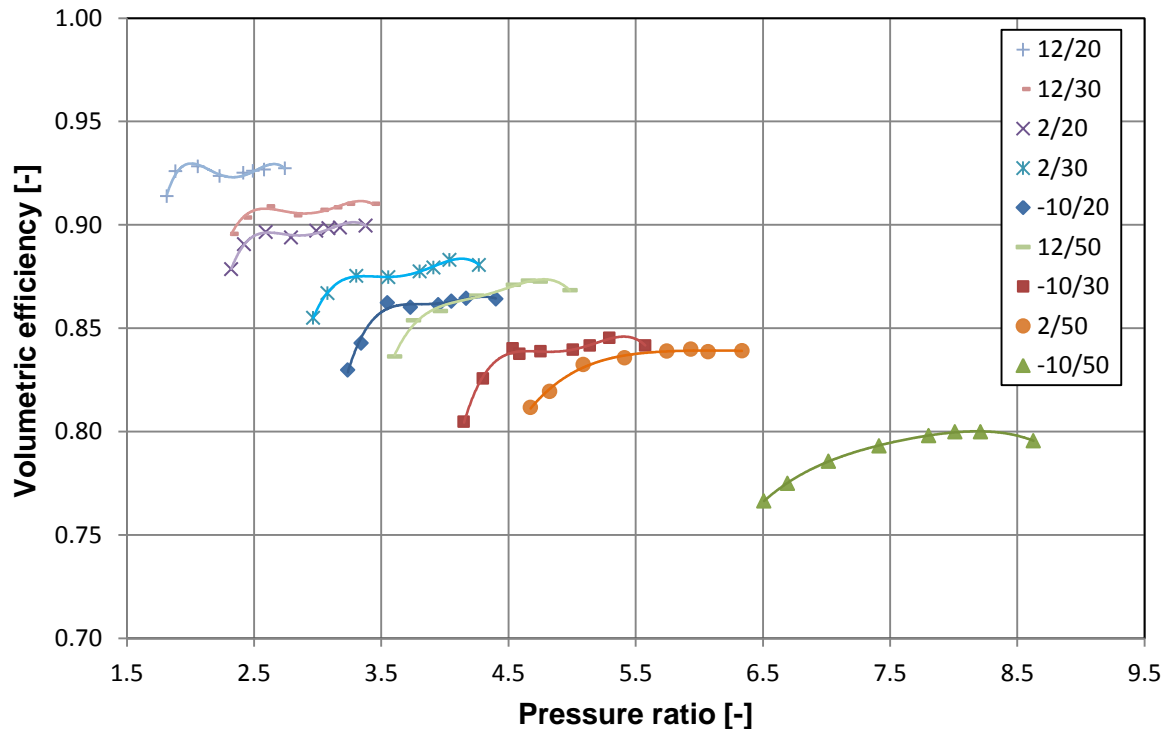


Figure 5-8: Volumetric efficiency for different operating points with different speeds

5.1.4 Influence of the vapour injection on the different efficiencies

For the measurement of the compressor performance map only operating points with ECO were recorded. For the evaluation of the cycle performance operating points with (w)- and without (wo) ECO were measured. To get an impression of the influence of the vapour injection on the compressor efficiencies the measured points for the evaluation of the cycle are used to determine the influence of the ECO on the before discussed compressor losses, the isentropic- and the volumetric efficiency. The compared points have the same brine inlet temperature to the evaporator and the same water inlet temperature to the condenser. Altogether 18 operating points are compared in this chapter with four different speeds from 1800 to 5400 rpm, two brine inlet temperature of -15 and 2 °C and water inlet temperatures between 20 and 50 °C.

It has to be mentioned that this comparison shows the influence of the ECO in this system. The injection expansion valve was closed manually to disable the ECO. A compressor without vapour injection may perform better since it does not have the injection port in the compressor at all.

Compressor losses w/wo ECO

Figure 5-9 shows the compressor losses for three different speeds as a function of the pressure ratio with- and without ECO. Potential best fit curves are used to visualize the trend. For all three compressor speeds a similar trend can be seen, which is a higher compressor loss without ECO compared to the measured points with ECO. For 3000 rpm the difference in the

compressor losses increases with the pressure ratio, for the two other speeds the difference stays approximately the same.

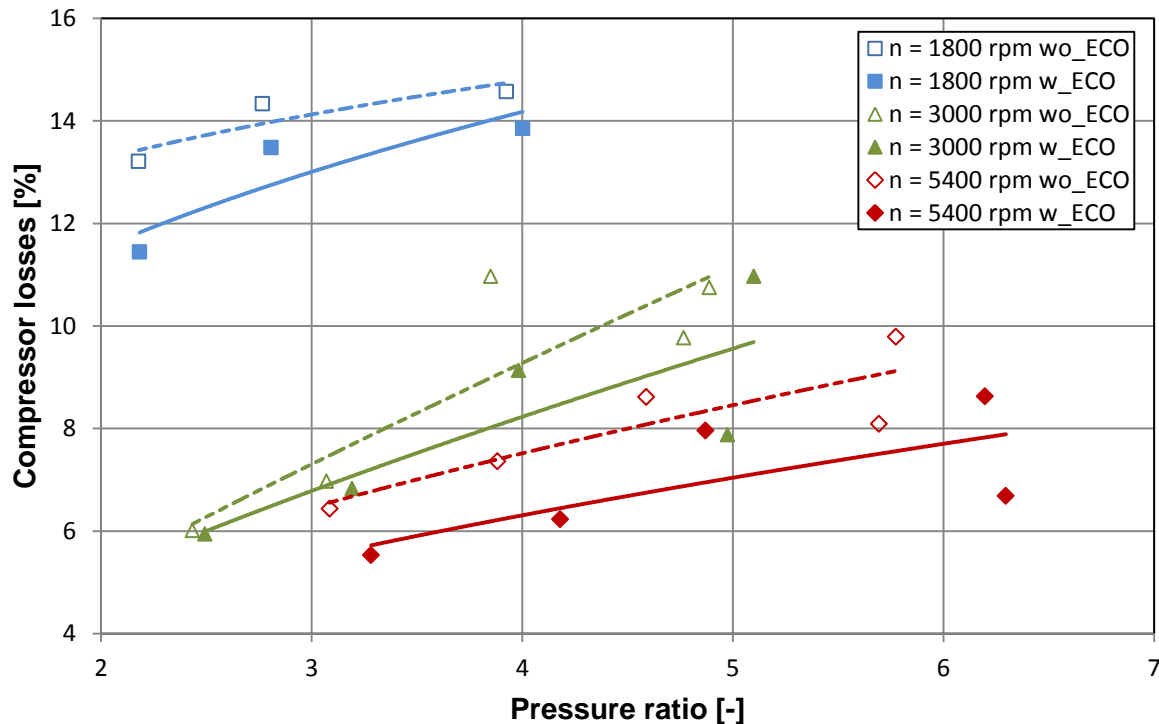


Figure 5-9: Comparison of the compressor losses as a function of the pressure ratio for three different speeds

One cause for the slightly increased compressor losses without ECO is the higher compressor outlet temperature, which can be seen in Figure 5-10. It is shown as a function of the pressure ratio for three different speeds with a brine inlet temperature to the evaporator of 2 °C. The compressor outlet temperature is far higher without ECO because there is no backcooling with injected vapour at the medium pressure level of the compressor. The temperature difference at the compressor outlet, for an operating point with- and without ECO, increases with the pressure ratio. This is because of the higher mass flow over the injection port with a higher pressure ratio, which can be seen in Figure 5-11.

It shows the mass flow over the evaporator and over the condenser for two compressor speeds for different pressure ratios with potential best fit curves. The points differ significantly because the mass flow also depends on the operating point (evaporation and condensation temperature). The injection mass flow is the difference of the condenser- and the evaporator mass flow. It increases with the pressure ratio, which reduces the compressor outlet temperature with ECO compared to the system without. Lower evaporation temperatures include a lower mass flow and with that lower cooling. Although the vapour injection at the medium pressure level, for a compressor with vapour injection, increases the mass flow over the compressor, the overall mass flow at the outlet of the compressor still decreases with the pressure ratio.

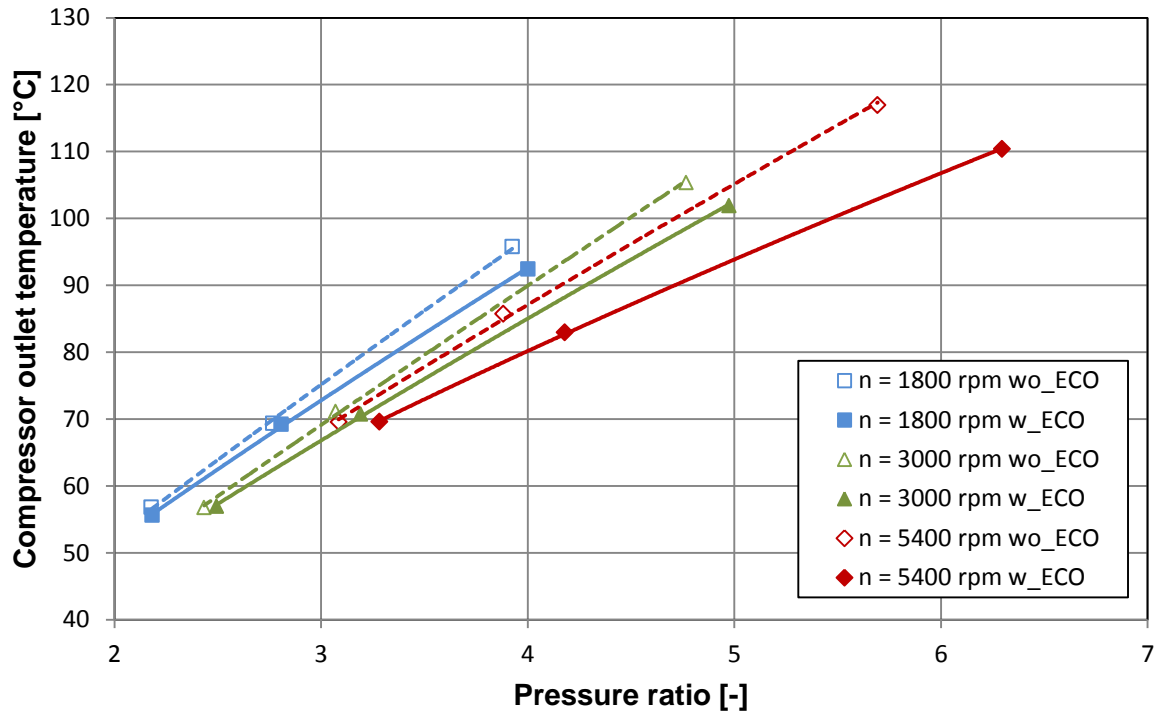


Figure 5-10: Compressor outlet temperature as a function of the pressure ratio for three different speeds with a brine inlet temperature in the evaporator of 2 °C

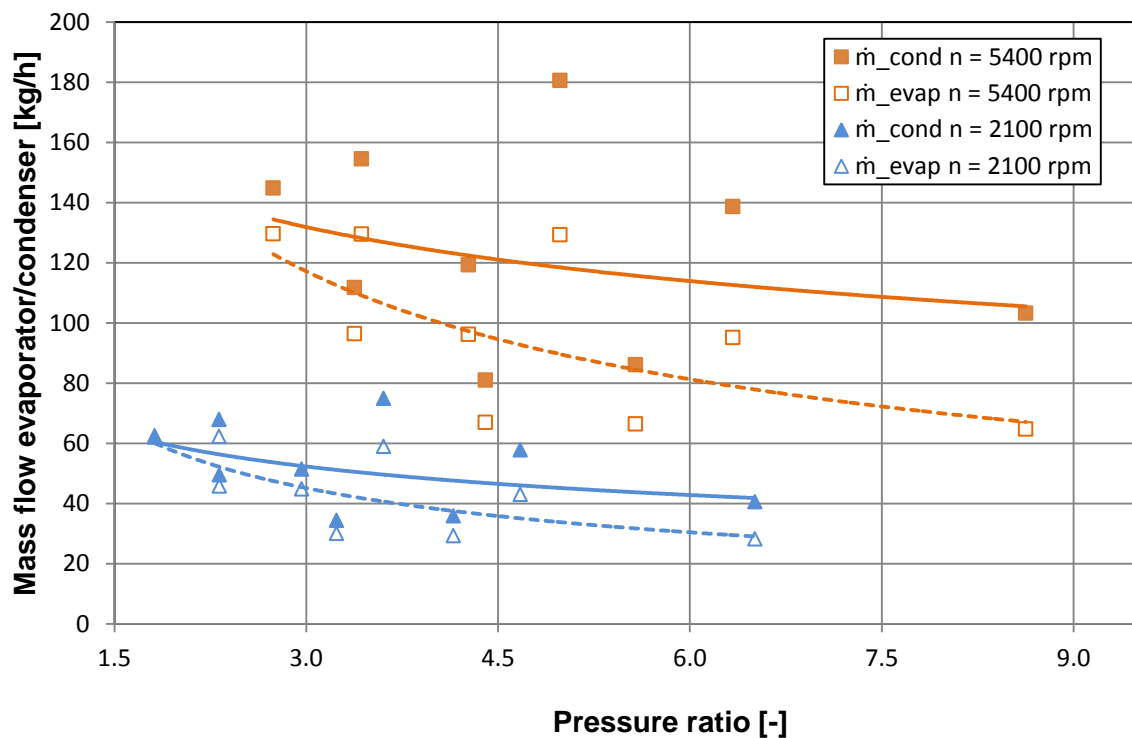


Figure 5-11: Mass flow as a function of the pressure ratio for two different compressor speeds

Furthermore Figure 5-10 shows that the outlet temperature of the compressor increases with decreasing compressor speed for the same pressure ratio. This also depends on the lower mass flow with lower compressor speeds.

For all 18 compared operating points the compressor losses increase by 0.77 % on average, from 8.24 to 9.01 %.

Overall isentropic efficiency w/wo ECO

Figure 5-12 shows the overall isentropic efficiency for different speeds and different operating points with- and without ECO. After the evaluation of the compressor losses without ECO, the isentropic efficiency shows the expected trend, which is a lower efficiency without ECO for nearly all compared points. The highest difference is measured for the operating point -15/30, which shows an about 0.05 lower isentropic efficiency for the three compared points on average. Furthermore all operating points show the trend that the difference in the isentropic efficiency with- and without ECO rises with the compressor speed. This is a result of the increasing influence of the ECO with increasing pressure ratio caused by the increasing capacities in the HX with higher compressor speeds.

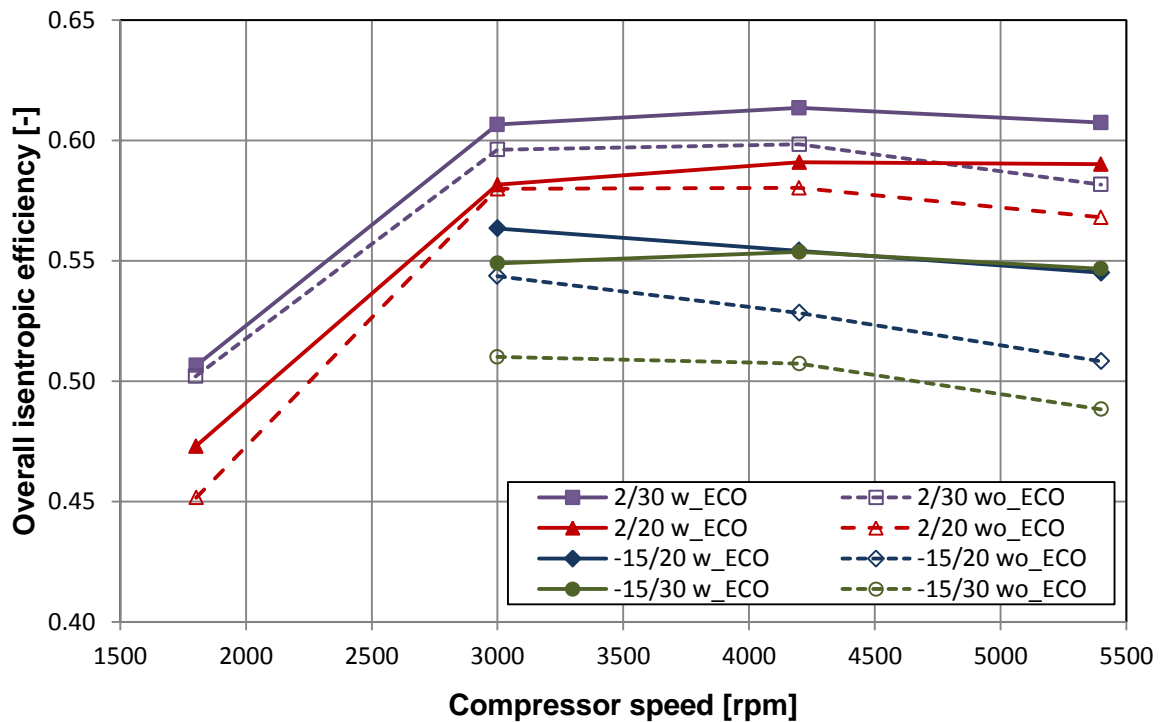


Figure 5-12: Isentropic efficiency for different operating points and different speeds with- and without ECO

The comparison of the overall isentropic efficiency for two different compressor speeds with- and without ECO as a function of the pressure ratio is shown in Figure 5-13. It shows the discussed trend that with increasing pressure ratio the difference in the overall isentropic efficiency with- and without ECO increases.

If all 18 operating points are compared, the overall isentropic efficiency decreases by 0.024 on average without ECO. This is a decrease of 4.3% if it is based on the average isentropic efficiency with ECO of 0.558.

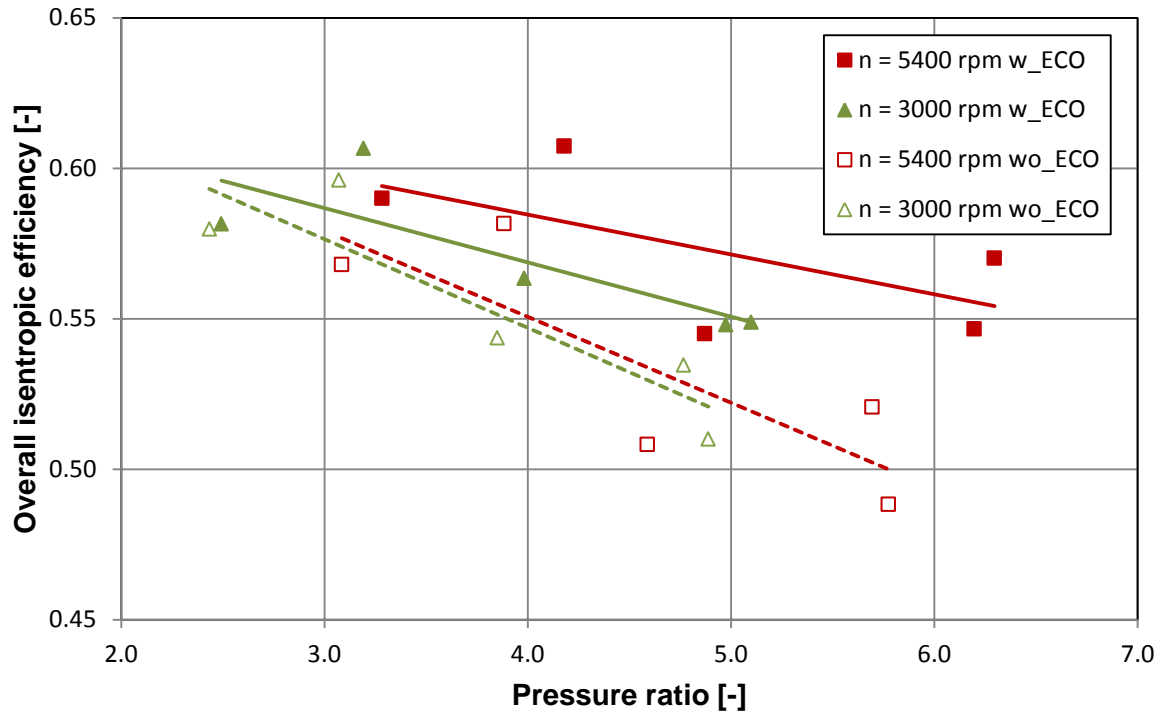


Figure 5-13: Overall isentropic efficiency as a function of the pressure ratio for different speeds with- and without ECO

Volumetric efficiency w/wo ECO

Figure 5-14 shows the volumetric efficiency for different pressure ratios and therefore different operating points with- and without ECO. Potential best fit curves are used to show the trend, same as for the evaluation of the volumetric efficiency in the previous chapter. Other than for the overall isentropic efficiency, the volumetric efficiency is higher without ECO for most of the operating points. For all speeds the best fit curve for the volumetric efficiency without ECO is higher than the trend line with ECO, except for the speed of 1800 rpm, where the volumetric efficiency for the operating point with the highest pressure ratio has a lower volumetric efficiency without ECO than with.

If all 18 operating points are compared, the average increase of the volumetric efficiency without ECO is 0.009, which is an increase of 1.1 % if it is compared to the average volumetric efficiency with ECO of 0.858.

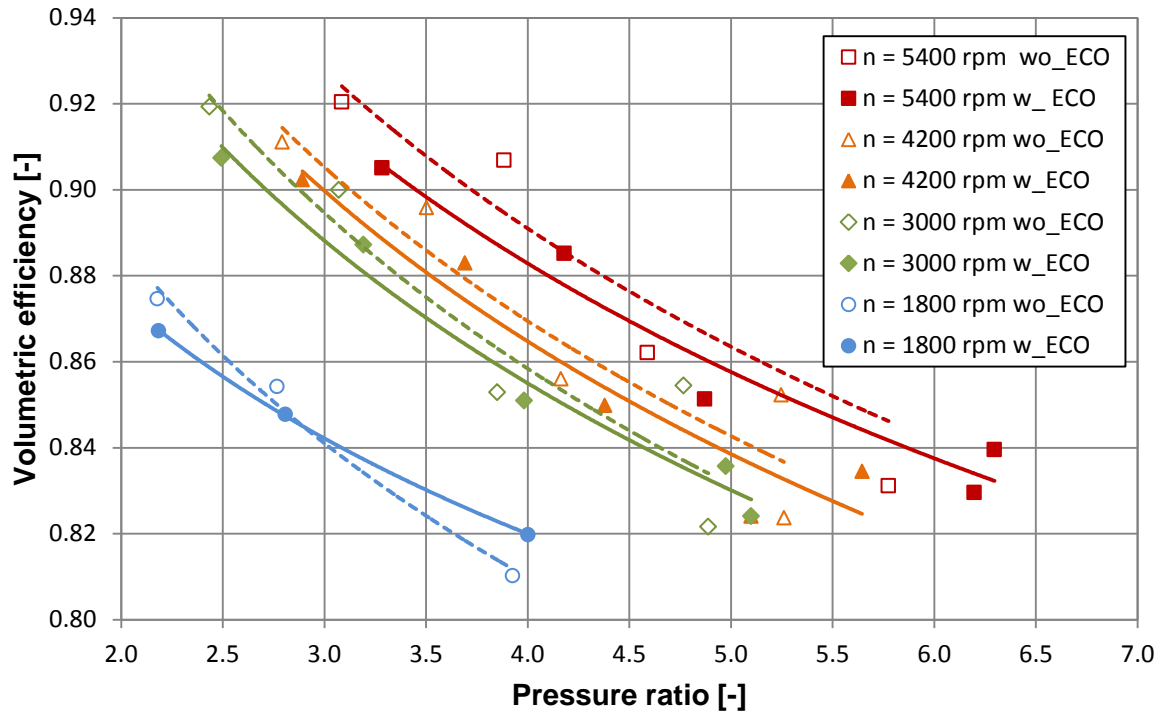


Figure 5-14: Volumetric efficiency for different compressor speeds and different pressure ratios with- and without ECO

5.2 Analysis of the heat pump cycle

For the evaluation of the cycle mainly the COP is used, with the definition of chapter 2.1.3 and 4.2. The cycle performance depends on the evaporation and condensation temperature, which also means the pressure ratio. Appendix A-4.2 shows the measurement matrix, which was recorded for the evaluation of the heat pump cycle. After the compressor performance map was measured different adjustments were made to improve the cycle performance. These improvements and their impact on the COP are described in chapter 5.2.1. The following chapter 5.2.2 deals with the evaluation of the cycle itself after the cycle optimization. Then the main innovations of this heat pump cycle, the economiser and the desuperheater and their impact on the cycle performance, are analysed in detail. The results of the error calculation verify the validity of the outcomes.

5.2.1 Improvements on the cycle performance

After the measurement of the compressor performance map, which was also used to get a first impression of the cycle performance, efforts were taken to improve the COP. As described in chapter 2.1.3, the evaporation and the condensing temperature are important for the cycle performance. If it is assumed that an operating point is given by a fixed water inlet temperature (condenser, return of the floor heating system) and a fixed inlet temperature to the evaporator (outside temperature for an air heat pump or brine temperature for a ground source heat pump with brine collector) the goal of the heat pump process is to work at this point with the minimum pressure ratio possible, which means that the evaporation temperature should be as high and the condensation temperature as low as possible. Figure 5-15 shows the heat pump cycle in the temperature-enthalpy diagram for the design point of the heat exchangers, which is $-10\text{ }^{\circ}\text{C}$ brine inlet temperature in the evaporator and $30\text{ }^{\circ}\text{C}$ water inlet temperature in the condenser.

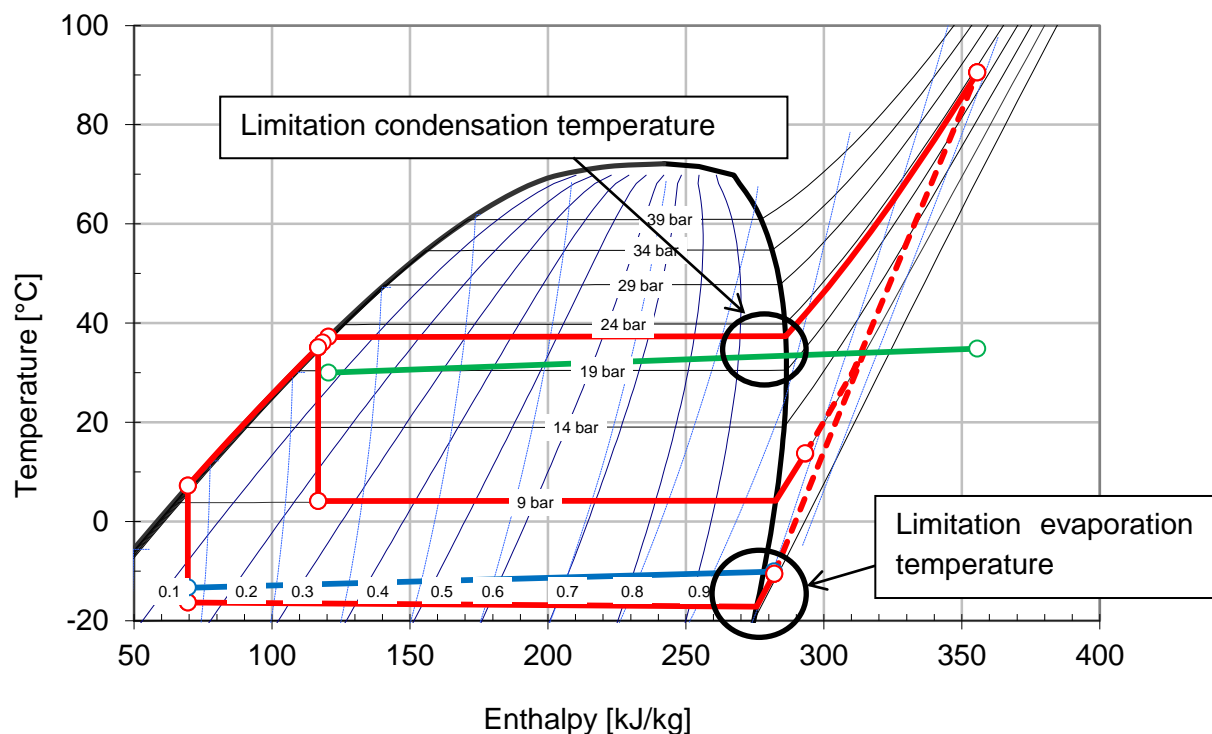


Figure 5-15: HP process in the temperature-enthalpy diagram for an operating point with $-10\text{ }^{\circ}\text{C}$ brine inlet- and $30\text{ }^{\circ}\text{C}$ water inlet temperature

Condensation temperature

For the condensation pressure the limitation is the temperature pinch point between the condensation temperature of the refrigerant and the water temperature. It is the minimum temperature difference between two fluids in a heat exchanger. In chapter 4.3 an UA calculation for the condenser and the evaporator is shown. A higher UA means that more capacity can be transferred per K temperature difference. As result of the dimensioning a heat exchanger with an UA of 1.095 kW/K was chosen (SWEF, 2013). After the first measurements showed a higher pinch point than expected, the already mentioned UA calculation was made, which only resulted in an UA value of about 0.7 kW/K, compared to the manufacture data (dimensioning point 5 kW heating capacity with water inlet temperature of 30 °C and condensation temperature of 40 °C). After the used condenser could not reach the expected values a condenser with 40 instead of 30 plates (pl.) was mounted, which increased the UA according to Figure 5-16 (second order polynomial best fit curves).

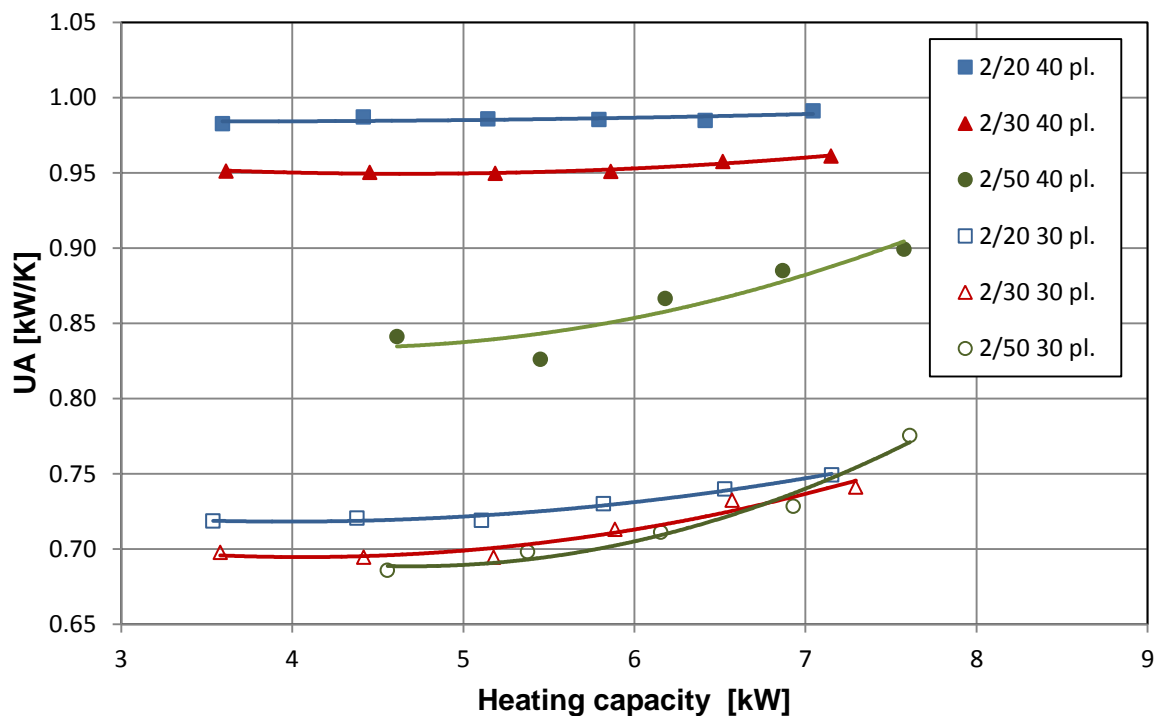


Figure 5-16: UA for three different operating points with different speeds and therefore heating capacity for the condenser HX with 40 plates and 30 plates

If it is referred to the condenser HX after the modifications with 40 plates the HX area increased by 25 %. The average increase in the UA for the operating point 2/20 was 27.5 % and 25.8 % for the operating point 2/30. This means that the UA increased nearly according to the increase in HX area and therefore the U value stayed approximately constant. For the operating point 2/50 the UA only increased by 15.4 % which means that the U value decreased. One cause for this is the different desuperheating and condensing area in the HX for different operating points. With the higher pressure ratio the desuperheating area increases, which influences the UA positive for the smaller heat exchanger compared to larger one. This includes a higher temperature difference between desuperheated refrigerant and water in the HX for a larger desuperheating area and contributes a larger part to the transferred capacity. The high enthalpy

difference of the desuperheating compared to the condensing for the operating point 2/50 can also be seen in Figure 5-32.

With the new heat exchanger the temperature difference between the condensation temperature and the water temperature (pinch point), which is indicated in Figure 5-15, is reduced. In Figure 5-17 the ΔT in the pinch point for the 30 and 40 plates HX is compared, whereby the absolute reduction of the pinch point for the same operating points with the different heat exchangers can be seen. The ΔT is reduced between 29 and 39 % for the compared operating points, if the two linear best fit curves are compared with the ΔT of the 30 plate HX as base. Since the operating points with the 30 plate HX show a high dependency on the operating point they are split up. The points with high pressure ratio (2/50) show a smaller pinch point with the 30 plate HX than the other operating points. For the 40 plate HX no significant dependency on the operating point can be seen, the ΔT in the pinch point rises almost linearly with the heating capacity.

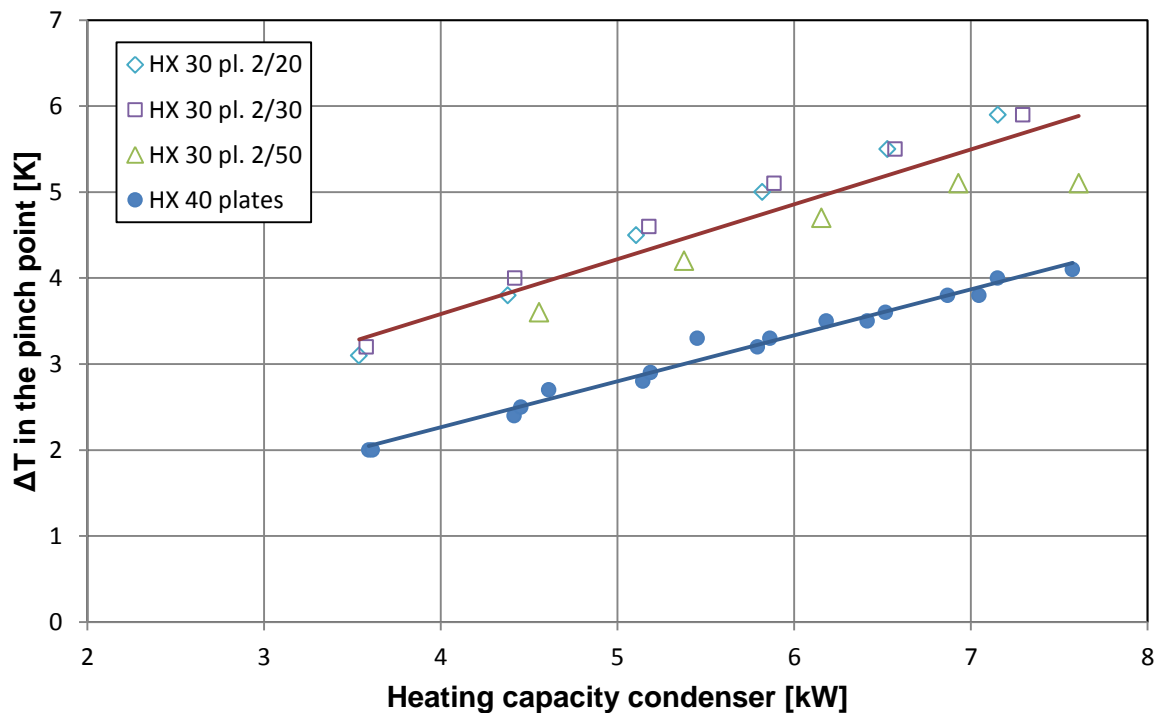


Figure 5-17: Reduction of the ΔT in the pinch point between condensation temperature and water temperature

The reduction of the ΔT in the pinch point results in a reduction of the condensation temperature by 0.6 to 2.1 K, depending on the operating point. This is shown in Figure 5-18. The reduction in the condensing temperature is lower for points with a higher pressure ratio and therefore with higher condensation temperature (0.6 to 1.1 K). The operating points with 20 and 30 °C water inlet temperature to the condenser show nearly the same values. This could already be expected after the evaluation of the reduction of the ΔT in the pinch point, which is shown in Figure 5-17. This can be explained by the smaller gain in the UA for high pressure ratios as discussed before.

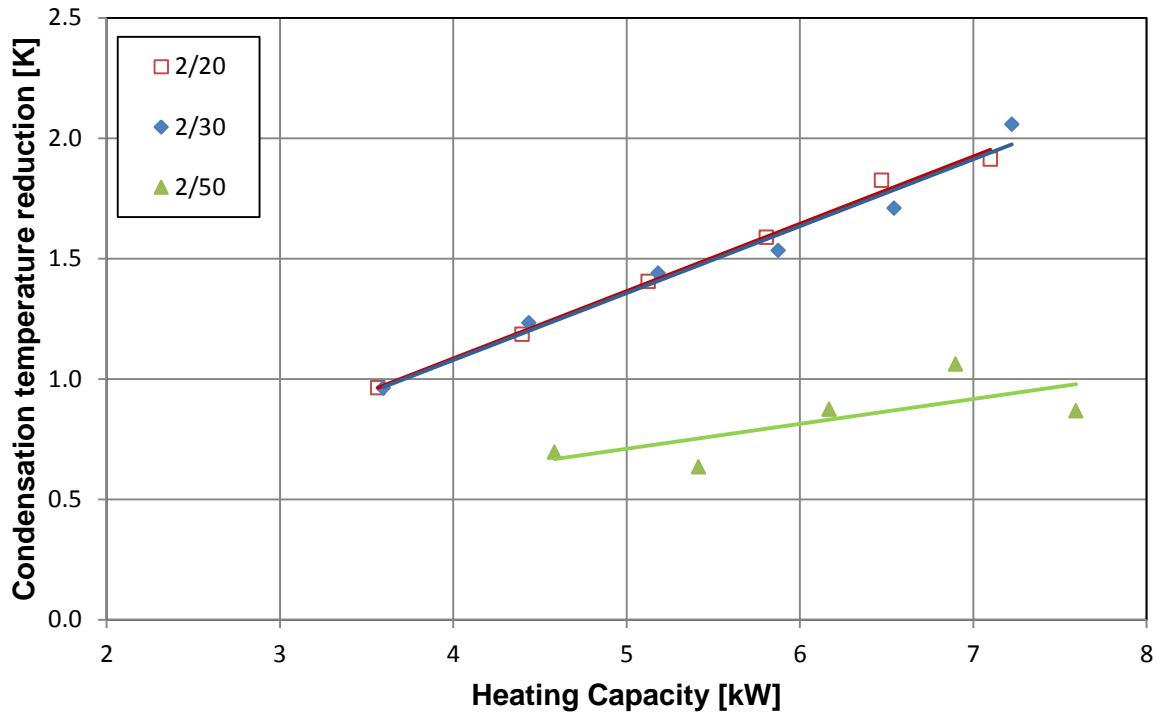


Figure 5-18: Condensation temperature reduction after condenser change

Evaporation temperature

The second possibility after the reduction of the condensation temperature is the increase of the evaporation temperature to reduce the pressure ratio. Compared to the condensation temperature there are two causes, which can limit the evaporation temperature. Figure 5-19 shows the same operating point with two different compressor speeds and thus two different evaporation capacities.

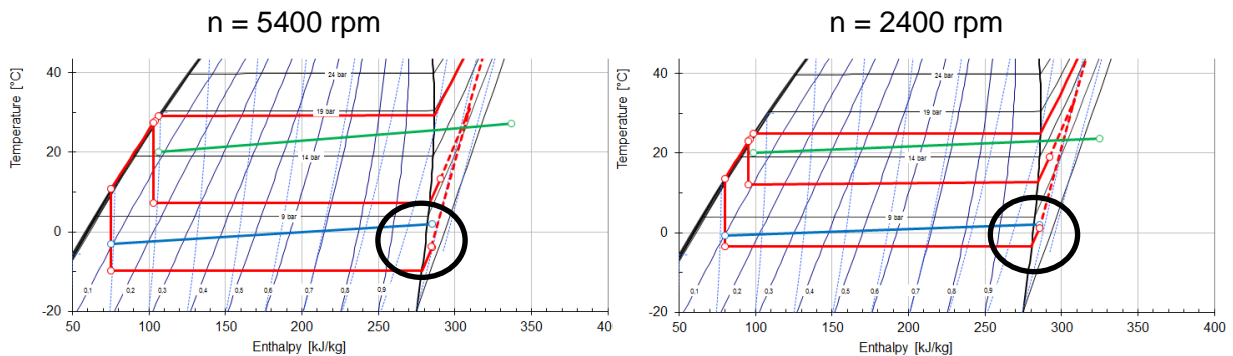


Figure 5-19: Comparison of the evaporation process for two different operating points

The operating point, which is compared in Figure 5-19, has a brine inlet temperature of 2 °C to the evaporator and a water inlet temperature of 20 °C to the condenser. The temperature-enthalpy diagram on the left side shows this operating point with a compressor speed of 5400 rpm and with that a cooling capacity of 5.5 kW, the temperature-enthalpy diagram on the right side with a compressor speed of 2400 rpm and with that a cooling capacity of 3 kW. For the lower cooling capacity the brine inlet temperature matches the superheated temperature of the refrigerant at the evaporator outlet. The superheating is the limiting factor for the evaporation

temperature. If the superheating can be reduced, the evaporation temperature increases and thus the COP. In the operating point with the higher heating capacity on the left side the superheating is not the limiting factor, because the temperature difference needed for the heat transfer is much higher than the superheating. The inlet temperature of the brine is higher than the temperature of the refrigerant at the evaporator outlet. In this case the performance can be improved by the same means as the reduction of the condensation temperature, which is a larger heat exchanger with a better UA. It has to be mentioned that the evaporator is dimensioned for a cooling capacity of 3.5 kW and that therefore the temperature-enthalpy diagram on the left side of Figure 5-19 shows a point, which does not correspond to the dimensioning of the heat pump cycle.

To increase the evaporation temperature, the first attempt was to reduce the superheat compared to the earlier measurement of the compressor performance map. This was done by using new parameters for the controlling of the expansion valve instead of the control system used before, which was provided by the manufacturer of the compressor. The result was a slight reduction of the superheating as well as a much more stable outlet temperature of the evaporator. A new software by the compressor manufacturer should improve the controlling of the expansion valves but this update was not delivered before this thesis was finished.

The second change on the evaporator side was the replacement of the distribution pipe at the evaporator inlet, which caused a high pressure drop, with a pipe with three boreholes instead of one for each refrigerant plate. This was already described in chapter 3.1.2. The pressure drop of the distribution pipe was removed almost completely but it had also an unexpected influence on the heat transfer capability of the evaporator. The results of these modifications on the low pressure side of the heat pump can be seen in Figure 5-20.

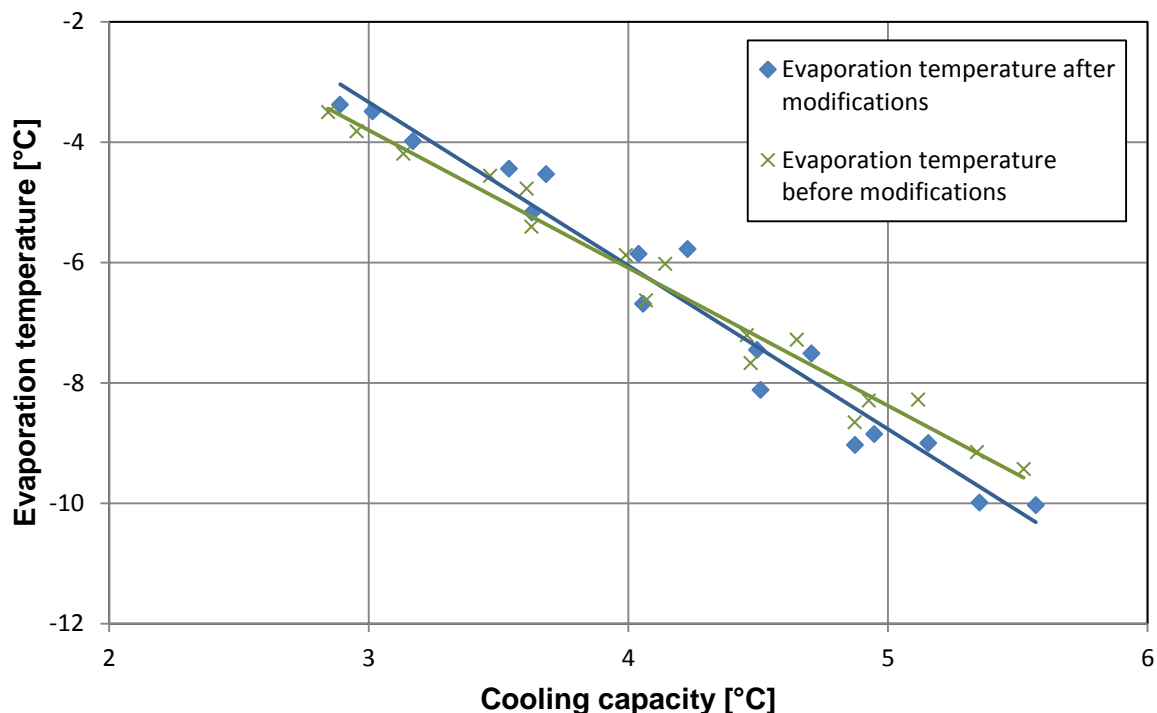


Figure 5-20: Change in the evaporation temperature after modifications

This figure shows the evaporation temperature of operating points with a brine inlet temperature to the evaporator of 2 °C for different compressor speeds and pressure ratios, whereby the same points were measured before and after the above described modifications. It shows that the modifications did not achieve the expected results. The reduction of the superheat increased the evaporation temperature for measured points with a low cooling capacity. As it can be seen in Figure 5-19 it only increased the evaporation temperature for points where the superheat is the limiting factor. The biggest improvement in the compared points is an increase of the evaporation temperature of 0.33 K. For the compared linear trend lines the evaporation temperature increases for operating points with less than 4 kW cooling capacity.

For operating points with a high cooling capacity the evaporation temperature decreased, which means that the change to a distribution pipe with more boreholes, and with that less pressure drop, did reduce the performance of the heat exchanger. The influence of the distribution pipe on the heat exchanger performance can still not be determined with certainty, because other causes could influence the cycle performance, for example that some plates got congested during the different modifications on the working fluid cycle. Up to now the assumption is that a distribution pipe with one borehole for every refrigerant channel of the HX, whereby the summed up area of all boreholes equals the area of the inlet pipe, shows the best performance of the evaporator, although it causes some pressure loss compared to a pipe with more boreholes.

If the results of the change of the distribution pipe and the reduction of the superheating are summed up it can be said that the cycle is improved for working points with less than 4 kW cooling capacity, whereby the cycle is dimensioned for 3.5 kW. If the cycle should be improved for higher capacities, test runs with different versions of the distribution pipe would have to be made to determine the impact of the distribution pipe with certainty. Another way to increase the evaporation temperature would be to use a larger heat exchanger similar to the condenser.

Coefficient of Performance

It has to be mentioned that after the measurement of the compressor performance map, the control board for the expansion valves and the drive (SEC board) was added to the electricity meter for the measurement of the compressor input power. The power needed by the control board alone was never measured separately during the operation of the heat pump, but it can be assumed that the gained improvements on the COP are higher than stated in the following description. A measurement of the input power with the compressor turned off resulted in a power input of 13.5 W with SEC board. If this power input would be added to the measurement of the compressor performance map, the increase in the COP would have been higher than stated on the next pages. 13.5 W less power input would increase the COP for another 0.4 to 2.7 % depending on the operating point and therefore compressor input power. The maximum power needed by the SEC board is stated with 20 VA by the compressor manufacturer (Copeland, 2013d). Since it cannot be ensured that the board needs the same amount of energy during operation, the evaluation of the improvements is made without considering the power input of the SEC board.

Now the improvements on the COP of the before described modifications are discussed. Figure 5-21 shows the COP for equal operating points before (b.) and after (a.) the modifications (m.).

The figure would appear similar if the COP would be shown as a function of the heating capacity. The improvement in the COP depends on the operating point. For the smallest pressure ratio, which equals the operating point 2/20, the COP improved the most with an average of 4.28 %. For the operating point 2/30 the average improvement was 3.94 %. For the operating point 2/50 the COP improved only slightly by 0.56 %. There are three causes which lead to this small improvement. First of all the lower increase in the UA for the high pressure ratio, as discussed in Figure 5-16, secondly the not considered increased power input for the SEC board, which also has an influence on the operating points 2/20 and 2/30, and lastly a slightly lower isentropic efficiency for the compressor speeds 3000, 3600, 4200 (only for the point 2/50) compared to measurements before the modifications.

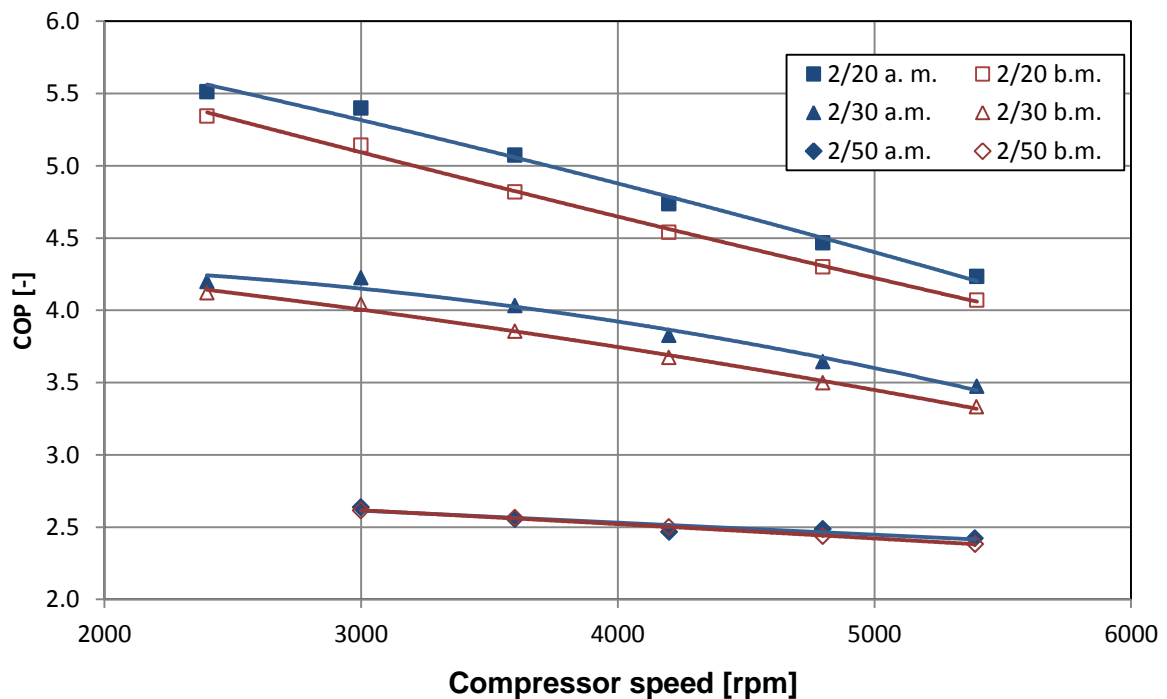


Figure 5-21: COP before and after the modifications for equal operating points

5.2.2 Cycle performance

After the cycle modifications were finished a measurement matrix to determine the cycle performance was recorded. The measured points as well as the most important results can be seen in Appendix A-4.2. The reached values for the COP vary between 1.92 and 7.38 for all the measurements. As already described in chapter 2.1.3 the COP mainly depends on the evaporation and condensation temperature. This can be expressed with the pressure ratio π . A high evaporation temperature and a low condensation temperature result in a small pressure ratio and a high COP. Figure 5-22 shows the COP as a function of the pressure ratio for different operating points.

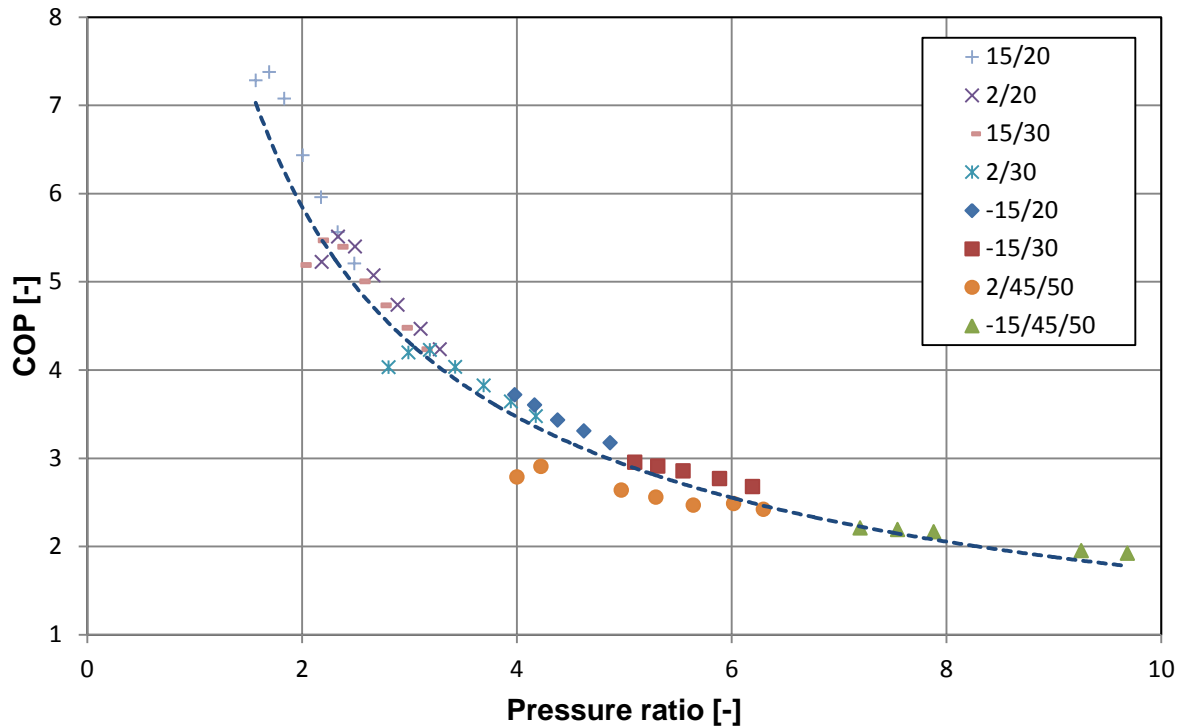


Figure 5-22: COP as a function of the pressure ratio for different operating points

As already used before, the legend shows the operating points with the brine inlet temperature to the evaporator and the water inlet temperature to the condenser. For the operating point 2/50 the first two measured points have a water inlet temperature of 45 °C and the same for the first three points of the operating point -15/50. This is done because the points are not in the operating area (envelope) of the compressor. For every operating point different compressor speeds are used. With the compressor speed the temperature differences in the heat exchangers increase, because of the higher capacity, which increases the pressure ratio. As expected the COP for all measured points depends on the pressure ratio. A potential best fit curve is used to show the trend. The point with the highest pressure ratio of 9.69 shows the lowest COP of 1.92, the second lowest pressure ratio of 1.70 shows the highest COP of 7.38.

Apart from the expected trend, two deviations can be seen. The measurement series 2/50 shows a lower COP than a measurement series with similar pressure ratio but lower condensation and evaporation temperature (-15/30). One cause is that the three measured points with 3000, 3600 and 4200 rpm show a slightly lower overall isentropic efficiency (around 0.02 lower) than comparable points measured for the compressor performance map. Causes for the lower overall isentropic efficiency for some of the last measurements, which were recorded are discussed in chapter 5.2.4.

The second deviation from the trend can be seen for measured points with low compressor speed. Figure 5-22 shows that for different measurement series the lowest pressure ratio, which corresponds to the lowest compressor speed, does not show the best performance. Figure 5-23 shows the COP for operating points with different compressor speeds. This figure only shows points with a low pressure ratio because the working area of the compressor (envelope) gets smaller with low compressor speed, which means that not all operating points could be measured for all speeds.

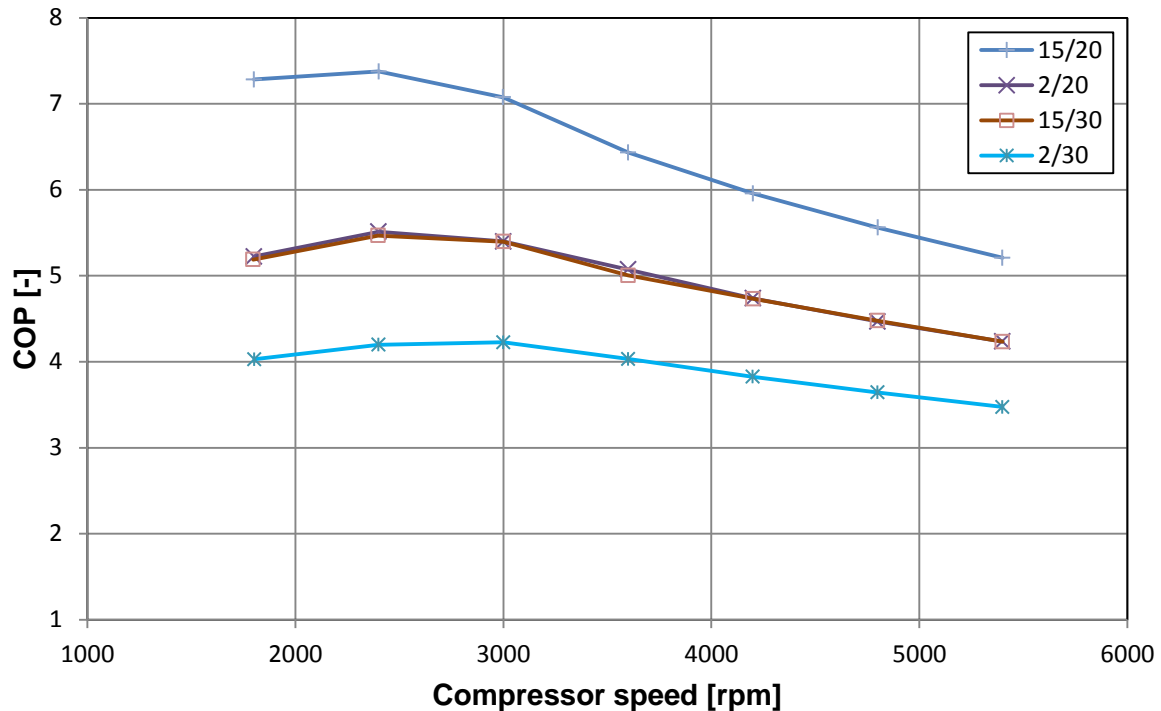


Figure 5-23: COP as a function of the compressor speed for different operating points

It can be seen that the maximum COP for four different operating points is not reached for the lowest compressor speed, which implies the lowest pressure ratio, the maximum COP is reached for measured points from 2400 to 3000 rpm. This can be explained with the already analysed compressor performance from chapter 5.1. The volumetric efficiency shows the lowest values for low compressor speeds and improves for every operating point from 2100 to 3000 rpm. The overall isentropic efficiency shows similar behaviour. The lowest compressor speed of 2100 rpm shows the lowest isentropic efficiency and the maximum is reached between 4000 and 5000 rpm. For measured points with low compressor speed the increase of the COP, because of the increasing compressor efficiency, is higher than the decrease of the COP because of the rising pressure ratio. In the range between 2400 and 3000 rpm the influence of the rising pressure ratio on the COP exceeds the influence of the rising efficiency, which leads to a decreasing COP with the compressor speed.

Figure 5-24 shows the COP as a function of the pressure ratio for different speeds. Potential best fit curves are used to show the trend of the COP for the different compressor speeds. It can be seen that the COP increases with the compressor speed. The biggest increase is between 1800 and 2400 rpm. This trend continues with higher compressor speeds as well, although the increase in the COP is lower than in the low compressor speed range. This behaviour is expected after the evaluation of the compressor performance, which shows an increasing volumetric efficiency with the compressor speed, also more pronounced for the lower speed range (Figure 5-6) and an increasing isentropic efficiency with the compressor speed, which is discussed in Figure 5-3.

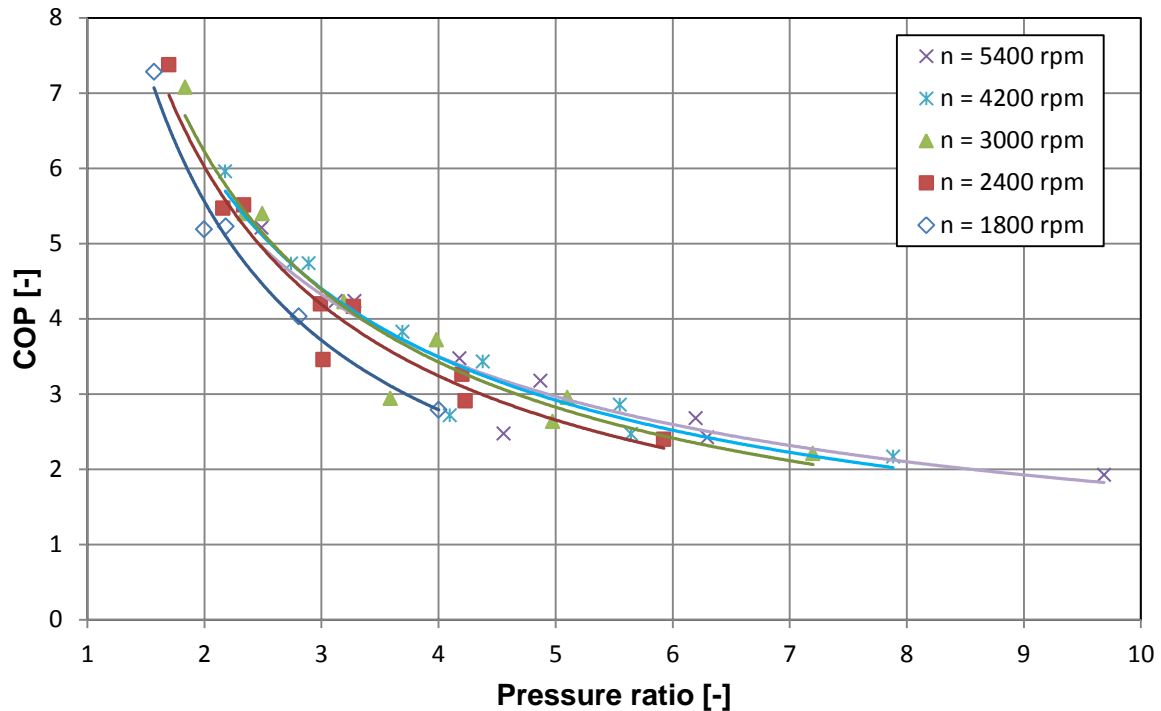


Figure 5-24: COP for different compressor speeds as a function of the pressure ratio

5.2.3 Influence of the economiser on the heat pump cycle

In chapter 2.1.7 the schematic view and the temperature-enthalpy diagram for a heat pump cycle with ECO are shown. In chapter 5.1.4 the influence of the vapour injection on the different compressor efficiencies is described. It was already discussed that the mass flow over the injection port of the compressor increases with the pressure ratio (Figure 5-11) and that the outlet temperature of the compressor decreases for the same pressure ratio with ECO (Figure 5-10). The decrease of the outlet temperature is higher for high pressure ratios because of the higher injection mass flow. This chapter deals with the impact of the ECO on the cycle performance. The compared points are the same as for the influence of the ECO on the compressor performance and can be seen in Appendix A-4.2 and A-4.3.

Figure 5-25 and Figure 5-26 show all compared operating points as a function of the pressure ratio. Potential best fit curves are used to show the overall COP trend with- and without ECO. Each operating point consists of different speeds, between 1800 and 5400 for the points 2/20 and 2/30, and three speeds, 3000, 4200 and 5400 rpm for the others.

Although it has to be considered that the COP for each operating point depends on the compressor efficiencies, the compressor speed, and the condensation and evaporation temperature, Figure 5-25 still shows the influence of the ECO on the COP as a function of the pressure ratio. If the two potential best fit curves are compared, and the COP without ECO is used as base, the improvement is 3.4 % for a point with a pressure ratio of 2.5 and 14.2 % for an operating point with a pressure ratio of 5.5. Figure 5-11 already showed that the injection mass flow is almost zero for a pressure ratio of 2, which means that the ECO has nearly no influence on the COP for smaller pressure ratios than that.

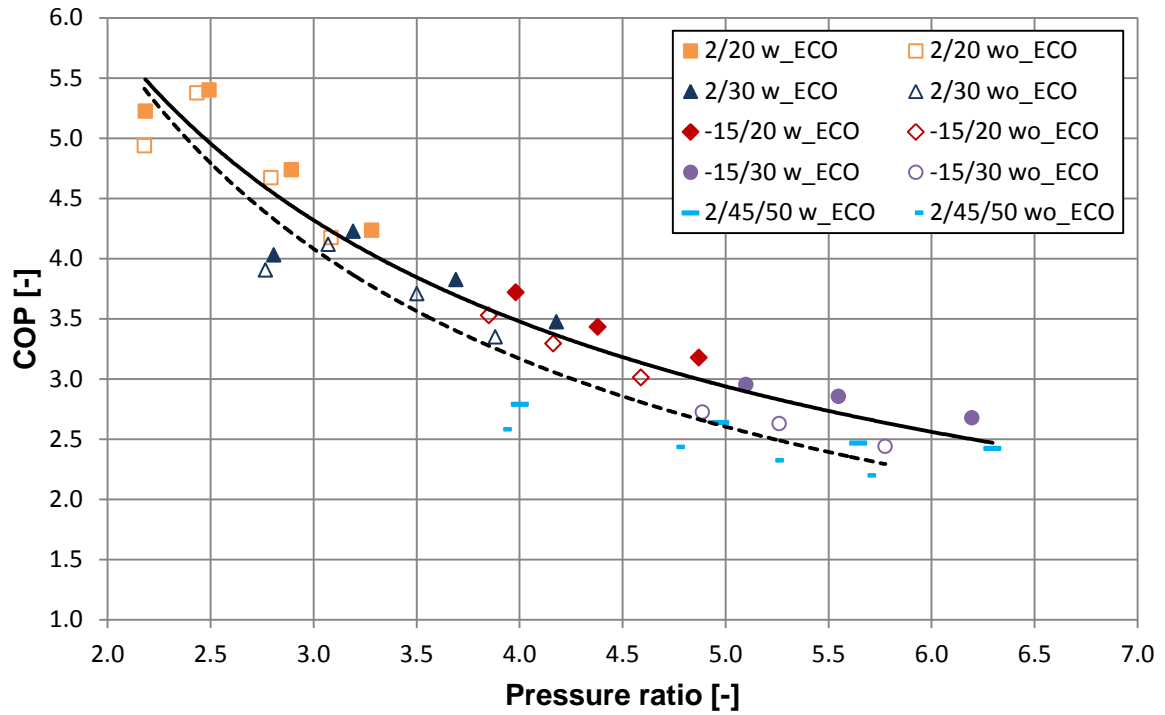


Figure 5-25: COP of all compared operating points with- and without ECO as a function of the pressure ratio (overall exponential trend)

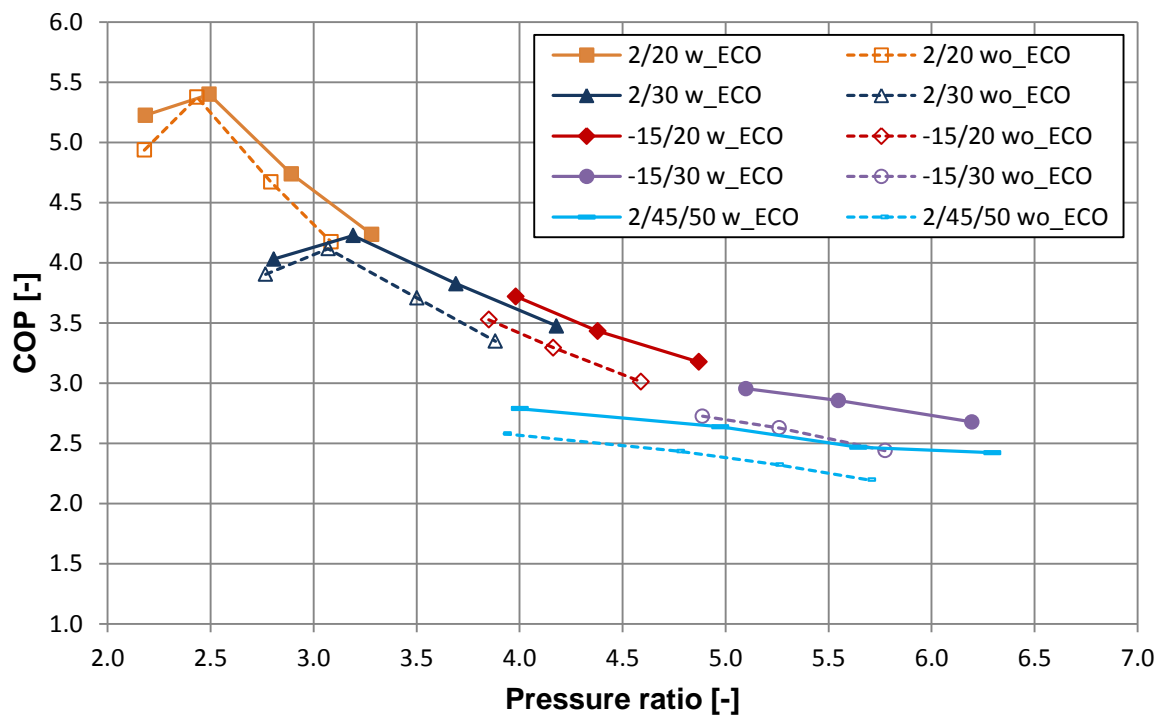


Figure 5-26: COP of all compared operating points with- and without ECO as a function of the pressure ratio (polynomial trend for each operating point with different speeds)

If the individual operating points are compared with- and without ECO, the already in chapter 5.2.2 discussed tendency can be seen, that the COP increases with low compressor speeds from 1800 to 3000 rpm because of the increasing compressor efficiencies, and then decreases,

because of the increasing pressure ratio caused by the higher capacities over the condenser and evaporator HX. The same trend also occurs for the operating points without ECO. Furthermore it can be seen that the improvement in the COP increases with the compressor speed because of the increasing pressure ratio.

Figure 5-26 also shows that the improvement in the COP is higher if it is based on the pressure ratio than if two working points with the same water inlet temperature to the condenser and brine inlet temperature to the evaporator are compared. This results from the higher pressure ratio caused by the higher capacities transferred in the condenser and evaporator HX with ECO. Because of the ECO the mass flow over the condenser increases and therefore the heating capacity. On the low pressure side the usable enthalpy difference increases because of the subcooling of the refrigerant mass flow before the evaporator in the ECO. The average COP improvement for the operating point -15/30 for all speeds is about 9 % for the average pressure ratio of 5.5. If the two potential best fit curves in Figure 5-25 are compared, the improvement for a pressure ratio of 5.5 is about 14 %.

Figure 5-27 shows the COP with- and without ECO for four different speeds with a brine inlet temperature to the condenser of 2 °C and three different water inlet temperatures to the condenser (20/30/50) as a function of the pressure ratio. The COP improvement increases with higher condensation temperature and therefore higher pressure ratio. This trend is indicated clearly for each compressor speed except 1800 rpm, where the improvement is nearly the same for all three pressure ratios. The COP for this speed without ECO is much lower than with ECO, whereby the cause cannot be determined, because of the lower pressure ratio these two points should be similar.

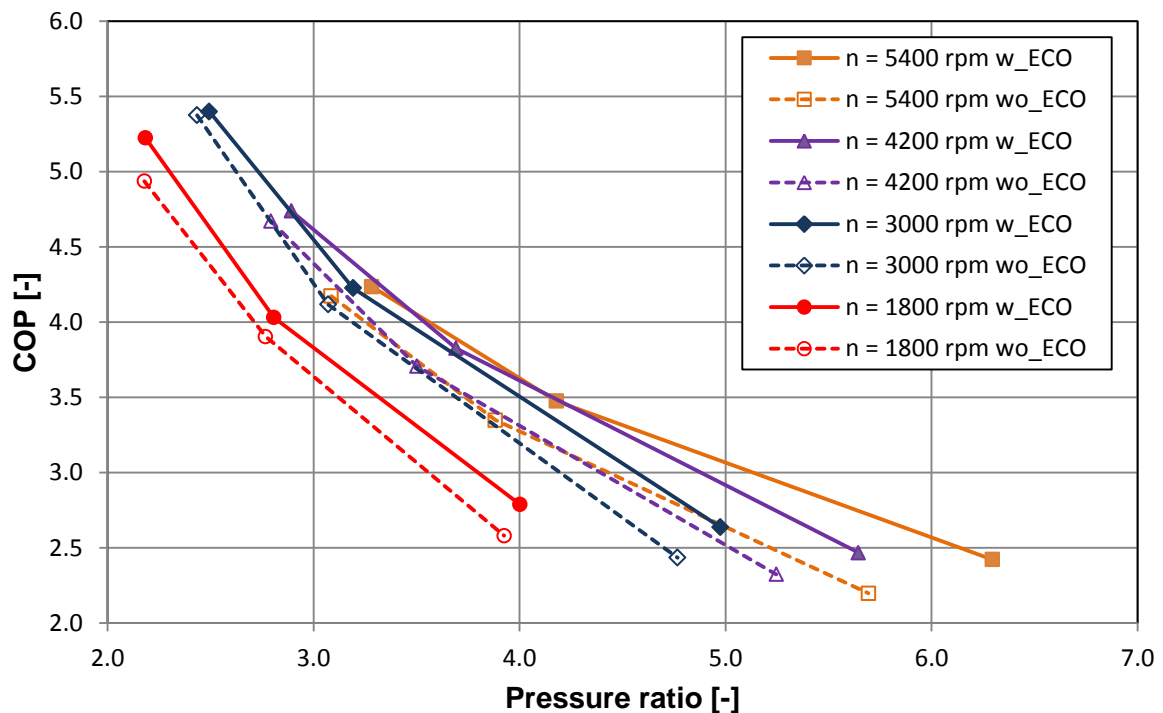


Figure 5-27: COP with- and without ECO for different speeds and different water inlet temperatures (20/30/50) to the condenser, as a function of the pressure ratio

The next two figures contain the same measured points which are discussed in Figure 5-27, to analyse if the COP improvement results from a higher heating capacity or a lower compressor input power.

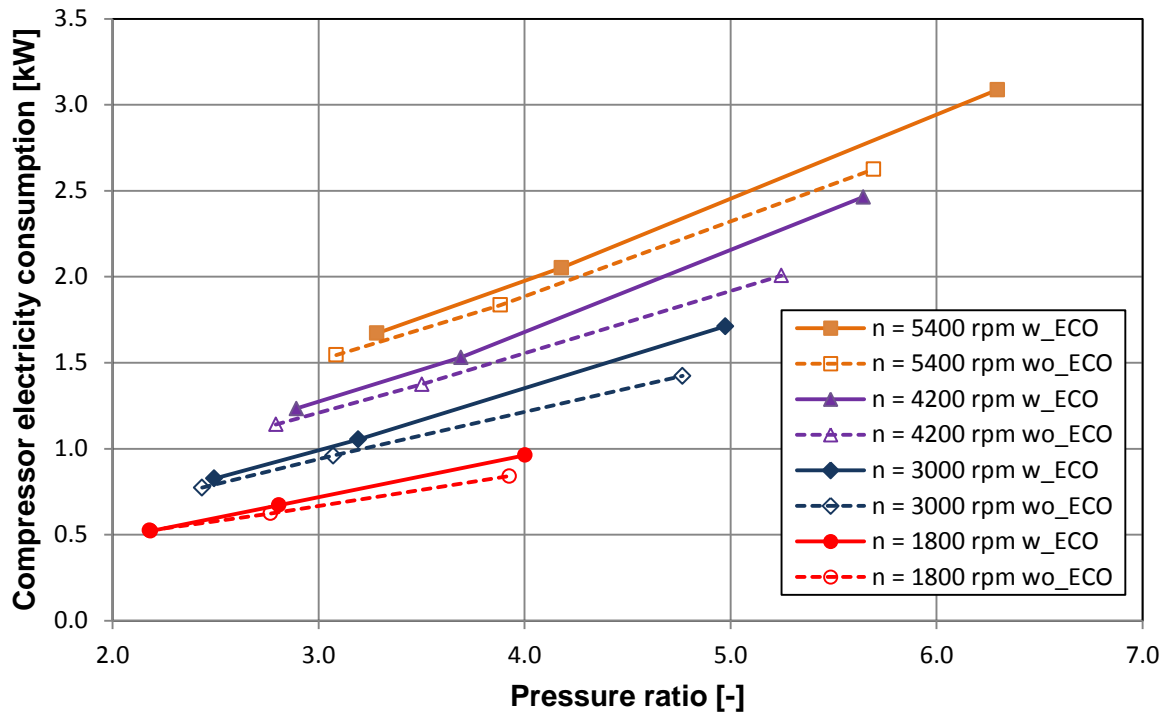


Figure 5-28: Compressor input power with- and without ECO for different speeds and different water inlet temperatures (20/30/50) to the condenser, as a function of the pressure ratio

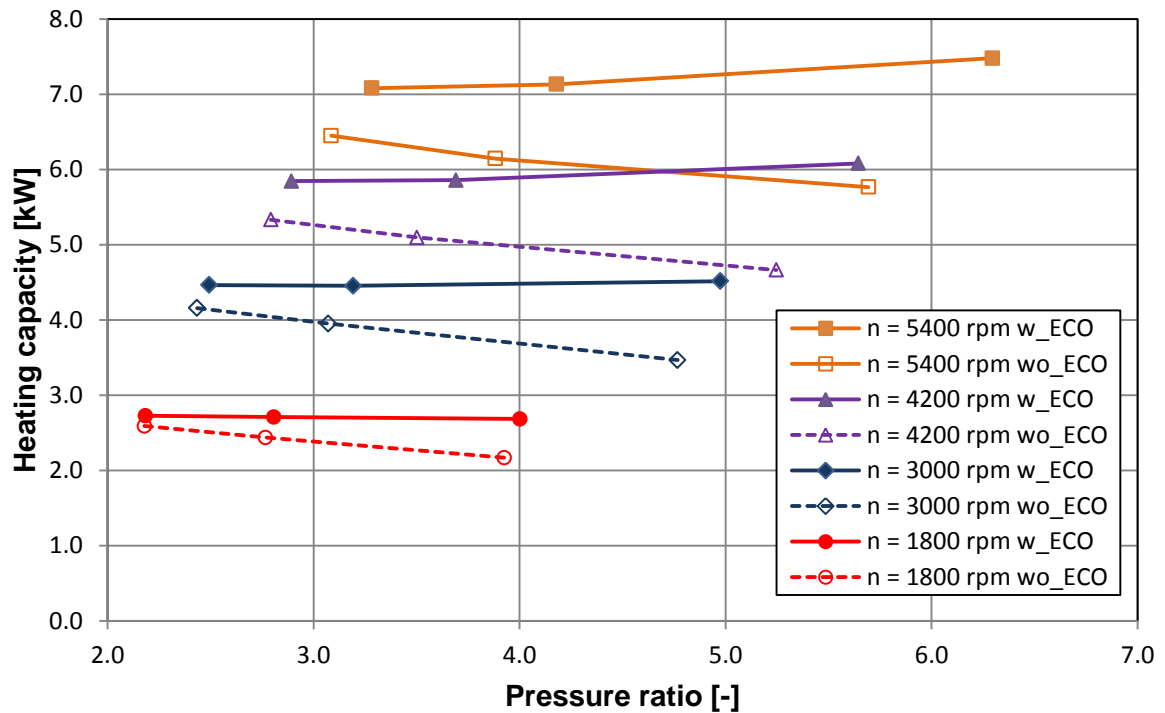


Figure 5-29: Heating capacity with- and without ECO for different speeds and different water inlet temperatures (20/30/50) to the condenser, as a function of the pressure ratio

Figure 5-28 shows the compressor input power and Figure 5-29 shows the heating capacity for four different speeds with- and without ECO with 2 °C brine inlet temperature to the evaporator and different water inlet temperatures (20/30/50) to the condenser, as a function of the pressure ratio.

Figure 5-28 indicates that the needed compressor input power is higher for the operating points with ECO. The difference in the input power, with- and without ECO, increases with the pressure ratio for all four speeds. This confirms the expected trend because with the ECO a higher mass flow has to be compressed from the medium to the high pressure level. This result already implies that for the improvement of the COP with the pressure ratio, the gain in the heating capacity with ECO has to be higher than the additional input power needed.

Figure 5-29 approves this assumption. For example for the operating point (2/50), for a speed of 5400 rpm, the heating capacity increases by nearly 30 %, based on the operating point without ECO, for a only 17 % higher power input of the compressor. The figure shows that for all compressor speeds the heating capacity increases with increasing condensation temperature for the same brine inlet temperature to the evaporator of 2 °C, except for 1800 rpm, where the heating capacity stays about the same for all three water inlet temperatures. Without ECO the heating capacity decreases with increasing condensation temperature. For the operating point 2/50 it even occurs that the heating capacity is higher with ECO and a compressor speed of 4200 rpm than for the compressor speed of 5400 rpm without ECO.

5.2.4 Analysis of the desuperheater

In chapter 3.1 the schematic view of the test rig with desuperheater is shown, in chapter 2.1.8 the temperature-enthalpy diagram of the heat pump process with desuperheater is described. In this chapter the influence of the desuperheater on the cycle performance is discussed as well as the usability of a desuperheater for hot water preparation.

During the evaluation of the measurement matrix with desuperheater, it showed up that the compressor performance was slightly worse than for the measurement matrix of the cycle performance. This was realized by a higher outlet temperature of the compressor and therefore a worse isentropic efficiency. This results in a lower COP for the measurements with desuperheater. The cause for this lower compressor performance is assumed to be the small increase in the compressor torque, which was measured for these operating points. This could be an indication for a compressor damage, or for a bad lubrication, as a late result of the four test rig modifications, in which the refrigerant, which contains a certain amount of compressor oil, was evacuated and then refilled again. Some oil also remained in the changed components like the condenser. Since the cause for the lower isentropic efficiency was still under investigation during the desuperheater evaluation, measurements before the last two test rig modifications, with the 30 plate condenser HX, and the manufacturer's superheating control system, are used to determine the influence of the desuperheater on the COP. This means that the COP of these measurements cannot be compared with the measurement of the cycle performance, they should only show the variation of the COP with the usage of the desuperheater.

Figure 5-30 shows the COP for three different operating points ($n = 5400$ rpm) with four different water mass flows over the condenser, whereby 0 equals the heat pump process without desuperheater use. The water mass flow over the condenser is 852 kg/h for all measured points. It occurs that the COP is higher for all measured points with desuperheater. The COP improvement increases with the water mass flow over the desuperheater. Although this trend can be seen for all three operating points, the COP improvements are quite low. If the operating point with the highest mass flow over the desuperheater and the operating point without desuperheater mass flow are compared, the COP improved by 2.2 % for the operating point 12/30 (8.8 kW heating capacity), 2.6 % for the point 2/30 (7.2 kW heating capacity) and 2.1 % for the point -10/30 (5.2 kW heating capacity).

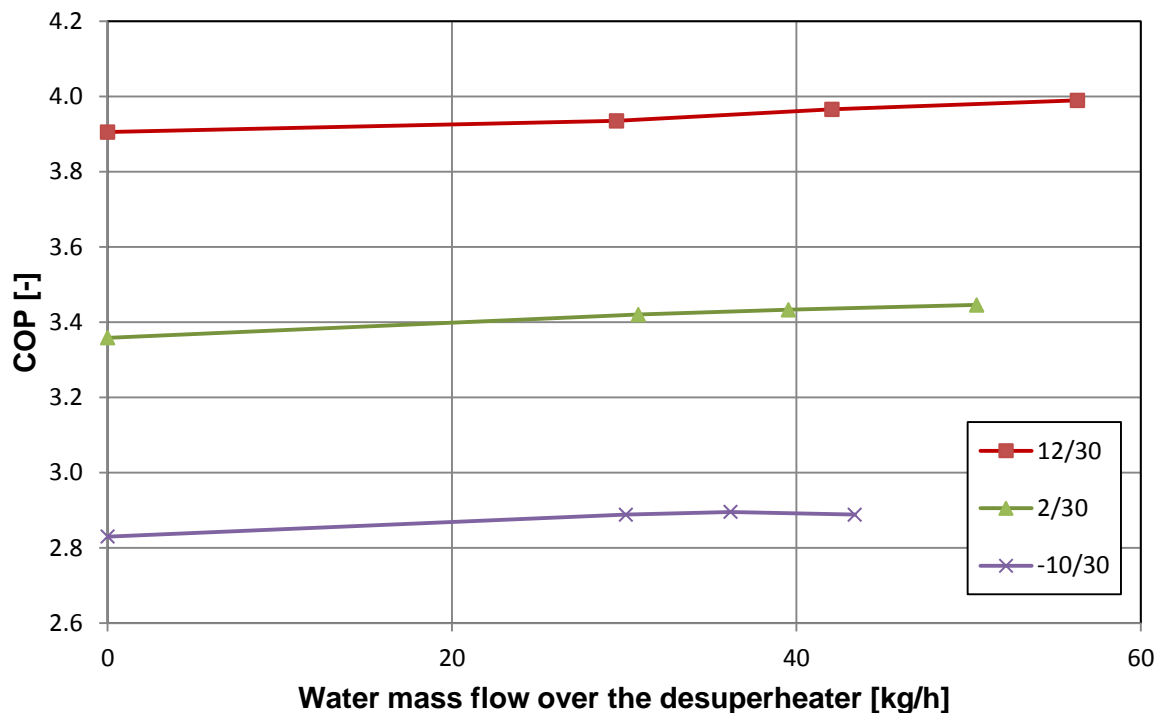


Figure 5-30: Influence on the COP of different water mass flow rates over the desuperheater for three different operating points and a compressor speed of 5400 rpm

Since the discussed operating points are all for a high heating capacity and the points were measured with the 30 plate condenser HX, it can be assumed that the increase in the COP mostly depends on the increased heat exchanger surface, because of the 10 additional plates of the desuperheater (Table 3-1). This is proven in Figure 5-31, which shows the condensation temperature for all discussed operating points. The condensation temperature is based on the water mass flow over the desuperheater to compare Figure 5-31 and Figure 5-30. If the same two points as for the COP discussion are compared, the decrease is 0.94 K for the operating point 12/30, 1.14 K for the point 2/30 and 0.77 K for the point -10/30. Why the decrease of the condensation temperature is the highest for the second highest heating capacity cannot be explained, but the decrease of the condensation temperature shows a similar trend as the increase in COP. The decrease of the condensation temperature leads to a similar reduction of the pressure ratio (2.1 %, 2.2 %, 1.4 %).

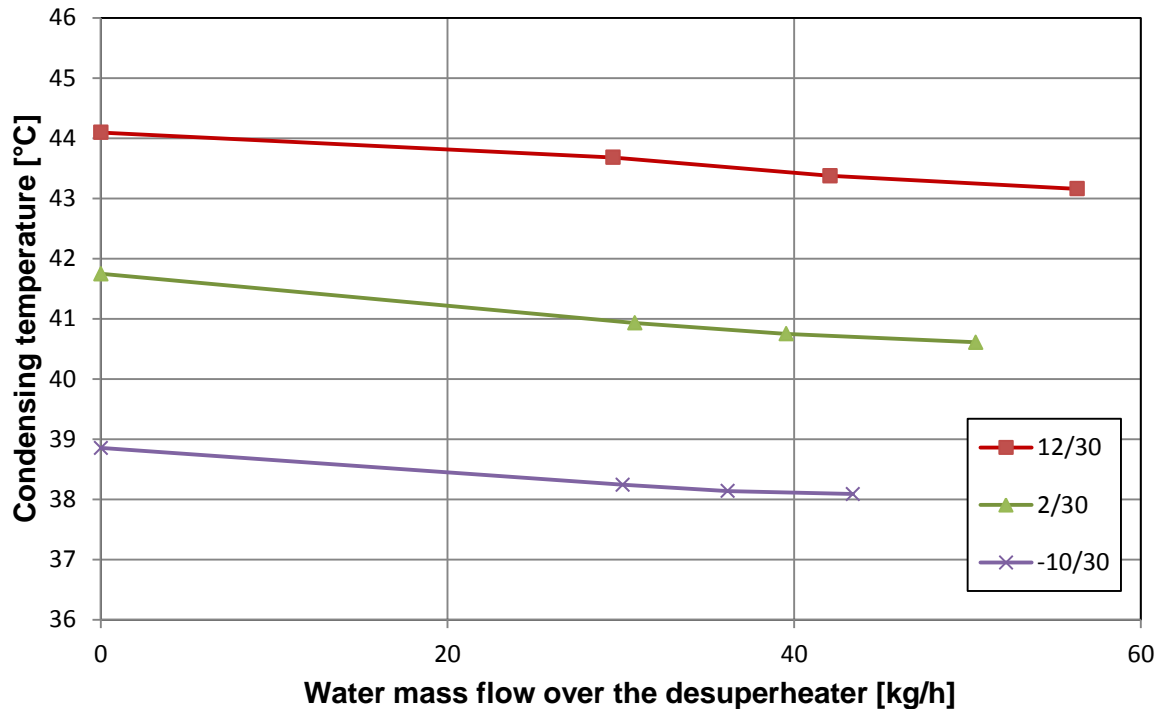


Figure 5-31: Decrease of the condensation temperature for three different operating points as a result of the increased HX area with the use of the desuperheater

The same result is gained if a point with the same isentropic efficiency (1800 rpm, $t_{b1} = 2\text{ °C}$, $t_{w1} = 20\text{ °C}$) with- and without desuperheater (Appendix A-4.4) is compared. With desuperheater the COP increases from 5.22 to 5.25 with a reduced condensation temperature of 0.11 K. This also shows that the COP stays nearly constant for low heating capacities and that the COP with desuperheater only varies because of the increased HX area.

As a result, the desuperheater makes it possible to produce a certain amount of hot water, for DHW preparation, without reducing the cycle efficiency. The big advantage can be described by comparing a point (3600 rpm, $t_{b1} = 2\text{ °C}$, $t_{w1} = 30\text{ °C}$) with desuperheater, which produces 62 kg/h water with a desuperheater outlet temperature of 50°C (COP 3.99). The same point was measured without desuperheater with a water inlet temperature to the condenser of 50 °C, which resulted in a water outlet temperature of 54.6 K. The COP reached was 2.64 because of the different condensation temperature and therefore higher pressure ratio.

Amount and temperature of the hot water for DHW preparation

The amount and the temperature of the hot water produced by the desuperheater depends on the operating point. The desuperheater outlet temperature can only be lower than the compressor outlet temperature at the discharge line. The discharge temperature depends on the compressor speed and the condensing and evaporation temperature. This was already discussed in Figure 5-10. With the pressure ratio the used enthalpy difference in the condenser that comes from the desuperheating of the refrigerant increases, compared to the enthalpy difference from the condensing. This is shown in Figure 5-32. The indexes for the enthalpy difference on the ordinate can be seen in Figure 4-1. It shows that with higher pressure ratio the enthalpy difference by desuperheating the refrigerant from the discharge line increases and that the enthalpy difference by condensing the refrigerant decreases. Points with lower evaporation

temperature tend to be beneath the linear best fit curve, the point 2/50 shows a significantly higher desuperheating enthalpy difference compared to the other points.

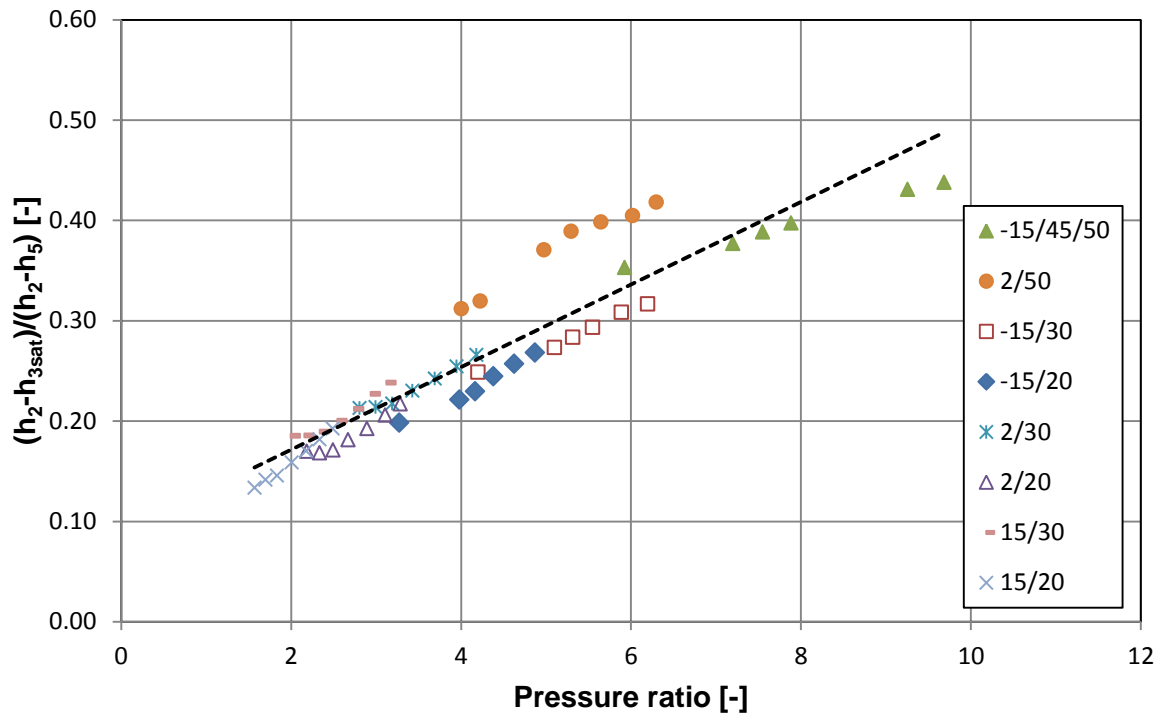


Figure 5-32: Enthalpy difference from desuperheating the refrigerant compared to the enthalpy difference from condensing in the condenser

Figure 5-33, Figure 5-34 and Figure 5-35 sum up the compressor outlet temperature and pressure ratio dependency by comparing two different operating points with a compressor speed of 5400 rpm and inlet temperatures to the condenser and evaporator as stated in the figures. The operating point with $-15\text{ }^{\circ}\text{C}$ brine inlet temperature (right) has a higher compressor outlet temperature, which makes it possible to produce hot water with higher temperature. Compared to that the operating point with $2\text{ }^{\circ}\text{C}$ brine inlet temperature (left) has a nearly 20 K lower compressor outlet temperature.

In Figure 5-33 the desuperheater outlet temperature is set to $80\text{ }^{\circ}\text{C}$. For the operating point on the left side, this temperature is very close to the compressor outlet temperature, only 15 kg/h of hot water with $80\text{ }^{\circ}\text{C}$ can be produced, which corresponds to a desuperheating capacity of 0.8 kW. The operating point on the right side with $-15\text{ }^{\circ}\text{C}$ brine inlet temperature to the evaporator produces 23 kg/h hot water with $80\text{ }^{\circ}\text{C}$, which corresponds to a desuperheating capacity of 1.3 kW. This is in this case 26 % of the whole heating capacity of 5 kW, compared to the operating point with the higher evaporation temperature, which transfers 11 % of the whole heating capacity of 7.2 kW in the desuperheater.

In Figure 5-34 the desuperheater outlet temperature is reduced to $70\text{ }^{\circ}\text{C}$. For this operating point, the figure on the left side shows already a higher hot water mass flow of 35 kg/h, which corresponds to 1.4 kW desuperheating capacity, compared to 33 kg/h at the operating point with the lower evaporation temperature and therefore lower total heating capacity. In Figure 5-35 the desuperheater outlet temperature is set to $60\text{ }^{\circ}\text{C}$, whereby the operating point on the

left side produces 58 kg/h and the point on the right side only 48 kg/h. The described points are listed in Appendix A-4.4.

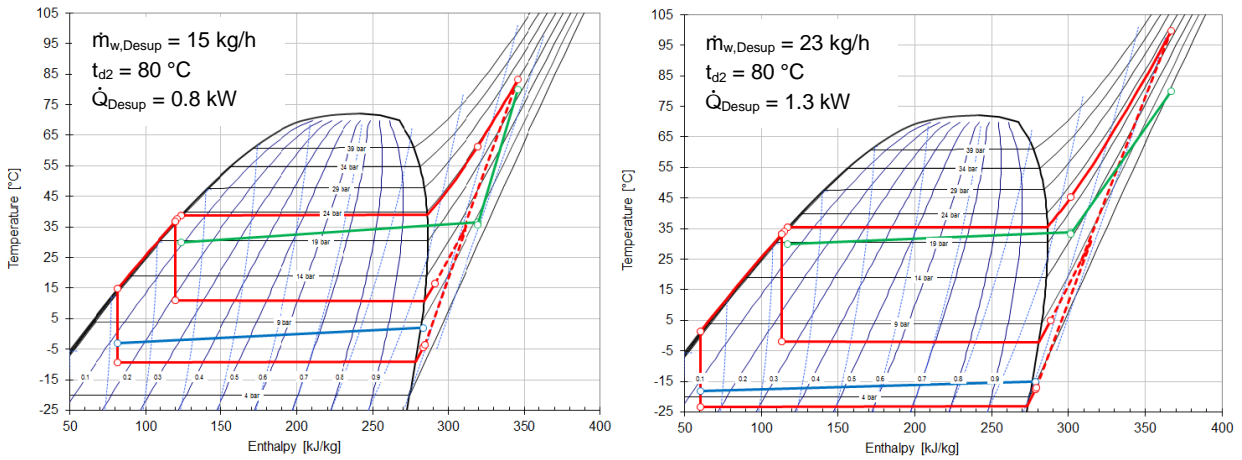


Figure 5-33: Comparison of two different operating points with desuperheater (left: $t_{w1} = 30\text{ °C}$ $t_{b1} = 2\text{ °C}$; right $t_{w1} = 30\text{ °C}$ $t_{b1} = -15\text{ °C}$)

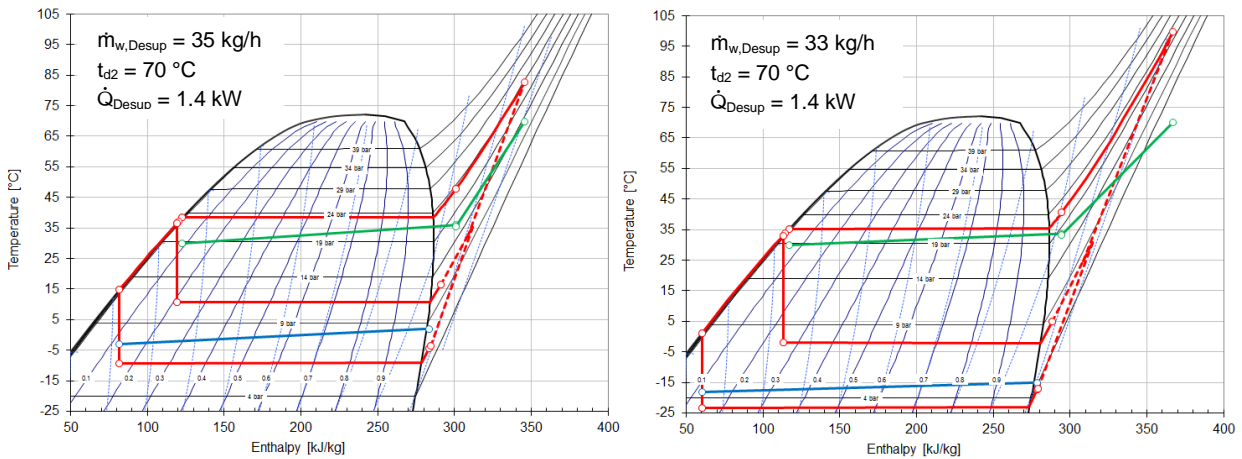


Figure 5-34: Comparison of two different operating points with desuperheater (left: $t_{w1} = 30\text{ °C}$ $t_{b1} = 2\text{ °C}$; right $t_{w1} = 30\text{ °C}$ $t_{b1} = -15\text{ °C}$)

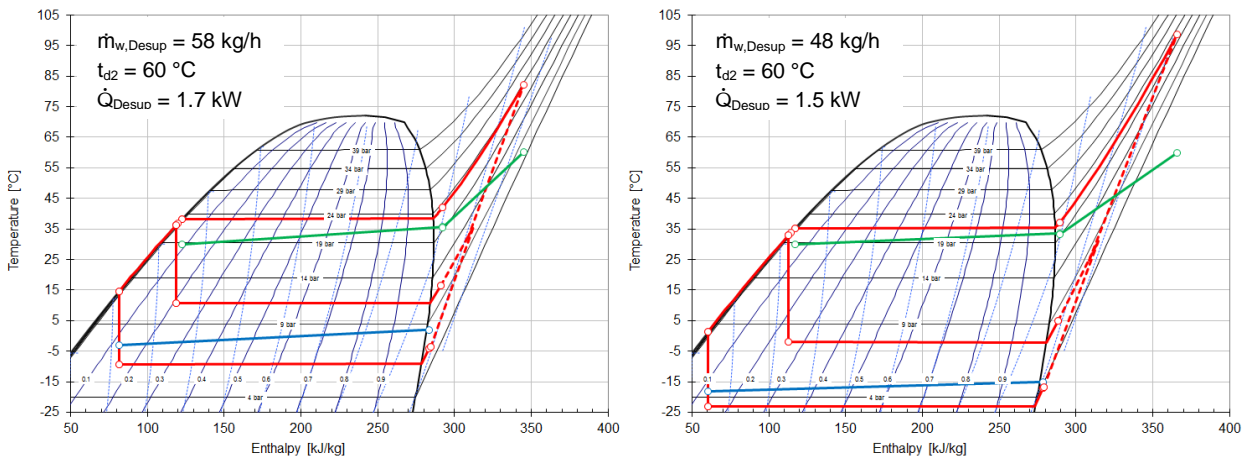


Figure 5-35: Comparison of two different operating points with desuperheater (left: $t_{w1} = 30\text{ °C}$ $t_{b1} = 2\text{ °C}$; right $t_{w1} = 30\text{ °C}$ $t_{b1} = -15\text{ °C}$)

5.2.5 Results of the error calculation

The calculation of the error of measurement for the COP is discussed in chapter 4.4. Table 3-2 shows the accuracy of the used measurement devices. The results of the error calculation are listed in the Appendix A-4 for each point. Table 5-1 shows the maximum error which appeared for all measured values from the cycle evaluation, the ECO evaluation and the evaluation of the desuperheater. The maximum error of measurement is given as percentage of the measured value.

Table 5-1: Maximum error for three measurement matrices

	$f_{\max}(P_{el})$ [%]	$f_{\max}(\dot{Q}_{cond})$ [%]	$f_{\max}(\dot{Q}_{desup})$ [%]	$f_{\max}(COP)$ [%]
Cycle evaluation	0.91	0.61	-	1.09
ECO evaluation	0.91	0.75	-	1.11
Desuperheater evaluation	0.84	0.74	11.65	2.44

The maximum error for the cycle evaluation (COP) is ± 1.09 % for an operating point with 1800 rpm, an electric input power of 0.52 kW and a heating capacity of 2.7 kW. It is expected that the maximum error occurs for small heating capacities because the error of the Pt100 and TC are stated with a constant value (0.02 K / 0.2 K), which leads to a higher measurement error with a smaller temperature difference. The same applies to the electrical input power. With higher power the electricity meter counts more often, which leads to a higher accuracy (could be compensated with longer measurements). Both together sum up to the measurement error of the COP, which has a maximum of ± 1.09 % for the mentioned operating point. These results are very satisfying.

For the evaluation without ECO the results are similar, whereby the highest error of measurement for the COP is ± 1.11 % for an operating point with 1800 rpm, an electrical power input of 0.52 kW and a heating capacity of 2.6 kW.

For the evaluation of the desuperheater the error of measurement shows a worse result. The highest deviation is ± 2.44 % for the COP. Table 5-1 shows that this error depends mostly on the calculation of the heating capacity of the desuperheater. Since the temperature difference of the water flow at the inlet and the outlet of the desuperheater is very high, nearly the whole error comes from the volumetric flow measurement over the desuperheater.

Figure 3-15 shows how the MID devices for the measurement of the flow rate are placed. It is measured as difference of the flow rate over the condenser and the flow rate over the condenser without desuperheater flow. This was done because of the higher accuracy of the MID devices for higher flow rates. The accuracy of 0.2 % of the measured value after the calibration is very good for each device but the placement in the cycle is not suitable for measuring small flow differences, which leads to a maximum error of ± 11.65 % for a mass flow of 11.9 kg/h.

6 SUMMARY AND CONCLUSION

Summary

A brine/water heat pump with speed control, economiser and desuperheater was investigated experimentally in this thesis. A performance map of the compressor was recorded and analysed as well as the influence of the ECO on the different compressor efficiencies. The heat pump test rig was modified to improve the cycle performance, whereby the cycle performance was evaluated including the influence of the ECO on the COP. Furthermore the impact of a desuperheater on the cycle performance was analysed as well as the ability for hot water preparation.

After the test rig start-up phase different modifications were made to enable the measurement of the compressor performance map. The LabVIEW program, for the data acquisition and the control of the heat pump system and the periphery, had to be extended and different controllers were implemented to ensure a safe and reliable operating of the test rig. This also included the parameter setting for the controllers of the different circuits. Valves for the bypassing of the desuperheater had to be changed to reduce the pressure losses of the cycle and TC in the refrigerant cycle had to be replaced with plugless types, which were not influenced by the vibrations of the test rig. An evaluation sheet for the measurements was created and continuously extended.

A compressor performance map was recorded and the compressor losses, the isentropic efficiency and the volumetric efficiency were analysed. The compressor losses vary between 4 and 16% of the electric power input for the whole compressor performance map. The losses consist of the heat losses of the motor, the compressor and the inverter. The compressor losses increase with increasing pressure ratio, and in similar manner with increasing compressor outlet temperature. The losses decrease with increasing compressor speeds and are also slightly higher with lower evaporation temperature.

The overall isentropic efficiency varies with the compressor speed and the condensation and evaporation temperature between 0.48 and 0.64 for the whole compressor performance map. The lowest compressor speed shows the lowest isentropic efficiency. The increasing efficiency with the compressor speed is more pronounced in the low compressor speed range than for speeds between 4000 and 5000 rpm, where the isentropic efficiency is quite similar. The efficiency decreases with the pressure ratio, but it also depends on the evaporating and condensing temperature. The operating point 12/30 shows the highest isentropic efficiency with an evaporation temperature between -0.85 and 6.05 °C and a condensation temperature between 36.81 and 44.10 °C for eight different speeds, nearly 0.05 higher than the operating point 2/20 with similar pressure ratio.

Compared to the isentropic efficiency, the volumetric efficiency mainly depends on the pressure ratio and the compressor speed. The volumetric efficiency varies between 0.77 and 0.93 for the whole measurement matrix. Similar to the overall isentropic efficiency it increases with higher compressor speeds for most of the operating points, and it decreases with increasing pressure

ratio. The operating point 12/20, which is the operating point with the lowest pressure ratio, shows the best volumetric efficiency.

After the measurement of the compressor performance map, attempts were made to improve the cycle efficiency. The intended goal was to reduce the condensation temperature and to increase the evaporation temperature. On the high pressure side of the HP the condenser with 30 plates was replaced with a HX with 40 plates to increase the UA and therefore decrease the ΔT in the pinch point between the condensation temperature of the refrigerant and the water temperature. The 25 % higher HX area resulted in a 25 to 28 % higher UA for the operating points 2/20 and 2/30 (U value nearly equivalent), and an improvement of the UA of 16 % for the operating point 2/50. As a result the condensation temperature decreased between 0.6 and 2.1 K for the compared points.

To increase the evaporation temperature, self-generated controller parameters were used to control the superheating at the evaporator outlet, instead of using the control system of the manufacturer. This resulted in a much more stable superheating signal and increased the evaporating temperature for low cooling capacities. The greatest improvement of all compared points was 0.33 K. Furthermore it decreased the oscillations of the mass flow in the heat pump cycle. A new software update by the compressor manufacturer for the superheating control was still under investigation while this thesis was finished.

Both improvements together increased the COP of the compared operating points up to 4.3 %. For this comparison measurements of the compressor performance map and measurements for determining the cycle performance after the modifications were used.

The evaluation of the cycle shows a COP between 1.92 (-15/50 5400 rpm, pressure ratio 9.69) and 7.28 (15/20 2400 rpm, pressure ratio 1.70) for all measurements. The COP depends on the compressor efficiencies as discussed before and the evaporation and condensation temperature. For an operating point with a fixed brine inlet temperature to the evaporator and water inlet temperature to the condenser the COP increases with the compressor speed between 1800 and 2400 rpm because of the increasing compressor efficiencies, and decreases with higher speeds because of the increasing capacities over condenser and evaporator HX and therefore higher pressure ratios. If the COP is shown as a function of the pressure ratio, the COP increases with the compressor speed, according to the compressor efficiencies.

After the evaluation of the cycle performance, measurements without ECO were made to determine the influence on the cycle performance. Compared with potential best fit curves for all measured points, the use of an ECO showed 3.4 % improvement for a pressure ratio of 2.5 and 14.2 % improvement for a pressure ratio of 5.5. For small pressure ratios no mass flow is injected at the medium pressure level, which leads to similar cycle performance with- and without ECO, but with increasing pressure ratio the advantage of the ECO increases. The increase in the COP comes from the far higher heating capacity compared to a smaller increase in electric power consumption as well as the slightly increased isentropic efficiency with ECO, because of the lower compressor outlet temperature.

Finally the use of a desuperheater in the cycle was evaluated. The influence on the COP is minor, the highest improvement was 2.6 % for all compared points, which mainly results from

the increased HX area for higher heating capacities. With lower heating capacities the increase in COP is lower. This finding is still very positive because it shows the possibility to produce hot water for DHW preparation without a significant reduction of the COP.

Conclusion

The treated innovations in this thesis, which are the speed control, the economiser and the desuperheater, are steps toward increasing the efficiency of today's heat pump systems.

The compressor speed range from 1800 to 7020 rpm makes it possible to adapt the heating capacity of the HP perfectly to the needed heating demand of the building, especially for different ambient temperatures. The compressor shows reliable performance for all tested compressor speeds although the isentropic and volumetric efficiency decrease drastically for speeds lower than 2400 rpm.

The economiser shows an improvement of the COP of up to 15 % for high pressure ratios (5.5). Especially for cold climates in ASHP the use of an economiser is a possibility in the future HP generation to provide a highly efficient system, which is competitive to other domestic heating alternatives.

In addition to the improved efficiency, based on the speed control and the economiser, the desuperheater contributes the possibility to produce hot water without any losses in COP. In a standard HP without desuperheater the DHW preparation would cause a significantly lower cycle efficiency. With the desuperheater no additional heating unit for DHW preparation is needed, which makes it a promising combination to supply a building with both, space heating and DHW.

REFERENCES

Copeland (2011), *Variable Speed Solutions For Heat Pump Applications*, Emerson Climate Technologies, Senefelder Str. 3 DE-63477 Maintal.

Copeland (2013a), *Select Version 7.7 (Copeland compressor software)*, Emerson Climate Technologies, Senefelder Str. 3 DE-63477 Maintal.

Copeland (2013b), *Emerson Inverter Drives for ZHW and ZPV Compressors - Technical Information*, Emerson Climate Technologies, Senefelder Str. 3 DE-63477 Maintal.

Copeland (2013c), *Superheat & Envelope Controller - SEC Modbus Interface Description - Technical Information*, Emerson Climate Technologies, Senefelder Str. 3 DE-63477 Maintal.

Copeland (2013d), *SEC - User Guideline Preliminar*, Emerson Climate Technologies, Senefelder Str. 3 DE-63477 Maintal.

Copeland (2014a), *Evaporator Valve for ZHW08/16K1P*, Emerson Climate Technologies, Senefelder Str. 3 DE-63477 Maintal.

Copeland (2014b), *R410A Vapour Injection ZHI K1P Scroll Compressors*, Emerson Climate Technologies, Senefelder Str. 3 DE-63477 Maintal.

Danfoss (2005), *Filtertrockner und Schaugläser - Tips for mechanic*, Danfoss-Straße 8A-2353 Guntramsdorf.

Danfoss (2013), *Druckschalter und Thermostate Typ KP - Refrigeration and air conditioning*, Danfoss GmbH, D-63004 Offenbach Postfach 100453.

DIN19227 (1993), *Graphische Symbole und Kennbuchstaben für die Prozessleittechnik*, Deutsches Institut für Normung, DIN, Berlin.

Emerson (2013), *Pressure Transmitter PT5*, Emerson Climate Technology, Pascalstraße 65, 52076 Aachen.

Endress+Hauser (2013a), *Proline Promag 50P, 53P*, Endress+Hauser Ges.m.b.H., Lehnergasse 4 1230 Wien.

Endress+Hauser (2013b), *Proline Promass 80A, 83A*, Endress+Hauser Ges.m.b.H., Lehnergasse 4 1230 Wien.

Endress+Hauser (2013c), *Proline Promass 80F, 83F*, Endress+Hauser Ges.m.b.H., Lehnergasse 4 1230 Wien.

FLICA (1990), *UKR 60/60 Absaug- und Umfüllgerät*, FLICA.

- FP7 (2011), *Annex 1 - Description of Work*, Seventh Framework Programme, Project acronym: MacSheep.
- Görtler, G. (2007), *Regelungs- und Leittechnik*, Fachhochschule Pinkafeld, Masterstudiengang Gebäudetechnik und Gebäudemanagement, Steinamangerstraße 21 A-7423 Pinkafeld, Skriptum.
- Görtler, G. (2010a), *Regelungstechnik*, Fachhochschule Pinkafeld, Masterstudiengang Gebäudetechnik und Gebäudemanagement, Steinamangerstraße 21 A-7423 Pinkafeld, Skriptum.
- Görtler, G. (2010b), *Angewandte Messtechnik*, Fachhochschule Pinkafeld, Masterstudiengang Gebäudetechnik und Gebäudemanagement, Steinamangerstraße 21 A-7423 Pinkafeld, Skriptum.
- Hauser, P. (2009), *Analyse einer multifunktionalen R744-Wärmepumpe*, Master's thesis, Technical College Wels in cooperation with Graz University of Technology.
- Heinz, A., Hengel, F., Baur, G., Haller, M. Y., Mojic, I., Matuska, T., Sedlar, J., Petrak, J., Sourek, B., Bales, C. & Poppi, S. (2013b), *Interim report on heat pump developments in WP 4*, Graz University of Technology, Final Draft.
- Heinz, A., Hengel, F., Haller, Y. M., Mojic, I., Matuska, T., Simek, P., Sedlar, J., Poppi, S. & Bales, C. (2013a), *System Simulations and Cost Analysis for Breakthroughs in Advanced Heat Pumps and Heat Pump Cycles*, Interim Report MacSheep for Seventh Framework Programme.
- Hengel, F. (2012), *Labor - MSR, Heizungsregelung I + II*, Fachhochschule Pinkafeld.
- IEA (2013), *Key world energy statistics*, 9, rue de la Federation 75739 Paris Cedex 15.
- IMPRESS (2013), *XMD Differential Pressure Transmitter for Process Industry with HART-Communication*, IMPRESS Sensors & Systems, Unit 6 Mercury House, CALleva Park, Aldermaston, Berkshire, RG7 8PN.
- Jakobs, R. (2010), *Kältemittel für Gewerbe- . Prozess- u. Industrieanwendungen bei der Erzeugung, Lagerung u. Verteilung von Nahrungsmitteln*, Seminar: Energieeffizienz in der Gewerbe-, Prozess- und Großkälte, Netzwerk Kälteeffizienz Hamburg.
- NI (2012), *LabVLab 2012*, 2012 edn, National Instruments, Plainbachstraße 12 5101 Salzburg-Bergheim.
- PMR (2013), *Pressure Industrial Transmitter (PIT-C) / Druckmessumformer für industrielle Anwendungen*, PMR HandelsgmbH, St. Peter Hauptstraße 50 8010 Graz.
- Pohlmann (2010), *Pohlmann Taschenbuch der Kältetechnik*, 20te auflage edn, VDE Verlag GMBH, Berlin, Offenbach, Bismarckstr. 33, 10625 Berlin.
- Rieberer, R. (2013), *Energie- und umwelttechn. Mess- und Versuchswesen Block "Wärmetechnik"*, Graz University of Technology, 8010 Graz Inffeldgasse 25b, Skriptum.

References

Rieberer, R., Moser, H. & Halozan, H. (2009), *Wärmepumpentechnik*, Graz University of Technology, 8010 Graz Inffeldgasse 25b, Skriptum.

Schiessl (2013), *Flüssigkeitssammler Klimal*, Schissl, Plainbachstraße 1, Postfach 101, 5101 Bergheim b. Salzburg.

SWEP (2010), *Installations- und Wartungshandbuch für hartgelötete Kompaktwärmetauscher*, SWEP International AB, Box 105, Hjalmar Brantings väg 5, SE-261 22 Landskrona, Sweden.

SWEP (2013), *Spezifikationen für das SWEP Angebot 22840DESL*, Dimensioning, SWEP International AB, Box 105, Hjalmar Brantings väg 5, SE-261 22 Landskrona, Sweden.

TA (2011), *Terminal balancing valve for modulating control*, TA Hydronics, Industriestraße 9, Objekt 5, Postfach 45, AT-2353 Guntramsdorf.

TA (2013), *Electrical linear actuator MC15/24-C*, TA Hydronics, Industriestraße 9, Objekt 5, Postfach 45, AT-2353 Guntramsdorf.

Treichl, D. (2013), *Documentation Test Rig*, Graz University of Technology, Project MacSheep.

Trnsys (2010), *TRNSYS 17*, University of Wisconsin, 22 N Carroll St- Suite 370 Madison, WI 53703.

Zamana, L. (2010), *Heat Pump Compressors Overview*, Copeland, Emerson Climate Technologies.

SYMBOLS

Abbreviations

A	heat exchanger area [m ²]	NoC	number of channels
AI	analog input	NoP	Number of plates
a.m.	after modification	ODP	ozone depletion potential
AO	analog output	p	pressure [bar]
ASHP	air source heat pump	P	Power [kW]
b.m.	before modifications	\dot{Q}	heat transfer rate [kW]
BPM	brushless permanent magnet	rpm	rounds per minute
CHR	Chien Hrones Reswick	RTD	resistance temperature detector
COP	coefficient of performance [-]	s	empirical standard deviation
cp	specific heat capacity [kJ/kg·K]	SEC	superheat and envelope control
D	diameter [mm]	SH	space heating
DHW	domestic hot water	SPF	seasonal performance factor
DI	digital input	SZK	Summenzeitkonstantenmodell
DMS	dehnmessstreifen (pressure gauge)	t	temperature [°C]
DO	digital output	T	temperature [K]
ECO	economiser	Ta	compensation time [s]
EXV	expansion valve	TC	thermocouple [s]
f_{loss}	relative heat losses [%]	Tu	dead time [s]
FPGA	field programmable gate array	U	heat transfer coefficient [W/m ² K]
FSO	full scale output	v	specific volume [m ³ /kg]
GWP	global warming potential	\dot{V}	volumetric flow rate [m ³ /h]
h	specific enthalpy [kJ/kg·K]	VI	virtual instrument
HP	heat pump / high pressure	w/wo	with/without
h.c.	hydrocarbons	WT	Wendetangentenmodell
I	input	x	measurement result
K	gain factor	x_m	measured value
L	low pressure	x_{true}	true value of a measurement
\dot{m}	mass flow rate [kg/s]	x_0	arithmetic
MHSi	mobile heat sink	ΔT_{log}	logarithmic mean temperature difference [K]
MHSo	mobile heat source	Δx	measurement error
MID	magnetic inductive	Δx_{sys}	systematic measurement error
MP	medium pressure	Δx_{rand}	random measurement error
n	speed [rpm]		
NI	national instruments		

Subscripts

b	brine	loss	heat losses
C	cooling	N	nominal (diameter)
comp	compressor	r	refrigerant
cond	condenser	sat	saturated
desup	desuperheated	sup	superheated
el	electric	swept	swept volume of the compressor
ECO	economiser	vol	volumetric
evap	evaporation	w	water
H	heating	wodes	without desuperheater
inj	injection	woloss	without heat losses
is	isentropic		

Greek symbols

η	compressor efficiency [-]	π	pressure ratio [-]
μ	expected value	σ	standard deviation

LIST OF FIGURES

Figure 2-1: Functional principle of a compression heat pump (http://ecoairsystems.ie/heat-pumps/ , 21.04.2014).....	4
Figure 2-2: Schematic view of a compression heat pump (left) and an absorption heat pump (right) (Rieberer et al., 2009)	5
Figure 2-3: Reference cycle for the heat pump process (Rieberer et al., 2009)	6
Figure 2-4: Compression process in a scroll compressor (http://www.baulinks.de/webplugin/2012/0001.php4 , 22.04.2014)	10
Figure 2-5: Hourly values of the heating capacity: radiator (Pheat), HP in SH mode (PCondSH) and DHW mode (PCondDHW for ASHP Zur45; left: without speed control, right: with speed control. (Heinz et al., 2013a).....	11
Figure 2-6: Heat provided by the condenser with different inlet and outlet water temperatures; left: without speed control, right: with speed control (Heinz et al., 2013a).....	12
Figure 2-7: Comparison of the schematic view of a heat pump without- (left) and with ECO (right).....	13
Figure 2-8: Comparison of the heat pump process without (left) and with ECO (right) in a temperature- enthalpy diagram.....	13
Figure 2-9: Temperature-enthalpy diagram of the heat pump cycle with desuperheater	14
Figure 2-10: Block diagram of a control circuit (Görtler, 2010a)	15
Figure 2-11: Response characteristic of a PID controller (http://www.geltec.de , 26.03.2014) ...	16
Figure 2-12: Step response of control systems with and without compensation (Görtler, 2007)	17
Figure 2-13: WT model compared to the SZK model (Hengel, 2012).....	18
Figure 2-14: Linear propagation of uncertainty (Rieberer, 2013).....	22
Figure 3-1: Schematic view of the working fluid cycle of the heat pump (Heinz et al., 2013b)...	24
Figure 3-2: Front view of the heat pump prototype (Treichl, 2013).....	25
Figure 3-3: Copeland system configuration with system controller (Copeland, 2013d)	26
Figure 3-4: Copeland compressor with nomenclature (Copeland, 2011)	27
Figure 3-5: Cross section ZHW08 (Copeland, 2011)	28
Figure 3-6: Simulation of the compression process in the scroll compressor (http://www.youtube.com/watch?v=dsabYhhOko0 , 16.04.2014).....	28
Figure 3-7: Inverter cooling.....	29
Figure 3-8: SWEP plate heat exchanger counterflow (SWEP, 2010).....	30
Figure 3-9: Distribution pipe at the evaporator inlet before (left) and after the modifications (right).....	32
Figure 3-10: Filter dryer Danfoss DML083 structure	32
Figure 3-11: Electronic expansion valve (http://www.danfoss.com , 12.03.2014).....	33
Figure 3-12: Diameter of the connection (copper) pipes in the refrigerant cycle (mm)	34
Figure 3-13: Schematic layout of the mobile heating moped used as brine source.....	35
Figure 3-14: Schematic view of the sink side with water cycle and secondary heat exchanger.	36
Figure 3-15: Test rig layout with points of measurement (Heinz et al., 2013b).....	39
Figure 3-16 "Seebeck" effect used in thermocouples (Rieberer, 2013).....	40
Figure 3-17: Resistance thermometer structure and wiring (Rieberer, 2013) and (http://www.omega.com/pptst/F_Series.html , 16.04.2014).....	41
Figure 3-18: Absolut pressure sensor from PMR on the left, Copeland pressure sensor in the middle and differential pressure sensor from XMD on the right.....	42
Figure 3-19: Functional principle of a coriolis mass flow meter (Rieberer, 2013)	43

Figure 3-20: Measurement principle of a MID volumetric flow meter left (Rieberer, 2013) and Promag 50P right (Endress+Hauser, 2013a).....	44
Figure 3-21: NI system configuration for communication	45
Figure 3-22: User interface for controlling the heat pump test rig.....	47
Figure 4-1: Temperature-enthalpy diagram of the working fluid cycle with high pressure ratio..	51
Figure 4-2: Energy balance over the compressor	52
Figure 4-3: Theoretical points for the calculation of the isentropic efficiency in the temperature-enthalpy diagram.....	53
Figure 4-4: Temperature-enthalpy diagram of the evaporation in the heat exchanger	58
Figure 4-5: Temperature-enthalpy diagram of the condensing process in the heat exchanger .	60
Figure 5-1: Compressor losses for different speeds depending on the pressure ratio.....	65
Figure 5-2: Compressor losses for different speeds depending on the compressor outlet temperature.....	66
Figure 5-3: Overall isentropic efficiency as a function of the pressure ratio for different compressor speeds	67
Figure 5-4: Overall isentropic efficiency for different speeds and three different operating points	68
Figure 5-5: Overall isentropic efficiency for the whole compressor performance map.....	69
Figure 5-6: Volumetric efficiency for different compressor speeds.....	69
Figure 5-7: Volumetric efficiency for different operating points and pressure ratios	70
Figure 5-8: Volumetric efficiency for different operating points with different speeds	71
Figure 5-9: Comparison of the compressor losses as a function of the pressure ratio for three different speeds.....	72
Figure 5-10: Compressor outlet temperature as a function of the pressure ratio for three different speeds with a brine inlet temperature in the evaporator of 2 °C.....	73
Figure 5-11: Mass flow as a function of the pressure ratio for two different compressor speeds	73
Figure 5-12: Isentropic efficiency for different operating points and different speeds with- and without ECO.....	74
Figure 5-13: Overall isentropic efficiency as a function of the pressure ratio for different speeds with- and without ECO.....	75
Figure 5-14: Volumetric efficiency for different compressor speeds and different pressure ratios with- and without ECO.....	76
Figure 5-15: HP process in the temperature-enthalpy diagram for an operating point with -10 °C brine inlet- and 30 °C water inlet temperature.....	77
Figure 5-16: UA for three different operating points with different speeds and therefore heating capacity for the condenser HX with 40 plates and 30 plates.....	78
Figure 5-17: Reduction of the ΔT in the pinch point between condensation temperature and water temperature	79
Figure 5-18: Condensation temperature reduction after condenser change.....	80
Figure 5-19: Comparison of the evaporation process for two different operating points	80
Figure 5-20: Change in the evaporation temperature after modifications.....	81
Figure 5-21: COP before and after the modifications for equal operating points	83
Figure 5-22: COP as a function of the pressure ratio for different operating points.....	84
Figure 5-23: COP as a function of the compressor speed for different operating points.....	85
Figure 5-24: COP for different compressor speeds as a function of the pressure ratio	86

Figure 5-25: COP of all compared operating points with- and without ECO as a function of the pressure ratio (overall exponential trend)	87
Figure 5-26: COP of all compared operating points with- and without ECO as a function of the pressure ratio (polynomial trend for each operating point with different speeds).....	87
Figure 5-27: COP with- and without ECO for different speeds and different water inlet temperatures (20/30/50) to the condenser, as a function of the pressure ratio	88
Figure 5-28: Compressor input power with- and without ECO for different speeds and different water inlet temperatures (20/30/50) to the condenser, as a function of the pressure ratio	89
Figure 5-29: Heating capacity with- and without ECO for different speeds and different water inlet temperatures (20/30/50) to the condenser, as a function of the pressure ratio	89
Figure 5-30: Influence on the COP of different water mass flow rates over the desuperheater for three different operating points and a compressor speed of 5400 rpm	91
Figure 5-31: Decrease of the condensation temperature for three different operating points as a result of the increased HX area with the use of the desuperheater	92
Figure 5-32: Enthalpy difference from desuperheating the refrigerant compared to the enthalpy difference from condensing in the condenser	93
Figure 5-33: Comparison of two different operating points with desuperheater (left: $t_{w1} = 30\text{ °C}$ $t_{b1} = 2\text{ °C}$; right $t_{w1} = 30\text{ °C}$ $t_{b1} = -15\text{ °C}$)	94
Figure 5-34: Comparison of two different operating points with desuperheater (left: $t_{w1} = 30\text{ °C}$ $t_{b1} = 2\text{ °C}$; right $t_{w1} = 30\text{ °C}$ $t_{b1} = -15\text{ °C}$)	94
Figure 5-35: Comparison of two different operating points with desuperheater (left: $t_{w1} = 30\text{ °C}$ $t_{b1} = 2\text{ °C}$; right $t_{w1} = 30\text{ °C}$ $t_{b1} = -15\text{ °C}$)	94
Figure A-1: Pattern for connecting the recycle device for evacuation.....	A-1
Figure A-2: Pattern for connecting the recycle device for filling.....	A-3
Figure A-3: Swagelok-Fitting for installation of the thermocouples.....	A-5
Figure A-4: Accuracy of the MID flow meter 50P DN15 (Endress+Hauser, 2013a).....	A-6

LIST OF TABLES

Table 2-1: Properties of R-410a compared to other refrigerants (Jakobs, 2010).....	8
Table 2-2: Difficulty of controlling a system (Görtler, 2010a).....	18
Table 2-3: Chien Hornes Reswick parameterization (Görtler 2007).....	19
Table 3-1: Specifications of the used brazed plate heat exchangers (SWEP, 2013).....	30
Table 3-2: Measuring points and sensor properties on the test rig (Heinz et al., 2013b).....	38
Table 3-3: Description of the different I/O Modules.....	46
Table 3-4: Control circuit overview	49
Table 3-5: Final parameters calculated by CHR	50
Table 5-1: Maximum error for three measurement matrices	95
Table A-1: Configuration of the I/O modules.....	A-9
Table A-2: Overview of all measurement points taken for the compressor evaluation	A-11
Table A-3: Measurement matrix for cycle evaluation	A-14
Table A-4: Measurement matrix for the evaluation of the influence of the economiser	A-16
Table A-5: Measurement matrix for the evaluation of the cycle performance with desuperheater	A-18

APPENDIX

A-1 Filling and evacuating the heat pump

A-1.1 Recycling of the refrigerant

This should be a short summary of points which have to be considered if the heat pump cycle has to be evacuated. Because it often happens that a modification at a prototype has to be made, it is important to recycle the refrigerant to reuse it after the changes on the test rig are made. For this test rig the recycle device UKR 60/6 was used to exhaust the working fluid from the cycle. The instruction manual of this device contains detailed information about how to use it. This instruction will contain references to the instruction manual which is enclosed to the device (FLICA, 1990).

Connecting the recycling device

The recycling device UKR 60/6 has to be connected to the refrigerant cycle and the recycle flask. An armature with pressure indication is used to connect the recycling device to the refrigerant cycle. Figure A-1 shows the structure of the system.

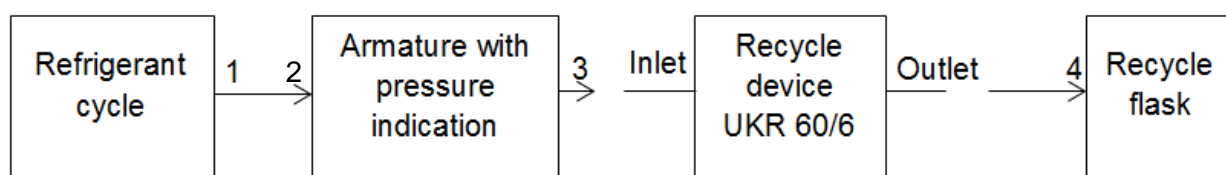


Figure A-1: Pattern for connecting the recycle device for evacuation

First of all the armature has to be connected to the refrigerant cycle, for this the valve at the liquid receiver is used. The armature has to be closed. First the armature has to be connected to the pipe (2) then to the valve of the refrigerant cycle (1). If no special connector for fast clipping is available, gloves have to be worn while connecting the pipe to the valve! During connecting the pipe a small amount of refrigerant escapes and because of the expansion of the working fluid it cools down, which can lead to icing of arms and fingers. Next step is to connect the armature (3) to the inlet of the recycling device. Then the outlet of the recycling device has to be connected with the recycling flask (4). Everything has to be tight except the connections for flushing the pipes (step 2).

Recycling of the refrigerant

First of all the pipes have to be flushed to assure, that there is no air in the pipes left and so only refrigerant comes into the recycling flask. The valve at the armature has to be slowly opened till a small amount of refrigerant comes out at the end of the connection pipe. Then the connection has to be closed immediately. This ensures that there is no air left in the pipes. This also has to be repeated for the pipe between recycling device and recycling flask. Before starting the recycling the magnetic and the expansion valves of the working fluid cycle should be opened, in this test rig this was done with LabVIEW. Then the UKR 60/6 can be used to get the refrigerant out of the heat pump cycle and into the recycling flask. A more detailed description how to do that can be found in the instruction manual. There are three different switch positions. First the

switch is put on position one. The liquid refrigerant flows through the recycling device as long as the pressure in the heat pump cycle is higher than in the recycling flask. After equalization of pressure in about 90 seconds the switch can be put in position two. The device increases the pressure in the working fluid cycle and pumps the rest of the liquid refrigerant in the recycling flask. After all the liquid refrigerant has passed to the recycling flask the control light (meaning of control lights see instruction manual) indicates to put the switch in position three. In this position the gaseous refrigerant is pumped into the recycling flask. The device stops when the absolute pressure drops below 1.1 bar that no air enters the refrigerant cycle. A switch at the front side of the device can be turned to keep on with the evacuation till 0.4 bar in the refrigerant cycle. With the pressure indicators on the test rig or the armature can be determined when the refrigerant cycle is completely empty. An even better way is to weight the recycling flask during the process. If the weight does not increase anymore the process can be stopped. Before the process is stopped it is important to close the recycling flask first that the refrigerant does not escape after the evacuation. Then the recycling device can be shut off and the pipes can be detached. It helps to close both valves on the connection pipes of the recycling device because some refrigerant stays in the pipes. After these steps the test rig is ready for modification and the refrigerant can be used again.

A-1.2 Filling of the refrigerant cycle

The next steps describe what has to be done if heat pump should be filled with refrigerant. This includes a pressure test to assure that there is no leak in the cycle, the evacuation to remove all air and moist which is left in the system and the filling of the heat pump with the refrigerant.

First of all it has to be assured that there is no leak in the system after the modification. For that the heat pump is filled with nitrogen. The pressure depends on the used components in the cycle. In this case a pressure of 30 bar was used after the low pressure switch was removed. If the low pressure switch is removed a second pressure test has to be made after connecting the low pressure switch again, with 15 bar in this case. A special fluid can be used to search for leaks called leakfinder. If it is sprayed on the brazed point with the leak bubbles arise. After all obvious leaks are closed the heat pump should be at least a whole day under pressure to see if the pressure level stays constant.

After the pressure test is done the heat pump has to be evacuated to remove all air and moist out of the heat pump cycle. Before starting the expansion- and the solenoid valves have to be opened. The connection valve at the high pressure liquid receiver should be used for evacuation because it also has to be used for filling. A vacuum pump is needed for the evacuation. The pump should evacuate for at least two to three hours. The lowest pressure level is reached much faster but it is done to get the whole moist out of the system. For the connection of the vacuum pump the armature used for the evacuation should already be used (Figure A-2). Before shutting down the vacuum pump the inlet of the armature is closed and with that it is ensured that no air enters the refrigerant cycle. The second possibility is to use a special valve (fast coupling) at the inlet of the heat pump where the pipe only has to be plugged in and nothing escapes. This is strongly recommended for both, the evacuation and the filling (Figure A-2).

After evacuating the heat pump cycle it can be started with the filling. Figure A-2 shows the structure of the filling system.

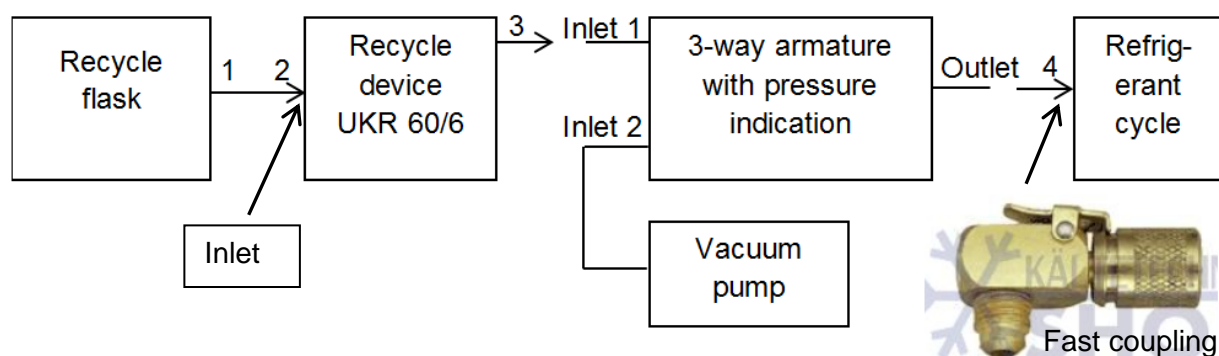


Figure A-2: Pattern for connecting the recycle device for filling

The recycling device is used in the same way as for the recycling of the refrigerant with the only difference that now the refrigerant is pumped from the recycling flask into the system. The recycling flask is connected to the recycling device inlet. The outlet of the recycling device is connected with the second inlet of the 3-way armature. The outlet should still be connected to the refrigerant cycle after the evacuation. Before the filling can be started the tubes have to be flushed with refrigerant. Then the recycling device should be put on switch position one which means pressure equalization between the recycling flask and the heat pump cycle. The 3-way armature should be still closed. Then the tube from the recycling device to the 3-way armature can be opened a bit just to fill the tubes with refrigerant and push out the air. Then the fitting should be closed fast. Then everything is prepared for filling the heat pump cycle.

The refrigerant has to be filled in liquid line into the cycle. For that it is important that the recycling flask is upside down. Secondly the expansion valves have to be closed that the refrigerant does not completely fill the low pressure side which would make it impossible for the compressor to start. The recycling device should still be in position one. Now the refrigerant can be slowly filled by opening the 3-way armature, slowly because of icing in case of a fast expansion of the whole refrigerant. After it is not possible to fill anymore the expansion valves can be opened 10% for a short time that the refrigerant can also flow into the low pressure side of the heat pump. If the whole liquid refrigerant is filled the recycling device can be put in position 2 and 3 like described before to get the gaseous refrigerant from the recycling flask into the heat pump cycle. A scale is used during the whole filling to determine how much refrigerant entered the heat pump cycle. If there is not enough refrigerant in the recycling flask, the flask has to be changed and then the missing amount filled. After the filling the devices are disconnected by opening the fast coupling. If there is no fast coupling available it cannot be prevented to lose a small amount of refrigerant during screwing off the tube to the valve at the liquid receiver.

It is also possible to fill the cycle without using the recycling device. The pressure is higher in the recycling flask and therefore most of the refrigerant passes to the heat pump cycle without the device, the pressure in the recycling flask can be additionally increased by heating it up. But this does not empty the flask fully, some of the refrigerant remains in the flask, this is why the recycling device should be used.

A-2 Considerations for installation

A-2.1 Test rig components

Scroll Compressor – Emerson ZHW08K1P-1E9-622

It is important to read the whole manual before installing the compressor, this paragraph only sums up the most important information. The compressor partly operates in natural frequencies. This leads to strong movement of the compressor and loud noise. The movements need to be absorbed by installing U-turns into the pipe routing. These U-turns make the connection more flexible and therefore are protecting the fixed braze or screw connections. Furthermore it was decided to install Swagelok-Fittings at the inlet and outlet ports of the compressor, to be able to switch the compressor more easily (2 compressors were delivered by Copeland). The plugs of the compressor are only allowed to be opened for a short time before starting the heat pump. The oil of the compressor is hygroscopic and therefore it absorbs the humidity of the air, leading to a change of the characteristics of the oil. When brazing the connection ports, the compressor inlet-ports need to be cooled (for example with wet cloth) as there are O-rings at the inside of the ports. Furthermore the pipes have to be flushed with nitrogen to prevent the formation of tinder and other reactions with the air. The inverter and the filter provide current and voltage for the compressor. These parts need to be cooled as a maximum temperature of 90°C must not be exceeded. This is realised, by guiding the condenser inlet piping over these two components. The water temperature varies between 20-50°C. The SEC is connected to 3 pressure transmitter (differential to ambient pressure), 3 temperature sensors (NTC) and the 2 expansion valves, whereby the temperature sensors are mounted as surface contact sensor. (Copeland, 2011)

Heat exchanger

For installation it is important to follow the manual. There are different configurations depending if the heat exchanger is used as condenser or evaporator or one phase applications. A small arrow on the front plate shows which port is which because the heat exchangers look symmetric. The manual recommends to install the refrigerant on the left side (when the arrow points upwards) as there is one channel more than on the right side. So the refrigerant is enclosed by the other fluid, in this case water or glycol/water-mixture. There are all kinds of ports available. Ports for brazing and welding should be chosen, if no exchange of the heat exchanger is considered and the possibilities of leakage shall be minimized. Ports for screw connections have a higher risk of leakage, though they ensure easier dismounting. Screw connections for copper pipes need to be realised by pipe screwing (Swagelok-Fitting), this can be expensive if it is not a standard dimension. (SWEP, 2010)

Filter dryer

The filter dryer is hygroscopic, so it should be closed as long as possible, that the filter dryer does not absorb the humidity of the air. The manual recommends exchanging the filter dryer every time after there has been a modification in the refrigerant cycle. One check valve including a schrader valve is positioned before and one after the filter dryer. Therefore, the filter dryer can be changed easily by closing the circuit before and after the dryer. According to the manufacturer it is no problem if the indication was already in contract with air humidity. When the system is dry, the indicator shows this. (Danfoss, 2005)

Expansion valves

Copeland recommends a straight pipe routing with a maximum length of 200 mm from the expansion valve to the heat exchanger inlet (evaporator/economiser). The valve cannot control the superheating exactly if it is influenced by gas, so it has to be ensured that only liquid refrigerant enters the expansion valve. Further guideline for placing the temperature sensors are in the manual for the heat exchangers (SWEP, 2010).

Pipes

It always has to be checked what kinds of copper-fittings (T-piece, reduction, bows, etc.) are needed for the individual pipe-section. This makes it much easier for the brazing, as it is not needed to search the single components, what is very time-consuming.

A-2.2 Measurement devices

Thermocouples

In the beginning the TC were installed with a Swagelok-Fitting, called Reducer (Figure A-3). After changing some of the TC the new ones were directly brazed in the cycle.

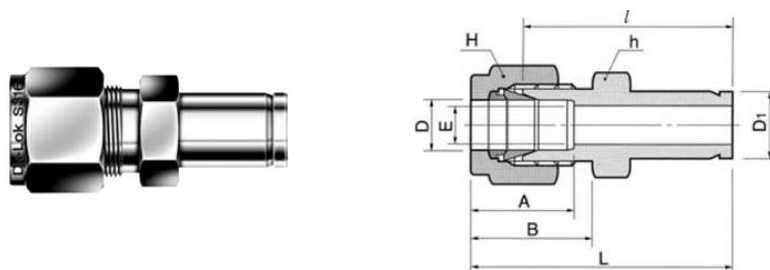


Figure A-3: Swagelok-Fitting for installation of the thermocouples

For the first option the tube is brazed to the refrigerant cycle (Figure A-3, right end) and on the other side, a male connector with a borehole of 3 mm outer diameter is chosen. The TC are brazed into a capillary pipe (outer diameter 3 mm, inner diameter 1.7 mm). With a tapered lock ring the connection is tightened. So no harm is done to the TC and it is possible to dismount the temperature sensor easily. Another possibility is to braze them directly into the cycle. Here, no T-pieces are needed and with that no additional fitting. Though, for dismounting, the TC needs to be brazed out of the cycle, leading to additional work that can only be done by special personnel. The reason why later on the TC were brazed directly into the cycle is that making modifications on the refrigerant cycle already includes a lot of work, mainly the evacuating of the test rig, the modifications itself, the pressure tests and the refill. So the time savings with the Swagelok-Fitting is rather small.

Pt100 resistance thermometer

The Pt100 are screwed to the cycle with Swagelok-Fittings with a 3 mm borehole. A lock ring made of Teflon is used for sealing. In the water and brine cycle the fast replaceability is a big advantage.

NTC resistors

For all surface contact temperature sensors, heat sink paste is used when the sensor is mounted on the pipe. The sensors should be insulated to minimize the influence from the environment.

Coriolis mass flow meter

This sums up the main points which are more detailed in the manuals for the mass flow meter Promass 83A DN04 (Endress+Hauser, 2013b) and the Promass 83F DN08 (Endress+Hauser, 2013b). The error of measurement depends on the mass flow and increases with lower mass flow. The function looks similar to Figure A-4, but with a better accuracy. The worst accuracies, which were reached with the lowest mass flows of all measurement points, were 0.3 % for the Promass 83F and Promass 83A. Subsequent are the most important points which have to be considered for the positioning:

- Do not put the device on the highest level of a pipe
- Do not put the device before a vertical or an open pipe
- Do not put the device into the suction line of a pump
- Do not stabilize the device at the housing
- No inlet or outlet length has to be considered compared to the MID measuring devices

MID volumetric flow meter

More accurate information can be found in the manual (Endress+Hauser, 2013a) but this is a summary of the most important points for the installation: The minimum inlet length, which should be a straight tube, should be at least $5 \cdot DN$, the minimum outlet length should be at least $2 \cdot DN$. The recommended flow rate is between 0.3 and 10 m/s whereby the accuracy increases with the flow speed, which can be seen in Figure A-4 (dotted line). The flow meter is dimensioned for a volumetric flow rate of 4 to 100 dm³/min for a diameter of 15 mm.

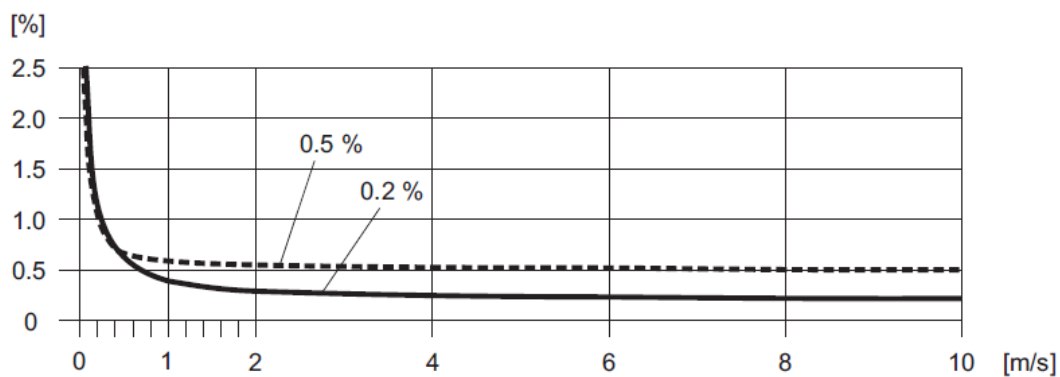


Figure A-4: Accuracy of the MID flow meter 50P DN15 (Endress+Hauser, 2013a)

The next list consists of some remarks for the positioning of the MID flow meter:

- Do not put the device on the highest level of a pipe
- Do not put the device before a vertical or an open pipe
- Do not put the device in the suction line of a pump
- Do not stabilize the device at the housing

Power consumption

In the beginning the power was measured with the transducer IME TM8P03120. This electric meter needs a measuring transformer which has, in this case, an accuracy of $\pm 3\%$. After significant deviations in the measured power with the pulse counter compared to the transducer, the more accurate pulse counter was used for further power measurements.

A-2.3 Calibration

Temperature sensors

Temperature sensors have different ranges of accuracy. Pt100 are more accurate than TC. The accuracy also differs within the product due to deviations in production. Therefore all temperature sensors need to be calibrated before installation. Both, Pt100 and TC have a linear dependency on the temperature (the linearity is approximated but it reflects the reality sufficiently). So the sensors are put in an environment with a constant temperature and are compared to a sensor that is gauged with a higher accuracy than the calibrated sensors need to be. At least two different temperatures need to be analysed to get the linear dependency, whereby a higher number of calibration points is preferable. The number of analysed temperatures also depends on the measuring range for which the sensor should be calibrated.

Equipment:

- Low-temperature thermostat (e.g. LAUDA RE310)
- Reference temperature sensor (e.g. Dostmann T900 with Pt100)

Procedure:

The thermostat keeps the temperature of the fluid inside at a constant level and has a cooling and a heating unit installed. It operates with desalted water for temperatures between 1 °C and 95 °C and with isopropanol for temperatures between -40 °C and 0 °C.

First of all it has to be determined in which measuring range the sensor should work. The isopropanol is not needed if the sensor does not have to measure temperatures less than 0 °C. If this is needed two thermostats have to be used parallel. Furthermore the pipe, which is used by the pump for the circulation of the isopropanol, has to be isolated because else it comes to icing at the outside of the tube which leads to unwanted heat input. If more than three temperature levels have to be used for calibration it is recommended to use two thermostats parallel. This saves some time as the thermostat needs a few minutes until it keeps the new temperature at a constant level.

The temperature sensors need to be wired and logged the same way as they are in the final set-up at the calibration. With this, the inaccuracy of the sensor itself, the wiring and the logging device are measured at the same time and can be minimized at once. The sensors always have to be calibrated at the same time. They have to be fixed together with a cable fixer, whereby the front of the sensors should be as close together as possible (length where the temperature is measured is about 3 mm for Pt100 and only a point for TCs). Within this bundle, the reference sensor should be in the middle. It has to be ensured that all fronts are at the same height in the middle of the thermostat as there are also temperature layers in the thermostat.

If possible, the signal of the reference sensor should be logged. For the Dostmann T900 an AI 0-10 V port is needed. When doing this, it is recommended to scale the signal for the wanted temperature range for a better resolution (e.g. when measuring at 20 °C, scale the signal from 19 to 21 °C). If logging is not possible, the value that is shown on the display has to be noted every minute (or every 30 seconds) and the mean value of these figures has to be calculated for the reference temperature. It is important that only stationary points are used for the calibration.

After all this work is done the calibration starts with one of the measuring points. The values of the sensors, which have to be calibrated, have to be recorded as well as the reference sensor for at least 2 minutes. Then the average of the recorded values has to be calculated. This has to be done for all calibration points, which will be the start and the end of the calibration range and some points in between. After all the data is taken, a compensation line has to be calculated from the difference between the values of the calibrated sensor and the reference sensor. For example Microsoft Excel can be used, the function RGP delivers the calibration factors ($k = \text{pitch}$ and $d = \text{offset}$). With this factors the new accuracy of the calibrated sensors can be determined, which is needed to know the measurement error. This was 0.02 K for the Pt100 and 0.18 K for the TC for this calibration, whereby most of the points were much more accurate.

One thing which is pointed out here is to be careful if it is the first calibration of the temperature sensor or if one of them gets replaced and the new one has to be calibrated again. If a sensor is replaced it is important not to forget to delete the old calibration line out of the system before starting the calibration! Else the calibrated old sensor is calibrated again and when the linear coefficients are replaced with the new ones the results are wrong. So it is important to calibrate the sensor without a calibration line deposited before.

Pressure sensor calibration

The calibration of the three absolute pressure sensors was done with a gauged reference sensor from VEGA type VEGABAR 52 with a measuring range from 0 to 60 bar. Each of the three absolute pressure sensors was calibrated individually because each of them has a different measuring range. Three measurement points were taken for each sensor. The low pressure sensor PE_r1 was calibrated between 5.8 and 20 bar, the medium pressure level sensor PE_r7i between 10 and 30 bar and the high pressure level sensor PE_r2 was calibrated between 20 and 50 bar. Both, the reference sensor and the sensor for calibration were connected to the same capillary tube where the pressure level for measuring was applied.

The further procedure is similar to the calibration of the temperature sensors. After all the values were recorded for the three calibration points of each sensor, the average of each measuring point was calculated. Then again a compensation line was determined with the difference of the measured values of the reference sensor and the sensors which had to be calibrated. The calibration factors were calculated and logged into the LabVIEW program, which reads the data from the sensors. The error of measurement before the calibration was up to 0.3 % of the measured value. This was reduced to an error of measurement of only 0.02 % after the calibration.

Mass flow meter calibration

The flow meters which are three MID volumetric flow meter and two coriolis flow meter were calibrated by measuring the weight of a container, which was filled over time. For the calibration a high-precision balance from Mettler Toledo type KC 120 with an accuracy of ± 5 g was used. Both the MID and the Coriolis devices were calibrated over three points. The MID measurement devices were calibrated from 200 kg/h to 800 kg/h and the Coriolis from 15 kg/h to 100 kg/h. First the time of filling a specific mass of water into the container was recorded with a stop watch. The stopped time for filling the container was approximately five minutes for every calibration point. Then the average mass flow was calculated. The container was filled again for every device which had to be calibrated with the same mass flow and exactly the same time. The measured mass flows and volumetric flows of the measurement devices were recorded and the average was calculated. The measuring points were 200, 600 and 800 kg/h for the MID and 15, 50 and 100 kg/h for the coriolis measurement devices. After the measurements the compensation lines were calculated in the same way as for the temperature and pressure sensors and logged into the LabVIEW file for recording the measured values. The deviation from the reference could be reduced to 0.2 % for the MID volumetric flow devices and to 0.3 % for the coriolis mass flow meter whereby this value is for a mass flow of 15 kg/h, which is lower than reached in any operating points.

A-3 Configuration of the Input and Output modules

The following Table A-1 shows the configuration of the I/O modules for the data acquisition and controlling described in chapter 3.5.1. For the designation of the different sensors is referred to chapter 3.4.

Table A-1: Configuration of the I/O modules

Module 1 (NI 9375)		Module 6 (NI 9213)	
I/O Nr.	Periphery	I/O Nr.	Periphery
DI (0)	Electric meter whole system (kWh)	TC (0)	TE_r1
DI (1)	Electric meter compressor (kWh)	TC (1)	TE_r2
DI (2)	SEC alarms	TC (2)	TE_r3
DI (3)	SEC components status	TC (3)	TE_r4
DO (1)	Solenoid valve main cycle	TC (4)	TE_r5
DO (2)	Solenoid valve injection cycle	TC (5)	TE_r6
Module 2 (NI 9871)		TC (6)	TE_r7
LAN	All SEC data (Modbus)	TC (7)	TC (7)
Module 3 (NI 9208)		TC (8)	TE_r9
AI (0)	PDE_r1	TC (9)	TE_r7i
AI (1)	PDE_r3	TC (10)	TC (10)
AI (2)	PDE_r4	TC (11)	TE_r10
AI (3)	PDE_r5	TC (12)	TE_r11
AI (4)	PDE_r7i	TC (13)	T_amb
AI (5)	PDE_r9	Module EC 1 (NI 9375)	
		DO (0)	Enable pump sink

List of tables

AI (6)	PE_r2	DO (1)	Enable pump source
AI (7)	PE_r7i	DO (2)	Enable pump system
AI (8)	PE_r1	DO (3)	Enable pump heating moped
AI (9)	FE_r5	DO (4)	Enable heating rod 1
AI (10)	FE_r7	DO (5)	Enable heating rod 2
AI (11)	IME		
Module 4 (NI 9217)		Module EC 2 (NI 9265)	
		AO (0)	Control heating rod 1
RTD (0)	TE_b1	Module EC 3 (NI 9263)	
RTD (1)	TE_b2	AO (0)	Control pump sink
RTD (2)	TE_d1	AO (1)	Control pump source
RTD (3)	TE_d2	AO (2)	Control pump system
		AO (3)	Control valve desuperheater
Module 5 (NI 9217)		Module EC 4 (NI 9208)	
RTD (0)	TE_w1	AI (0)	FE_w4
RTD (1)	TE_w2	AI (1)	FE_b1
RTD (2)	TE_c1	AI (2)	FE_w5
RTD (3)	TE_c2		

A-4 Measurement matrixes for compressor and cycle evaluation

This chapter includes all measurement points, which were you used in this thesis for the evaluation. For all points the volumetric flow of the brine on the source side was 1178 l/h and the volumetric flow of the water on den sink side was 857 l/h.

A-4.1 Measurement matrix for the compressor evaluation

Table A-2 shows all measurement points, which were used for the evaluation of the compressor performance.

List of tables

Table A-2: Overview of all measurement points taken for the compressor evaluation

Compressor speed	Brine inlet temperature	Water inlet temperature	Evaporation temperature	Condensing temperature	Electric power input	Compressor losses	Isentropic efficiency (Overall)	Volumetric efficiency	Cooling capacity	Heating capacity	Cycle performance (COP)	Error of measurement (COP)
[rpm]	[°C]	[%]	[°C]	[°C]	[kW]	[%]	[-]	[-]	[kW]	[kW]	[-]	[%]
2100	-10	20	-14.20	23.92	0.58	14.5	0.520	0.830	1.90	2.32	3.96	1.04
2100	-10	30	-14.00	33.75	0.74	14.0	0.519	0.805	1.80	2.30	3.12	1.01
2100	-10	50	-13.55	53.25	1.14	16.0	0.480	0.766	1.63	2.29	2.02	0.97
2100	2	20	-3.20	25.49	0.58	9.9	0.537	0.879	2.60	3.12	5.40	0.93
2100	2	30	-3.08	35.15	0.75	10.4	0.556	0.855	2.50	3.08	4.12	0.90
2100	2	50	-2.79	54.75	1.21	12.3	0.519	0.812	2.25	3.04	2.52	0.86
2100	12	20	5.65	26.74	0.55	10.1	0.512	0.914	3.27	3.79	6.90	0.89
2100	12	30	6.05	36.81	0.74	9.4	0.575	0.898	3.22	3.85	5.19	0.84
2100	12	50	6.48	56.12	1.31	11.6	0.511	0.836	2.87	3.76	2.88	0.79
2400	-10	20	-14.71	24.43	0.66	11.1	0.541	0.843	2.16	2.64	3.99	0.96
2400	-10	30	-14.59	34.33	0.83	12.5	0.549	0.826	2.08	2.63	3.18	0.94
2400	-10	50	-13.98	53.82	1.28	13.7	0.496	0.775	1.88	2.66	2.07	0.90
2400	2	20	-3.82	26.32	0.66	7.7	0.561	0.891	2.95	3.55	5.34	0.87
2400	2	30	-3.50	36.09	0.86	8.4	0.579	0.867	2.85	3.53	4.12	0.84
2400	2	50	-3.26	55.49	1.36	10.6	0.537	0.819	2.55	3.50	2.56	0.81
2400	12	20	5.38	27.81	0.63	7.4	0.545	0.926	3.73	4.30	6.85	0.84
2400	12	30	5.47	37.90	0.85	7.9	0.602	0.903	3.69	4.39	5.15	0.80
2400	12	50	5.85	57.09	1.45	12.8	0.549	0.854	3.29	4.29	2.95	0.76
3000	-10	20	-15.46	25.67	0.83	12.4	0.569	0.862	2.72	3.28	3.94	0.87

List of tables

3000	-10	30	-15.37	35.33	1.03	14.5	0.574	0.840	2.63	3.28	3.20	0.85
3000	-10	50	-14.71	54.75	1.59	10.8	0.513	0.786	2.37	3.37	2.12	0.81
3000	2	20	-4.77	27.73	0.85	5.2	0.583	0.897	3.60	4.39	5.14	0.80
3000	2	30	-4.57	37.55	1.08	6.7	0.605	0.875	3.47	4.37	4.04	0.78
3000	2	50	-4.20	56.48	1.68	7.9	0.566	0.832	3.11	4.38	2.61	0.75
3000	12	20	4.05	29.65	0.86	6.1	0.570	0.928	4.64	5.44	6.32	0.77
3000	12	30	4.32	39.41	1.10	6.3	0.624	0.909	4.46	5.41	4.92	0.74
3000	12	50	4.80	58.12	1.77	6.4	0.581	0.858	3.96	5.35	3.02	0.71
3600	-10	20	-16.13	26.63	1.03	9.9	0.568	0.860	3.15	3.90	3.80	0.80
3600	-10	30	-15.89	36.47	1.25	8.9	0.580	0.839	3.04	3.92	3.14	0.79
3600	-10	50	-15.61	55.77	1.92	9.2	0.521	0.793	2.76	4.06	2.11	0.75
3600	2	20	-6.03	28.97	1.06	4.9	0.590	0.894	4.08	5.11	4.82	0.76
3600	2	30	-5.88	38.75	1.33	5.9	0.612	0.875	3.93	5.12	3.86	0.74
3600	2	50	-5.41	57.46	2.03	7.1	0.573	0.836	3.55	5.19	2.56	0.71
3600	12	20	2.65	31.06	1.09	5.2	0.584	0.924	5.25	6.33	5.83	0.73
3600	12	30	2.78	40.67	1.37	6.2	0.630	0.905	5.00	6.29	4.61	0.71
3600	12	50	3.38	59.30	2.11	6.3	0.607	0.866	4.48	6.30	2.98	0.69
4200	-10	20	-16.98	27.64	1.22	7.3	0.572	0.861	3.59	4.47	3.68	0.76
4200	-10	30	-16.68	37.42	1.48	7.4	0.582	0.840	3.45	4.52	3.06	0.75
4200	-10	50	-16.49	56.64	2.27	8.4	0.524	0.798	3.08	4.72	2.08	0.72
4200	2	20	-7.28	30.01	1.28	5.5	0.593	0.897	4.55	5.82	4.54	0.72
4200	2	30	-7.21	39.68	1.58	6.1	0.613	0.877	4.36	5.82	3.67	0.71
4200	2	50	-6.63	58.32	2.39	6.9	0.576	0.839	3.94	5.97	2.50	0.69
4200	12	20	1.15	32.38	1.33	5.0	0.595	0.925	5.77	7.17	5.40	0.70
4200	12	30	1.41	41.89	1.65	5.5	0.634	0.907	5.50	7.16	4.35	0.69
4200	12	50	1.98	60.27	2.51	6.0	0.612	0.871	4.92	7.21	2.88	0.67
4500	-10	20	-17.41	28.03	1.31	6.9	0.573	0.863	3.77	4.75	3.61	0.75
4500	-10	30	-17.28	37.60	1.59	7.5	0.580	0.842	3.62	4.77	3.01	0.74

List of tables

4500	-10	50	-17.01	56.97	2.43	8.0	0.525	0.800	3.15	5.03	2.07	0.71
4500	2	20	-7.83	30.50	1.39	5.3	0.594	0.898	4.77	6.16	4.42	0.71
4500	2	30	-7.69	40.17	1.72	6.0	0.613	0.879	4.58	6.18	3.60	0.70
4500	2	50	-7.13	59.02	2.59	6.7	0.577	0.840	4.12	6.35	2.46	0.68
4500	12	20	0.63	32.98	1.46	4.7	0.597	0.926	6.04	7.62	5.23	0.69
4500	12	30	0.78	42.48	1.79	5.4	0.635	0.909	5.75	7.58	4.23	0.68
4500	12	50	1.41	60.66	2.70	6.1	0.615	0.873	5.16	7.62	2.82	0.67
4800	-10	20	-17.94	28.35	1.41	7.2	0.572	0.865	3.98	4.99	3.54	0.74
4800	-10	30	-17.72	38.14	1.73	8.6	0.576	0.845	3.78	5.06	2.93	0.72
4800	-10	50	-17.56	57.18	2.60	8.4	0.524	0.800	3.25	5.34	2.05	0.70
4800	2	20	-8.28	31.05	1.51	5.3	0.593	0.899	4.99	6.51	4.30	0.70
4800	2	30	-8.30	40.64	1.85	8.1	0.614	0.883	4.82	6.48	3.50	0.69
4800	2	50	-7.68	59.22	2.76	6.2	0.577	0.839	4.30	6.73	2.44	0.68
4800	12	20	-0.04	33.48	1.58	4.9	0.599	0.927	6.28	8.01	5.06	0.68
4800	12	30	0.18	43.02	1.94	5.2	0.635	0.910	5.99	8.01	4.12	0.67
4800	12	50	0.86	60.75	2.89	5.9	0.613	0.872	5.37	8.10	2.81	0.65
5400	-10	20	-18.86	29.15	1.63	7.7	0.566	0.864	4.28	5.49	3.38	0.72
5400	-10	30	-18.65	38.86	1.98	7.4	0.569	0.842	4.02	5.60	2.83	0.70
5400	-10	50	-18.51	57.82	2.96	9.7	0.520	0.796	3.31	5.93	2.00	0.68
5400	2	20	-9.43	31.91	1.75	6.0	0.591	0.900	5.38	7.13	4.07	0.69
5400	2	30	-9.15	41.75	2.16	7.4	0.604	0.881	5.20	7.20	3.33	0.67
5400	2	50	-8.66	59.66	3.11	7.1	0.577	0.839	4.61	7.42	2.38	0.66
5400	12	20	-1.15	34.53	1.85	4.7	0.601	0.927	6.75	8.79	4.76	0.67
5400	12	30	-0.85	44.10	2.26	5.3	0.631	0.910	6.44	8.82	3.91	0.66
5400	12	50	-0.13	61.52	3.29	5.9	0.611	0.868	5.75	8.93	2.71	0.65

A-4.2 Measurement matrix for the cycle evaluation

Table A-3 shows all measured points, which were used for the cycle evaluation.

Table A-3: Measurement matrix for cycle evaluation

Compressor speed	Brine inlet temperature	Water inlet temperature	Evaporation temperature	Condensing temperature	Electric power input	Compressor losses	Isentropic efficiency (Overall)	Volumetric efficiency	Cooling capacity	Heating capacity	Cycle performance (COP)	Error of measurement (COP)
[rpm]	[°C]	[%]	[°C]	[°C]	[kW]	[%]	[-]	[-]	[kW]	[kW]	[-]	[%]
1800	2	20	-2.44	24.13	0.52	11.4	0.473	0.867	2.28	2.73	5.22	1.09
1800	2	30	-2.33	33.94	0.67	13.5	0.507	0.848	2.19	2.71	4.03	1.03
1800	2	45	-2.28	48.68	0.96	13.9	0.500	0.820	2.04	2.68	2.79	0.97
1800	15	20	9.42	25.50	0.51	16.2	0.398	0.918	3.26	3.68	7.28	0.93
1800	15	30	9.73	35.23	0.70	11.9	0.464	0.893	3.07	3.61	5.19	0.95
2400	-10	20	-14.42	24.05	0.65	9.5	0.555	0.865	2.17	2.72	4.16	1.04
2400	-10	30	-14.30	33.81	0.83	12.0	0.548	0.835	2.09	2.70	3.26	1.00
2400	-10	45	-13.96	48.52	1.14	11.6	0.519	0.795	1.93	2.73	2.40	0.94
2400	2	20	-3.50	25.36	0.66	6.7	0.548	0.901	3.07	3.63	5.51	0.96
2400	2	30	-3.38	35.13	0.86	9.7	0.566	0.878	2.94	3.61	4.20	0.91
2400	2	45	-3.10	49.90	1.25	9.4	0.537	0.838	2.70	3.62	2.91	0.85
2400	15	20	8.24	27.13	0.65	8.2	0.482	0.950	4.22	4.78	7.38	0.92
2400	15	30	8.58	36.96	0.88	6.9	0.549	0.920	4.10	4.82	5.47	0.85
2400	15	45	9.05	51.59	1.38	9.8	0.515	0.878	3.76	4.78	3.46	0.79
3000	-15	20	-19.62	24.28	0.80	9.1	0.563	0.851	2.31	2.97	3.72	0.97
3000	-15	30	-19.48	34.02	1.00	11.0	0.549	0.824	2.22	2.97	2.95	0.93
3000	-15	45	-19.18	48.74	1.37	12.1	0.515	0.785	2.08	3.03	2.21	0.89

List of tables

3000	2	20	-4.54	26.55	0.83	5.9	0.582	0.907	3.76	4.46	5.40	0.87
3000	2	30	-4.44	36.32	1.05	6.8	0.607	0.887	3.60	4.45	4.23	0.83
3000	2	50	-3.99	55.79	1.71	7.9	0.548	0.836	3.23	4.51	2.64	0.77
3000	15	20	6.82	28.50	0.81	5.2	0.539	0.951	5.02	5.73	7.08	0.85
3000	15	30	7.12	38.48	1.09	5.5	0.604	0.923	4.96	5.86	5.40	0.80
3600	-15	20	-20.37	24.93	0.97	8.9	0.564	0.850	2.72	3.50	3.60	0.89
3600	-15	30	-20.16	34.65	1.21	10.0	0.552	0.823	2.62	3.52	2.91	0.86
3600	-15	45	-19.98	49.49	1.66	10.6	0.518	0.788	2.45	3.64	2.19	0.82
3600	2	20	-5.78	27.56	1.02	5.5	0.588	0.903	4.32	5.19	5.07	0.82
3600	2	30	-5.86	37.31	1.29	5.6	0.613	0.882	4.12	5.19	4.03	0.79
3600	2	50	-5.18	56.83	2.09	6.6	0.546	0.832	3.72	5.36	2.56	0.73
3600	15	20	5.14	30.02	1.06	3.9	0.559	0.939	5.87	6.81	6.43	0.79
3600	15	30	5.29	39.67	1.34	5.4	0.617	0.916	5.65	6.72	5.00	0.75
4200	-15	20	-21.26	25.55	1.17	7.9	0.554	0.850	3.08	4.00	3.43	0.84
4200	-15	30	-20.86	35.33	1.43	9.0	0.554	0.827	2.99	4.08	2.86	0.81
4200	-15	45	-20.73	50.18	1.95	10.1	0.519	0.794	2.80	4.23	2.17	0.78
4200	2	20	-7.52	28.42	1.23	5.5	0.591	0.902	4.78	5.84	4.74	0.78
4200	2	30	-7.46	38.15	1.53	5.3	0.613	0.883	4.57	5.86	3.83	0.75
4200	2	50	-6.69	57.45	2.46	7.8	0.546	0.835	4.16	6.08	2.47	0.71
4200	15	20	3.55	31.27	1.29	3.6	0.577	0.939	6.53	7.70	5.96	0.75
4200	15	30	3.83	40.84	1.61	4.8	0.628	0.919	6.31	7.64	4.73	0.73
4800	-15	20	-22.30	26.10	1.35	7.8	0.550	0.850	3.38	4.46	3.31	0.80
4800	-15	30	-22.04	35.91	1.64	8.7	0.552	0.831	3.27	4.55	2.77	0.78
4800	-15	50	-21.55	55.87	2.53	13.2	0.507	0.796	2.99	4.94	1.95	0.73
4800	2	20	-9.00	29.22	1.45	5.2	0.594	0.905	5.20	6.46	4.47	0.75
4800	2	30	-8.85	38.93	1.78	5.4	0.613	0.886	5.00	6.50	3.64	0.73
4800	2	50	-8.12	58.16	2.72	6.5	0.573	0.843	4.60	6.77	2.49	0.69
4800	15	20	2.27	32.41	1.54	4.4	0.587	0.942	7.18	8.57	5.56	0.72

List of tables

4800	15	30	2.41	41.91	1.91	4.3	0.631	0.922	6.88	8.54	4.48	0.70
5400	-15	20	-23.30	26.62	1.54	8.0	0.545	0.851	3.66	4.89	3.18	0.77
5400	-15	30	-22.99	36.50	1.87	8.6	0.547	0.830	3.54	5.02	2.68	0.75
5400	-15	50	-22.38	56.49	2.86	13.8	0.503	0.787	3.32	5.51	1.92	0.71
5400	2	20	-10.03	30.00	1.67	5.5	0.590	0.905	5.63	7.08	4.23	0.73
5400	2	30	-9.99	39.69	2.05	6.2	0.607	0.885	5.41	7.13	3.47	0.71
5400	2	50	-9.04	58.79	3.09	6.7	0.570	0.840	4.99	7.48	2.42	0.68
5400	15	20	1.09	33.47	1.80	4.9	0.590	0.940	7.76	9.39	5.21	0.70
5400	15	30	1.21	42.89	2.21	4.9	0.630	0.923	7.44	9.36	4.23	0.69

A-4.3 Measurement matrix for the cycle evaluation without economiser

Table A-4 shows all measurement points, which were used for the evaluation of the influence of the economiser.

Table A-4: Measurement matrix for the evaluation of the influence of the economiser

Compressor speed	Brine inlet temperature	Water inlet temperature	Evaporation temperature	Condensing temperature	Electric power input	Compressor losses	Isentropic efficiency (Overall)	Volumetric efficiency	Cooling capacity	Heating capacity	Cycle performance (COP)	Error of measurement (COP)
[rpm]	[°C]	[%]	[°C]	[°C]	[kW]	[%]	[-]	[-]	[kW]	[kW]	[-]	[%]
1800	2	20	-2.50	23.97	0.52	13.2	0.452	0.875	2.16	2.59	4.94	1.11
1800	2	30	-2.14	33.61	0.62	14.3	0.502	0.854	1.99	2.44	3.90	1.09
1800	2	45	-2.17	47.99	0.84	14.6	0.480	0.810	1.65	2.17	2.58	1.08
3000	-15	20	-19.00	23.89	0.72	11.0	0.544	0.853	1.99	2.55	3.53	1.04
3000	-15	30	-18.76	33.40	0.88	10.8	0.510	0.822	1.78	2.41	2.73	1.03
3000	2	20	-4.17	26.10	0.77	6.0	0.580	0.919	3.51	4.16	5.37	0.90

List of tables

3000	2	30	-3.82	35.58	0.96	7.0	0.596	0.900	3.20	3.95	4.12	0.87
3000	2	50	-3.65	54.39	1.42	9.8	0.535	0.854	2.48	3.47	2.43	0.85
3000	15	50	8.11	56.36	1.52	6.5	0.584	0.898	3.64	4.76	3.13	0.78
4200	-15	20	-20.41	24.85	1.05	9.2	0.528	0.856	2.65	3.45	3.29	0.89
4200	-15	30	-20.14	34.27	1.26	9.1	0.507	0.824	2.36	3.30	2.63	0.87
4200	2	20	-7.06	27.67	1.14	4.4	0.580	0.911	4.35	5.33	4.67	0.94
4200	2	30	-6.68	37.06	1.37	6.4	0.598	0.896	3.99	5.09	3.71	0.78
4200	2	50	-5.65	55.72	2.01	8.1	0.532	0.852	3.15	4.66	2.32	0.76
4200	15	50	5.85	57.95	2.14	5.4	0.595	0.899	4.61	6.30	2.94	0.71
5400	-15	20	-22.37	25.71	1.38	8.6	0.508	0.862	3.09	4.17	3.01	0.81
5400	-15	30	-22.00	35.19	1.65	9.8	0.488	0.831	2.77	4.02	2.44	0.80
5400	2	20	-8.92	29.08	1.55	6.4	0.568	0.920	5.15	6.45	4.17	0.78
5400	2	30	-8.84	38.30	1.84	7.4	0.582	0.907	4.67	6.14	3.35	0.73
5400	2	50	-7.39	56.78	2.62	8.1	0.521	0.867	3.71	5.77	2.20	0.71
5400	15	50	4.39	59.37	2.83	5.5	0.590	0.916	5.47	7.79	2.75	0.68

A-4.4 Measurement matrix for the desuperheater evaluation

Table A-5 shows all measured values recorded with desuperheater.

Table A-5: Measurement matrix for the evaluation of the cycle performance with desuperheater

Compressor speed	Brine inlet temperature	Water inlet temperature	Evaporation temperature	Condensing temperature	Electric power input	Cooling capacity	Heating capacity (Condenser)	Water outlet temperature (Desuperheater)	Mass flow (Desuperheater)	Heating capacity (Desuperheater)	Cycle performance (COP)	Error of measurement (COP)
[rpm]	[°C]	[%]	[°C]	[°C]	[kW]	[kW]	[kW]	[°C]	[kg/h]	[kW]	[-]	[%]
1800	2	20	-2.48	24.02	0.54	2.29	2.33	39.9	23.8	0.49	5.25	1.47
1800	2	25	-2.43	28.88	0.62	2.23	2.28	50.0	19.4	0.52	4.53	1.67
1800	2	30	-2.44	33.71	0.71	2.18	2.19	55.1	20.3	0.55	3.83	1.70
2100	-5	20	-9.36	23.96	0.61	2.17	2.25	45.0	19.2	0.51	4.51	1.69
2100	-5	25	-9.33	28.75	0.70	2.12	2.18	50.0	21.0	0.56	3.94	1.69
2100	-5	30	-9.25	33.72	0.79	2.08	2.19	65.0	13.9	0.54	3.47	2.20
2100	2	20	-3.03	24.60	0.61	2.69	2.76	44.9	20.5	0.53	5.43	1.48
2100	2	25	-2.93	29.44	0.70	2.63	2.67	50.0	22.5	0.59	4.69	1.47
2100	2	30	-2.90	34.27	0.80	2.55	2.61	60.0	19.0	0.61	4.03	1.67
2400	-10	20	-14.29	23.97	0.67	2.15	2.30	55.0	13.2	0.50	4.19	2.14
2400	-10	25	-14.18	28.79	0.77	2.10	2.23	59.9	14.6	0.56	3.63	2.15
2400	-10	30	-14.15	33.74	0.86	2.08	2.23	70.1	11.9	0.53	3.19	2.44
2400	-5	20	-9.92	24.38	0.68	2.48	2.61	50.0	16.6	0.53	4.63	1.72
2400	-5	25	-9.81	29.25	0.76	2.44	2.54	55.0	17.6	0.57	4.07	1.72
2400	-5	30	-9.70	34.14	0.87	2.39	2.52	65.0	15.4	0.59	3.56	1.94
2400	2	20	-3.54	25.26	0.68	3.08	3.22	50.0	16.5	0.52	5.48	1.49

List of tables

2400	2	25	-3.45	30.07	0.78	3.01	3.12	55.0	18.8	0.59	4.77	1.49
2400	2	30	-3.40	34.96	0.89	2.93	3.10	65.0	15.3	0.58	4.13	1.67
3600	-15	30	-20.27	34.38	1.24	2.60	2.61	60.0	28.7	0.92	2.85	1.51
3600	-15	30	-20.23	34.42	1.23	2.59	2.67	69.8	20.0	0.87	2.87	1.90
3600	-15	30	-20.21	34.51	1.23	2.59	2.80	79.9	13.4	0.74	2.87	2.33
3600	2	30	-5.55	36.83	1.32	4.16	4.08	50.2	62.2	1.17	3.99	0.92
3600	2	30	-5.56	36.92	1.32	4.16	4.26	60.0	32.8	0.99	3.98	1.11
3600	2	30	-5.59	37.13	1.33	4.15	4.53	70.0	17.6	0.73	3.97	1.34
5400	-15	30	-23.16	35.75	1.89	3.52	3.52	60.0	47.7	1.48	2.65	1.12
5400	-15	30	-23.30	35.83	1.88	3.49	3.60	70.0	32.7	1.39	2.65	1.39
5400	-15	30	-23.26	35.97	1.89	3.49	3.73	79.9	23.3	1.26	2.65	1.71
5400	2	30	-9.41	39.08	2.07	5.51	5.59	60.1	58.1	1.67	3.50	0.88
5400	2	30	-9.42	39.31	2.08	5.50	5.86	69.9	34.8	1.39	3.48	1.03
5400	2	30	-9.39	39.74	2.10	5.50	6.43	80	15.4	0.79	3.44	1.22